PERFORMANCE OF ECM CONTROLLED VAV FAN POWERED TERMINAL UNITS

A Thesis

by

ANDREW CRAMLET

Submitted to the Office of Graduate Studies of
Texas A&M University
in partial fulfillment of the requirements for the degree of

MASTER OF SCIENCE

August 2008

Major Subject: Mechanical Engineering

PERFORMANCE OF ECM CONTROLLED VAV FAN POWERED TERMINAL UNITS

A Thesis

by

ANDREW CRAMLET

Submitted to the Office of Graduate Studies of
Texas A&M University
in partial fulfillment of the requirements for the degree of

MASTER OF SCIENCE

Approved by:

Chair of Committee,	Dennis O'Neal
Committee Members,	Warren Heffington
	Jerry Jackson
Head of Department,	Dennis O'Neal

August 2008

Major Subject: Mechanical Engineering

ABSTRACT

Performance of ECM Controlled VAV
Fan Powered Terminal Units. (August 2008)
Andrew Cramlet, B.S., The Ohio State University
Chair of Advisory Committee: Dr. Dennis O'Neal

Empirical performance models of fan airflow, primary airflow and power consumption were developed for series and parallel variable air volume fan powered terminal units. An experimental setup and test procedure were created to test the terminal units at typical design pressures and airflows. Each terminal unit observed in this study used an 8 in (20.3 cm) primary air inlet. Two fan motor control methods were considered. The primary control of interest was the electronically commutated motor (ECM) controller. Data collected were compared with previous research regarding silicon rectified control (SCR) units. Generalized models were developed for both series and parallel terminal units. Coefficients for performance models were then compared with comparable SCR controlled units. Non-linear statistical modeling was performed using SPSS software (2008).

In addition to airflow and power consumption modeling, power quality was also quantified. Relationships between real power (watts) and apparent power (VA) were presented as well as harmonic frequencies and total harmonic distortion. Power quality was recorded for each ECM controlled terminal unit tested. Additional tests were also made to SCR controlled terminal units used in previous research (Furr 2006).

The airflow and power consumption performance models had an R^2 equal to 0.990 or greater for every terminal unit tested. An air leakage model was employed to account for leakage in the parallel designed VAV terminal units when the internal fan was turned off. For the leakage model, both ECM and SCR controlled units achieved an R^2 greater than or equal to 0.918.

ACKNOWLEDGMENTS

The work performed in this research project was organized and funded by a consortium of VAV fan powered terminal unit manufacturers. I would like to thank A.O. Smith Corp, General Electric, Krueger, Metalaire, and Nailor Industries for their financial contributions.

I would like thank Dr. Dennis O'Neal, Dr. Warren Heffington and Dr. Jerry Jackson for agreeing to serve as my committee advisors. To Dr. Leslie Feigenbaum, thank you for graciously agreeing to attend my defense in substitute of Dr. Jackson. I would also like to acknowledge Kelly Milligan and Carlos Ortiz for their dedicated support on site at the Energy Systems Lab. I would be remiss not to mention the efforts of Michael Davis and James Furr - individuals who were able to give project background, insight and assistance despite being removed from the project by both geography and professional occupation. I would also like to mention Jake Edmondson, the current student caretaker of this project. His recent addition to the team greatly eased my personal burden and without question his participation has strengthened the work in general.

I would also like to take a moment to thank my professional friends, colleagues and supervisors who supported my decision to return to academia. Specifically my former supervisor Hector Robledo and project manager Bill Mitchell, whose letters of recommendation were essential in gaining acceptance into graduate school.

To my friends and family, who have endured my various migrations from Ohio to Michigan and then to Texas, I offer a heartfelt thank you for your steadfast support.

Lastly to my Mum, Dad, and brother - your collective influence has been immeasurable, and any success I achieve is surely yours as well. Thank you for your encouragement, your patience, your example... and the occasional use of your Mastercard. "Priceless."

Thank you all.

NOMENCLATURE

AHU	Air Handling Unit
C	Capacitance
CAV	Constant Air Volume
cp	Specific heat capacity
DAQ	Data Acquisition
dE/dt	Change in energy per unit time
DP	Differential Pressure
ECM	Electronically Commutated Motor
f	Frequency
fb	Half-power frequency
FPTU	Fain Powered Terminal Unit
$\|H(f)\|$	Magnitude of output signal from low pass filter
h	Enthalpy
HVAC	Heating, Ventilation, & Air Conditioning
I_{RMS}	RMS value of current (amps)
$\dot{m}$	mass flow rate
P_{iav}	Inlet air velocity differential pressure
P_{down}	Downstream static pressure
P_{unit}	Static pressure inside terminal unit
P_{up}	Upstream static pressure
$P_{owerfan}$	Power consumption of terminal unit fan
PF	Power Factor
PSC	Permanent Split Capacitor
$\dot{Q}$	Change in heat input per unit time
Q_{fan}	Amount of airflow through terminal unit fan
$Q_{induced}$	Amount of airflow induced from plenum
$Q_{leakage}$	Amount of airflow leaked from a terminal unit
Q_{out}	Amount of parallel terminal unit airflow output
$Q_{primary}$	Amount of primary airflow
R	Resistance
RMS	Root Mean Square

S	Damper orientation (degrees)
SCR	Silicon Controlled Rectifier
T	Temperature
ΔT	Temperature differential
THD	Total Harmonic Distortion
V_{DAQ}	Voltage entering DAQ card
V_{fan}	Voltage entering terminal unit fan
V_{RMS}	RMS value of voltage (volts)
VA	Volt-Amps (apparent power)
VAV	Variable Air Volume
VSD	Variable Speed Drive
W	Watts (real power)
$\dot{W}$	Change in work per unit time

TABLE OF CONTENTS

LIST OF FIGURES

Page

Page

Page

LIST OF TABLES

CHAPTER I

INTRODUCTION

The United States consumes approximately 100 quadrillion BTU's (29.3 PW-h) of energy per year, of which approximately 30% is attributed to residential and commercial buildings. Of this 30%, the fraction of energy required to both heat and cool these buildings is between 25% in the commercial sector and 45% in the residential sector (Kreider et al. 2002). Therefore, between 7.5 to 13.5 quadrillion BTU's (2.2 to 4.0 PW-h) of energy are required for annual HVAC operation.

With crude oil prices exceeding $135 per barrel and natural gas prices approaching $12 per MMBTU, the cost of energy is at an all-time high. Energy conservation and efficiency are now being moved to the forefront of today's society and engineering community. With so much energy being required for heating and cooling residential and commercial buildings, millions of dollars are at stake when finding even the smallest of HVAC optimization.

The ultimate purpose of an HVAC system is to provide thermal comfort and healthy indoor air quality to the occupants of a building (Engdahl and Johannson 2003). In commercial buildings, this is achieved primarily by two systems: constant air volume (CAV) and variable air volume (VAV). In CAV systems, a constant flow of conditioned air is delivered to a space which meets demand by modulating supply air temperature . A VAV system adjusts to demand by modulating the quantity of incoming air which remains at a constant air temperature. In published reports, it has been shown that VAV systems can offer a 50% energy savings over CAV systems due to the difference in required fan operation (Ardehali and Smith 1996) which make it the preferred commercial HVAC system.

The supply air introduced by a VAV system into a zone is controlled by the VAV terminal unit (Figure 1-1). In its most simple form, terminal units do little more than reduce conditioned primary airflow supplied by an upstream supply fan via mechanical dampers. Most VAV terminal units have a fan that helps induce air from the return air plenum; these are known as fan powered terminal units (FPTU). There are two fundamental configurations of FPTUs: series and parallel. These more complex VAV systems allow a mixture of both primary air and recycled return air drawn from the return air plenum.

This thesis follows the style of *HVAC&R Research.*

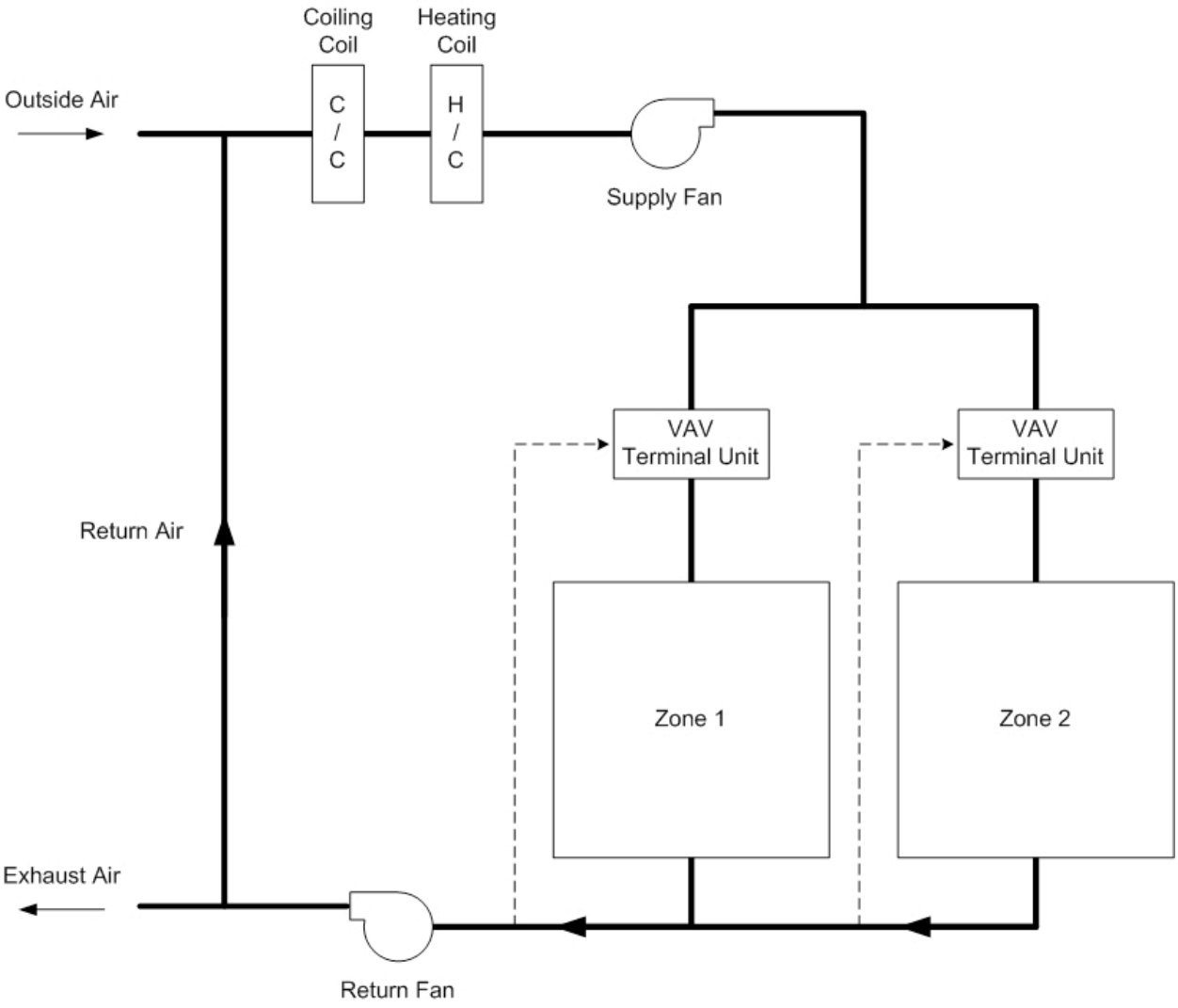

Figure 1-1: Airflow of classic VAV system

Series and parallel FPTUs mix primary and return air-streams differently (Figure 1-2). Terminal units are designated as "series" when the internal fan works in series with the primary system supply fan. The fan is always on, creating a vacuum inside the terminal unit, which draws air through the box. Terminal units are designated as "parallel" when the internal fan works in parallel with the primary system supply fan. The air-streams are mixed after the terminal fan which results in positive pressure inside the chamber. However, because the terminal fan is not required to pass primary air through the box in the parallel configuration, fan operation is not mandatory.

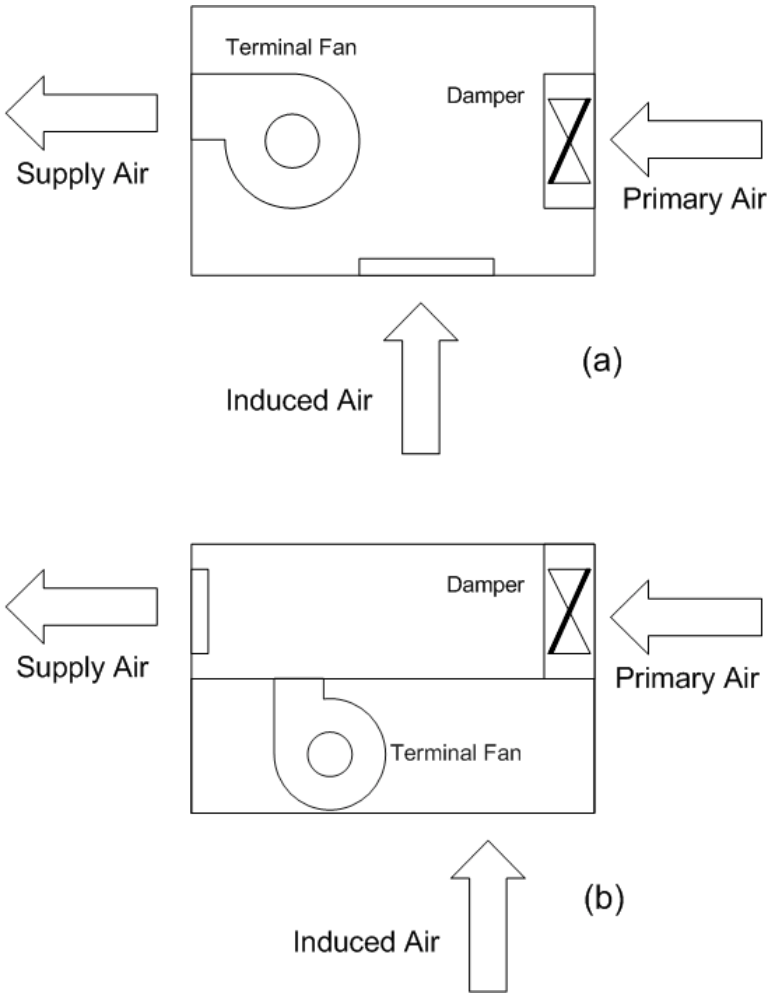

Figure 1-2: Generic VAV fan powered terminal unit design (a) series (b) parallel

This research had two primary objectives. The first was airflow performance modeling. Characteristics equations for both primary and fan airflow were established as a function of variables such as temperature, pressure and fan input voltage. The empirically driven models allowed prediction of terminal unit airflow over a large range of operating conditions. These FPTU models can be used in building simulation models to estimate the total energy use for heating and cooling in buildings.

The second research objective was FPTU energy performance. Authors from academia and the HVAC industry have long believed parallel FPTUs are more efficient than series units due to the mandatory fan operation of the series design (Elleson 1993, Wendes 1994, Chen and Demster 1996). This opinion has influenced energy codes and standards such as ASHRAE Standard-90.1 (2004) which states that all VAV systems be of parallel design. In design guidelines published by the California Energy Commission (Hydeman et al. 2003) it states that series fan powered terminal units should be avoided.

However, modern technology may narrow the differences between series and parallel performance. Specifically, terminal units which are controlled by electronically commutated motor (ECM) variable speed fan motors have not been adequately researched. In contrast to fixed speed AC induction motors, ECM motors use a fixed magnet, high efficiency brushless DC motor that can dynamically fan speed and torque to produce a uniform preset airflow. Power consumption performance models were empirically generated as a function of airflow demand and environmental conditions for both series and parallel FPTUs. Both ECM airflow and power consumption models were compared with SCR controlled FPTUs characterized in previous research (Furr et al. 2007).

Observation of fan power quality characteristics associated with the respective FPTU fan controller/motor combinations were also reported. Power quality is a set of boundaries that allow electrical systems to function in their intended manner without significant loss of performance or life (Sankaran 2002). Figure 1-3 is commonly referred to as a "power triangle."

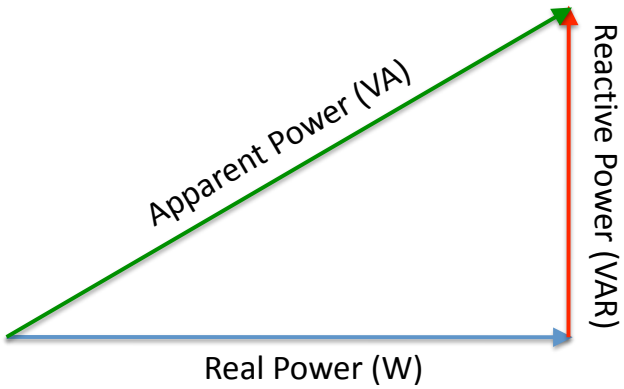

Figure 1-3: Power triangle

The relationship between real and apparent power can be expressed using the Pythagorean Theorem:

$$(\text{apparent power})^2 = (\text{real power})^2 + (\text{reactive power})^2 \quad (1.1)$$

The associated power factor is defined as the ratio of real power to apparent power:

$$\text{power factor} = \frac{\text{real power}}{\text{apparent power}} \quad (1.2)$$

Ideally, power factor (PF) is equal to 100%. However, in practice, PF is adversely affected by loads such as those found in inductors. The significance of power factor is that power utility companies supply volt-amps (apparent power) but typically charge for watts (real power). Power factors below 100% require a utility to generate more than the minimum volt-amperes necessary to supply the real power required of a given device. This increases generation and transmission costs which are often passed onto the customer, especially in large residential and commercial buildings.

Uncorrected power factor will cause increased losses in electrical distribution systems and limit capacity for expansion. Higher power factor will reduce voltage drop at the point of use. When voltage below equipment rating is used there is a loss in efficiency, increased current and reduced starting in torque motors. Under-voltage reduces the load motors can carry without overheating or stalling (EnergyIdeas 2003).

The power quality analysis also included harmonics associated with voltage, current and real power. Specific attention was given to the amperage triplen harmonics. Triplen harmonics are odd harmonics which are also multiples of 3. They represent zero sequence currents which are in phase with the 60 Hz fundamental current. Triplen current harmonics add to each other and cause heat gain and voltage drop along the neutral conductor and induce noise into nearby circuits (Kennedy 2000).

In addition to triplens, which are a select group of harmonics, total harmonic distortion (THD) was also reported in regards to power quality. THD accounts for all harmonics and is typically presented in percentage form. It is defined per Eq. (1.3) as the ratio of cumulative harmonic frequencies over the fundamental.

$$\text{THD} = \frac{\sum \text{harmonic powers}}{\text{fundamental frequency power}} = \frac{f_2 + f_3 + \ldots + f_n}{f_1} \tag{1.3}$$

Total harmonic distortion is a singular variable which represents the aggregate distortion to the ideal, sinusoidal supply waveform due to the interaction of distorting loads within the control volume. Adverse effects of THD are the overheating of induction motors, transformers and capacitors and the overloading of neutrals (Gosbell 2000).

CHAPTER II

LITERATURE REVIEW

Variable air volume (VAV) systems are widely considered the most efficient means of distributing conditioned air in commercial and industrial buildings. In the 1970's the Japanese created a simulation tool HASP/ACLD 7101 (1971) that assisted researchers in declaring a Tokyo-based VAV system could provide a 40% reduction in energy consumption versus a similarly constructed dual duct constant air volume (CAV) system (Inoue and Matsumoto 1979).

Sekhar (1997) reached similar conclusions while testing two buildings located in a hot, humid climate. His computer simulations yielded VAV energy savings of 10-20% versus their CAV counterparts. Johnson (1984) concluded in an experiment for testing various airflow control strategies, that an interior-zone retrofit of CAV to VAV could provide a 53% improvement in energy efficiency. However, none of the studies cited included modern-day fan powered terminal units. Instead they used damper-only VAV subsystems.

Ardehali and Smith (1996) included FPTUs in their computer modeling. Using the TRACE (1993) simulation program, they compared CAV and VAV system performance using Des Moines, Iowa weather data. The research was based on what they described as a "typical" office building configuration. The results of their study reflected the 1979 conclusions of Inoue and Matsumoto. They concluded that VAV-based HVAC systems could indeed result in energy savings up to 40% versus CAV-based systems.

Given the historical acceptance that VAV systems are the most practical, efficient means of air distribution, attention has turned towards optimizing this HVAC system design. VAV systems can incorporate one of two fundamental fan powered terminal unit (FPTU) designs: series or parallel construction. Parallel FPTU fans operate in parallel to incoming primary airstream and optional in operation. Series FPTU fans operate in series with the incoming primary air and their operation is mandatory. Proper application of these two systems is one aspect of HVAC design currently being studied by the community at large.

Elleson (1993) conducted a field study of cold air distribution systems with both series and parallel FPTUs in two separate buildings. Contrary to typical 55 oF (12.8 oC) supply air temperature, this study used 45 oF (7.2 oC) supply air. It was the purpose of this research to

document the benefits of the cold air distribution system. However, results from the simulation also provided a comparison of series and parallel FPTUs in the context of conventional air distribution systems. Regarding both cold air and conventional HVAC systems, the study concluded that parallel configured FPTUs were more energy efficient than their series counterparts.

The California Energy Commission (Hydeman et al. 2003) sponsored an energy study which included a comparison of series and parallel VAV terminal units operating in the perimeter zone. This research was based on the DOE-2 (1998) computer simulation tool and took into consideration the reduced static pressure of the main supply fan in series systems. The research concluded that the parallel FPTU offered a 9% energy savings over the series configuration. The improved performance was concluded to be due to the series configuration's mandatory use of it's internal fan. However, this simulation was based on the mild California climate. It was noted that in cooler climates, where the supply air reheat requirement is much larger, the parallel configuration's internal fan would require more frequent operation and narrow the performance advantage.

Commercial building's HVAC systems are commonly designed using building simulation software such as: DOE-2, BLAST (1992) or EnergyPlus (Crawley et al. 2000). However, these simulation tools are only as accurate the individual HVAC component models used inside them. The current FPTU-based VAV sub-system models are not adequate for accurate, comprehensive simulation; consequently, the entire HVAC system accuracy suffers. Therefore, there is still ongoing debate as to the correct application of series and parallel terminal units.

To date, there is very little experimental evidence to support the computer simulations by Elleson (1993) or the California Energy Commission (2003). The claim that parallel designed FPTUs outperformed their series counterpart was almost entirely on computer simulations with primitive VAV terminal models. Khoo et al. (1998) developed non-linear models for three damper-only controlled VAV terminal units. This study concluded that the damper-only approximations used in HVAC design software were not accurately representative of their real-world counterparts.

Furr et al. (2007) provided empirically-driven quantitative performance models for both series and parallel fan powered terminal units. Data were collected spanning several manufacturers and included industry standard inlet configurations of 8 in. (20.3 cm) and 12 in. (30.5 cm). The research focused on developing detailed performance models for both induced airflow and power

consumption. Models were developed as functions of upstream and downstream static pressure, inlet air velocity pressure, primary damper setting and SCR input control voltage.

However, Furr's research was limited to VAV FPTUs equipped with fixed speed SCR internal AC induction motors. Variable speed drive (VSD) fan motors are also commercially used inside both series and parallel terminal units. These electronically assisted motors allow a more dynamic range of operation. VAV systems with VSD fan controls allow the motor to reduce speed "on the fly" as the load decreases while maintaining a fixed volumetric airflow. For example, a 50% reduction in speed results in a 88% reduction in energy consumption (SEEP 2006). Such operation would reduce the energy use of series FPTUs during reduced loads.

One such VSD device is the ECM (Electronically Cummutated Motor) controller. These controllers are programable and use brushless DC motors with a permanent magnet rotor and built-in inverter. They have made it possible to achieve Seasonal Energy Efficiency Ratio (SEER) ratings of 12 and higher in residential air conditioners (Nailor Industries 2003). Widely used permanent split capacitor (PSC) induction motors typically achieve efficiencies in the range of 12-45% and suffer greatly at low speed. However, ECM motors in maintain a high efficiency of 65-72% at all operating speeds (Nailor Industries 2003).

Building HVAC simulation models are only as valid as the system models contained within it. Furr et al. (2007) advanced the research of Elleson (1993) and Kolderup et al. (2003) by empirically deriving characteristic equations for VAV fan powered terminal units using AC fan motors. Power and airflow models were created for SCR controlled FPTUs. An important contribution of Furr et al. (2007) was identifying and quantifying leakage in parallel FPTUs. While leakage does not affect series FPTUs, it does reduce the performance of parallel FPTUs. Furr et al. (2007) was able to empirically demonstrate that the gap between series and parallel performance was smaller than previously thought due to the leakage impact. At the terminal level, energy consumption differential could be as low as 8%. However, Furr et al. did not take into account the commercially available VSD controlled terminal units.

The literature review indicated that the development of analytical models for fan powered terminal unit simulation is still largely incomplete. Empirical data are still needed for modern VSD controlled motors and characteristic performance models still need to be generated. Power quality assessment is largely ignored or underdeveloped. Only after predictive computer simulation models are updated can informative conclusions be drawn regarding the recommendation and implementation of series and parallel fan powered terminal units.

CHAPTER III

EXPERIMENTAL APPARATUS

The test equipment used in this study can be categorized into two distinct groups: airflow and power. Data for each were collected in separate acquisition systems and then later merged into a single electronic data set. This chapter describes those respective systems.

3.1 Airflow Equipment

An overview of the test apparatus is shown in Figure 3-1. Two airflow chambers (AMCA 1999) were used to measure primary and supply air. The upstream flow chamber ("AMCA Figure 15") was used to measure the primary air delivered to the fan powered terminal unit (FPTU). The "AMCA Figure 12" chamber was used to measure the supply airflow provided by the FPTU.

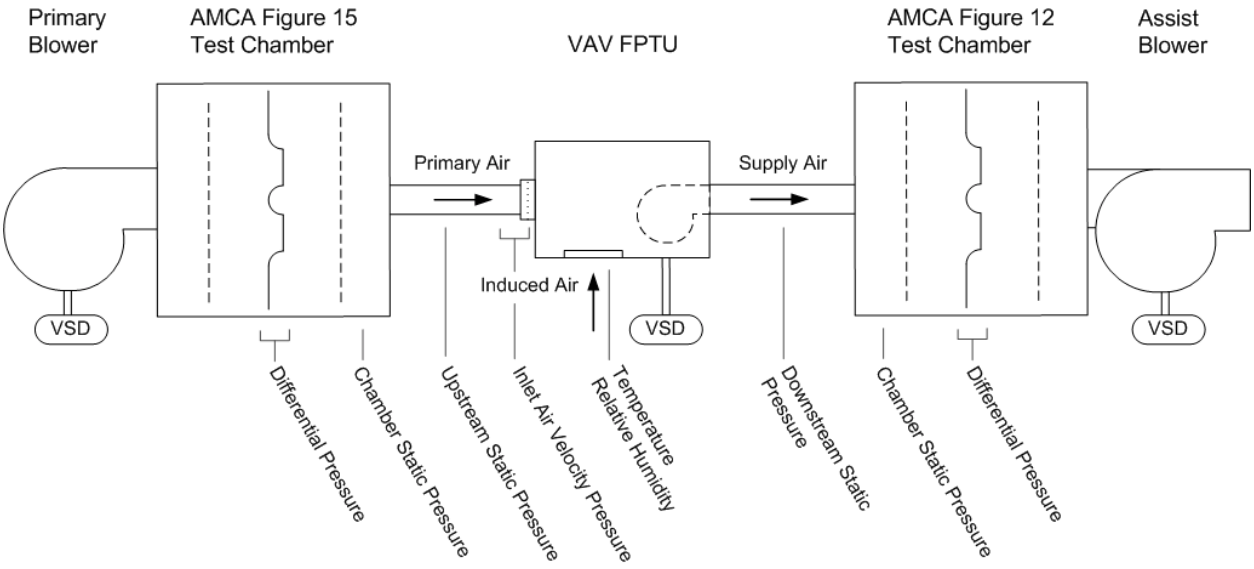

Figure 3-1: Airflow test apparatus including FPTU and airflow chambers

The individual airflow components referenced in Figure 3-1 are described in greater detail in the following sections of this chapter.

3.1.1 Variable Air Volume Terminal Units. The purpose of this study was to characterize the performance of variable air volume (VAV) fan powered terminal units (FPTUs). These HVAC devices draw available air from a building plenum space into the unit and mix it with the conditioned air-stream provided by an upstream supply fan and coiling coil. FPTUs include both series (Figure 3-2) and parallel designs (Figure 3-3).

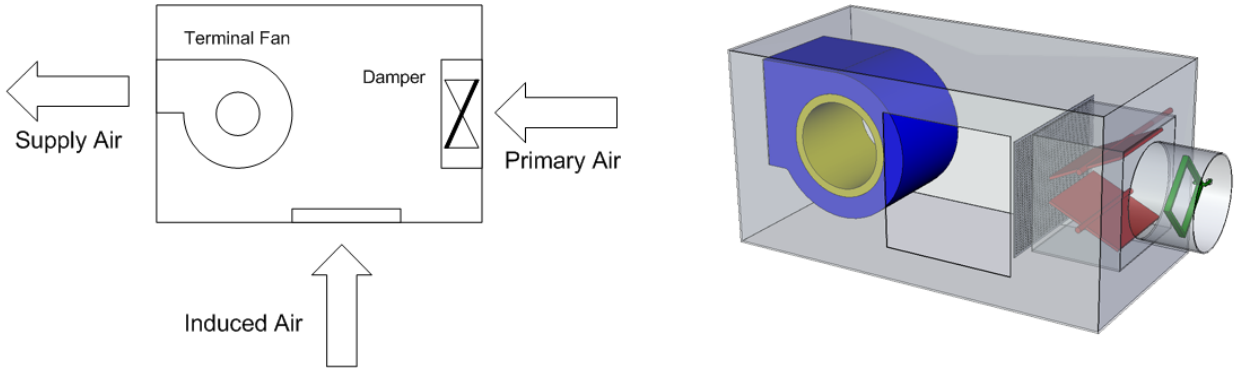

Figure 3-2: Typical VAV series fan powered terminal unit design

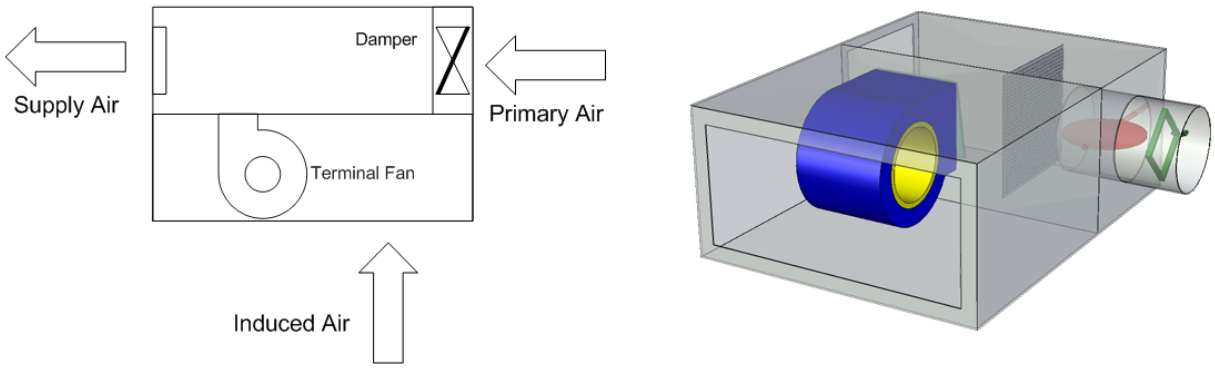

Figure 3-3: Typical VAV parallel fan powered terminal unit design

Although no two manufacturers produce identical terminal units, most designs share common elements. Using the designs in Figures 3-2 and 3-3 as reference, the internal components are discussed in greater detail.

Incoming primary air was received via an inlet duct which has an internal differential pressure sensor (Figure 3-4). In this case, the device was a multi-point averaging sensor which takes four location specific pressure measurements (labeled 1 through 4 on the figure) inside the inlet duct and averages them. Multiple measurements allow a better representation of the mean pressure differential throughout the entire duct cross-section in the case of uneven airflow. The averaged differential inlet pressure was then accessible to a pressure transducer via the two respective outlet taps.

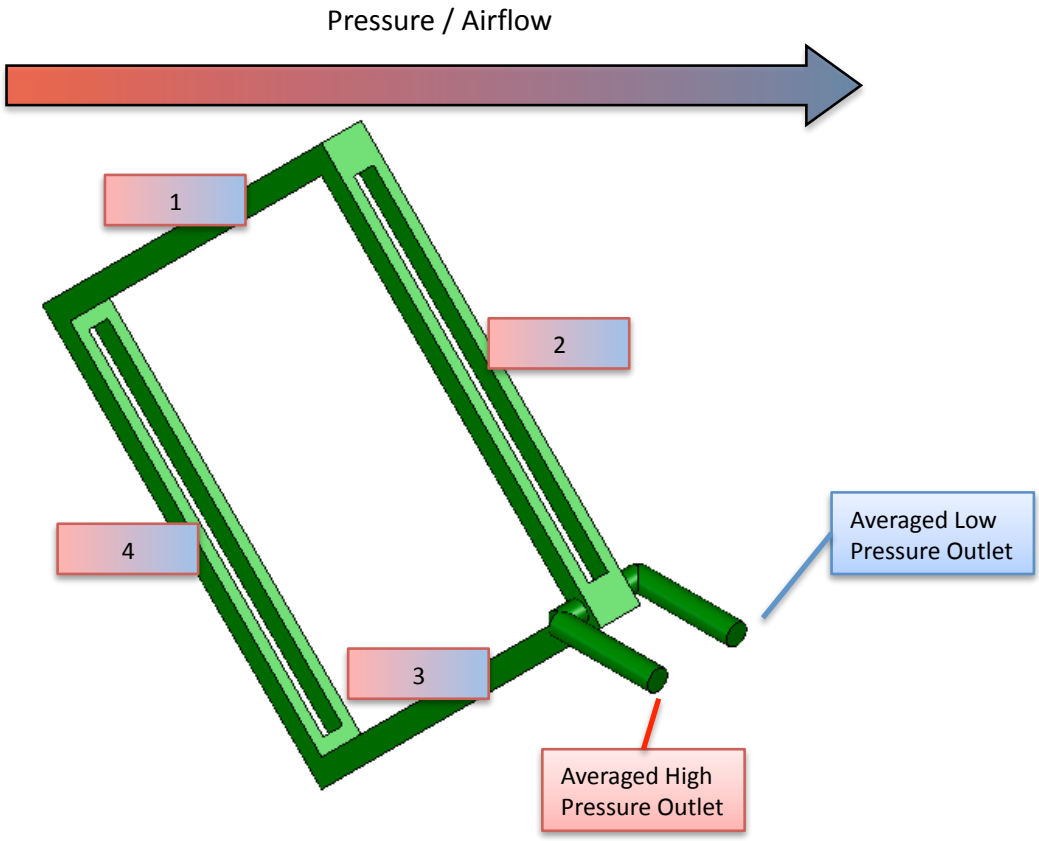

Figure 3-4: FPTU multi-point differential pressure sensor

The next internal FPTU element was a mechanical damper which regulates the flow rate of primary air and helps set the pressure differential across the entire terminal unit. Dampers typically come in one of two configurations (Figure 3-5). In some cases, a simple circular butterfly damper was utilized which has a 90º range of full operation. A more complex combination of mechanically linked opposing blades were also used which has an approximate 45º of operational range.

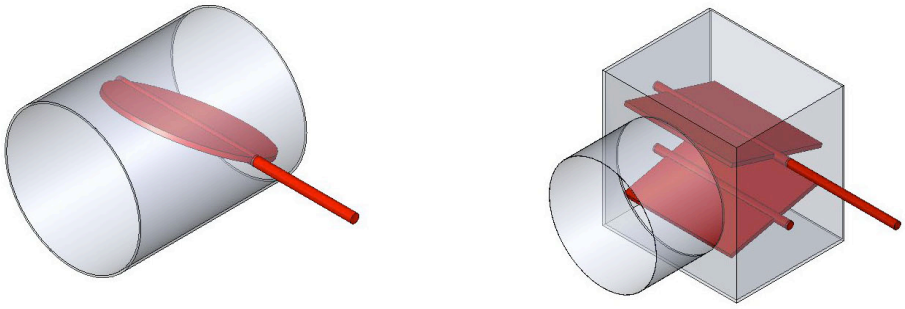

(a) (b)

Figure 3-5: Primary air damper designs: (a) butterfly vs. (b) opposing blade

The terminal units tested in this study use damper designs which are operated by simple rotation of a single input shaft. The respective angles of rotation were achieved by using an open-air damper actuator with 0-10 VDC input (Figure 3-6). The use of a remotely controlled actuator allowed precise control and repeatability of damper position.

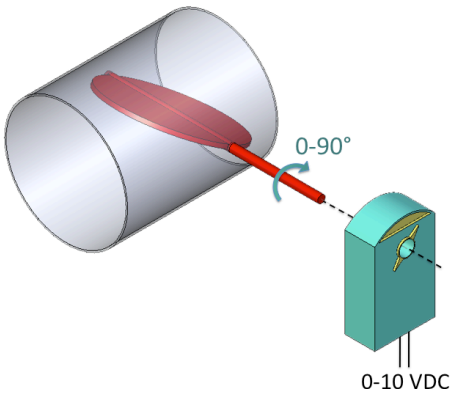

Figure 3-6: Butterfly damper with open-air actuator

Once the conditioned primary air passes through the inlet duct, some systems employ a form of diffuser to help make the airflow more uniform inside the terminal unit. The diffuser in this study was a simple perforated piece of sheet-metal placed orthogonal to the inlet just beyond the inlet damper (Figure 3-7).

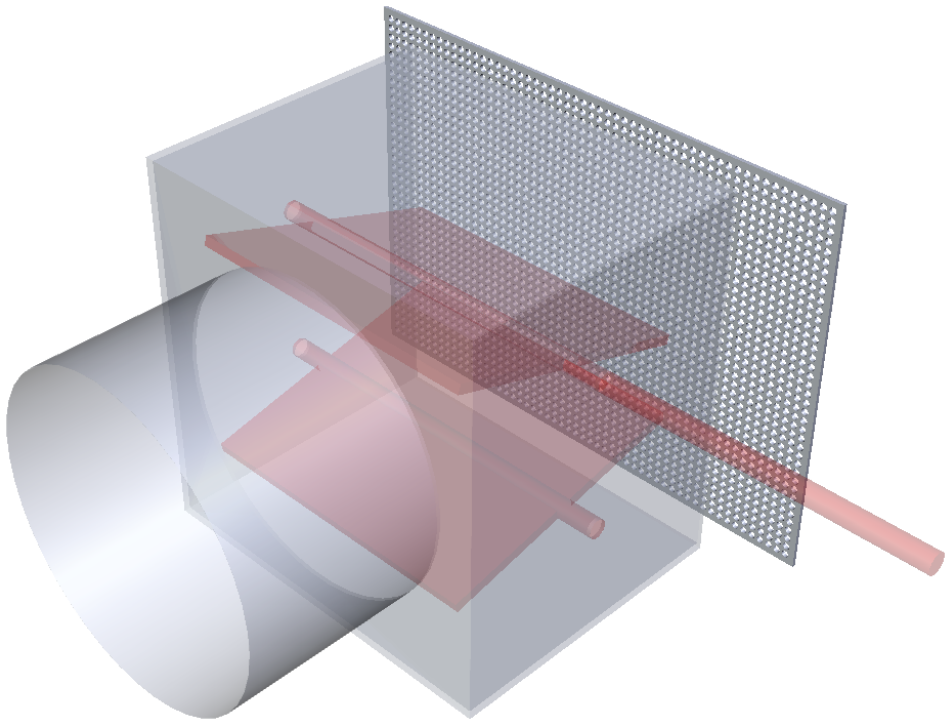

Figure 3-7: Perforated sheet-metal diffuser

The heart of the fan powered terminal unit is a centrifugal fan (Figure 3-8). Typically a single width, forward curved design, these fans can come in a range of sizes and capacities used to draw ambient air into the conditioned supply stream. The fan motors in this study were supplied with single phase 277 voltage AC power (Table 3-1).

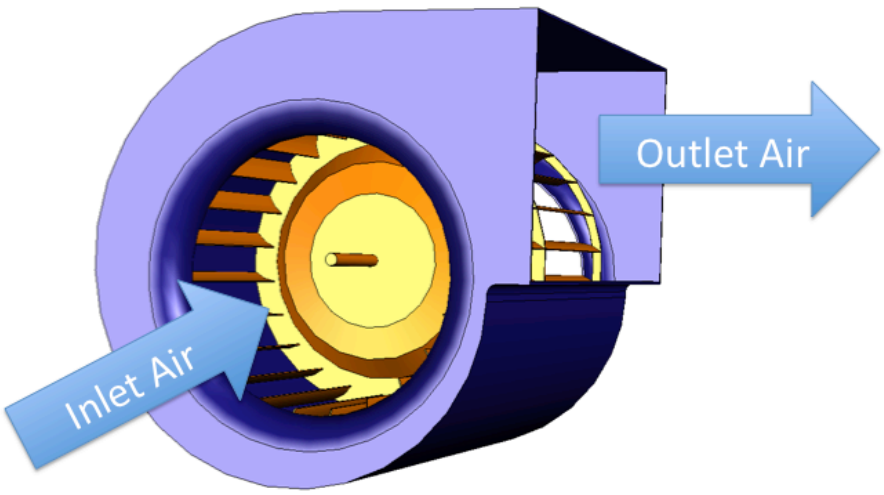

Figure 3-8: Typical FPTU centrifugal fan

Table 3-1: FPTU fan motor characteristics

	Fan Controller	Motor Type	Rated Fan Power
Series	ECM	Brushless DC	1/2 hp (373 W)
Parallel	ECM	Brushless DC	1/2 hp (373 W)
Series	SCR	Induction AC	1/2 hp (373 W)
Parallel	SCR	Induction AC	1/4 hp (186 W)

In contrast to older SCR controlled AC induction motors, the terminal fans used in this study were driven by electronically commutated motors (ECM). The brushless DC motor was designed with a built-in inverter and a microprocessor-based motor controller (Figure 3-9). The controller was matched to the unit's internal fan and pre-programmed by the supplier. The ECM motor can dynamically adjust fan torque and speed to maintain a preprogrammed airflow. The microprocessor and ECM motor controller for all FPTUs tested in this study were operated via a 0-10 VDC input signal.

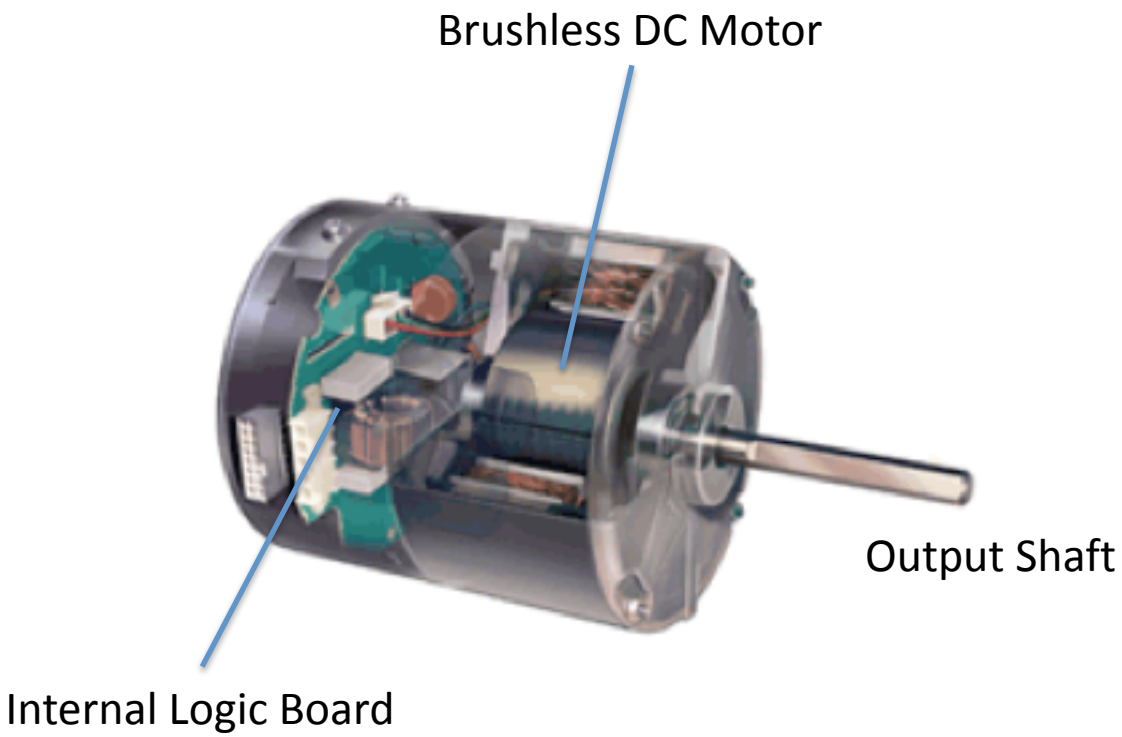

Figure 3-9: Typical electronically commutated motor controller (compliments of GE 2000)

The final feature of the fan powered terminal unit was the backdraft damper, which was only used on the parallel configuration. The purpose of the damper was to increase system efficiency by preventing conditioned supply air from leaking through the fan interface and escaping into the space adjacent to the FPTU. There were two designs typically employed by manufacturers: air-operated and gravity-operated (Figures 3-10 and 3-11, respectively). The air-operated damper was hinged along the fan outlet's upstream edge and closes due to the force of the primary air striking against the damper arm. The gravity-operated design was hinged along the fan outlet's upper edge and closes by virtue of the damper's inherent weight. In both cases, the backdraft damper was intended to fully close and seal only when the internal fan was powered off. When the terminal fan was engaged, the fan's outlet pressure then exceeded the FPTUs internal pressure and the damper opened.

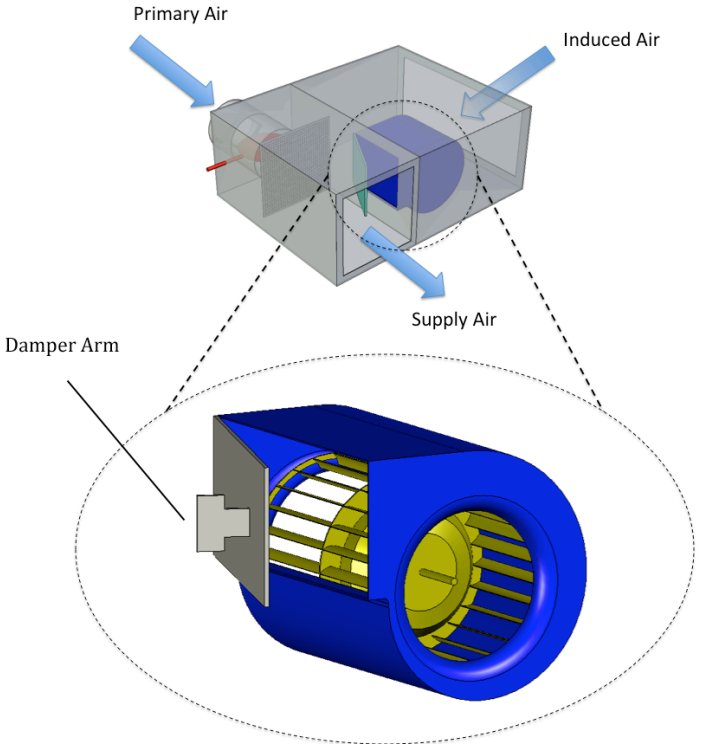

Figure 3-10: Parallel FPTU air-operated backdraft damper

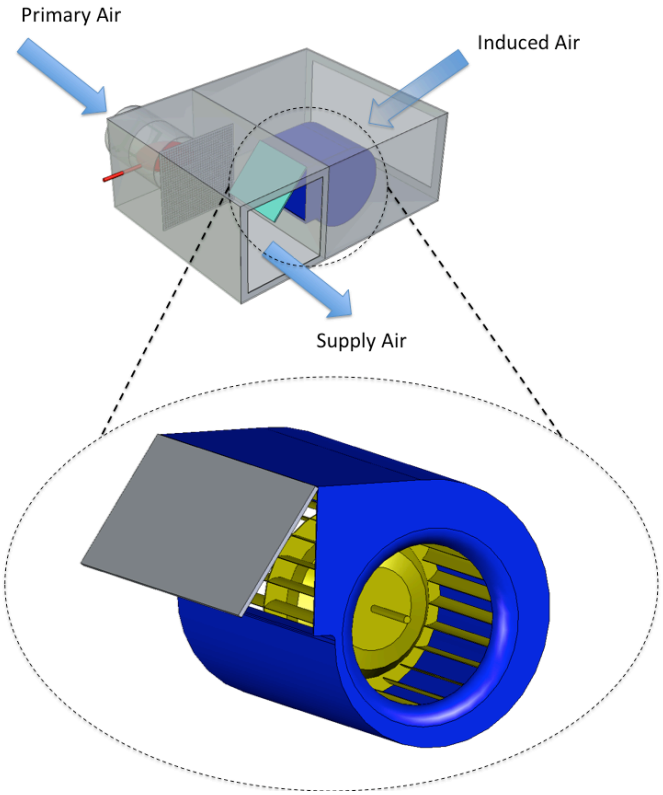

Figure 3-11: Parallel FPTU gravity-operated backdraft damper

3.1.2 Primary and Assist Fans. Airflow quantities were calculated using the techniques found in ASHRAE Standard-120 (1999). Figure 3-1 showed the experimental airflow configuration while Figure 3-12 and Figure 3-13, respectively, showed the form and feature set of an "AMCA Figure 15" and "AMCA Figure 12" flow chamber as defined by Air Movement & Control Association International, Inc. (AMCA) Standard-210 (1999).

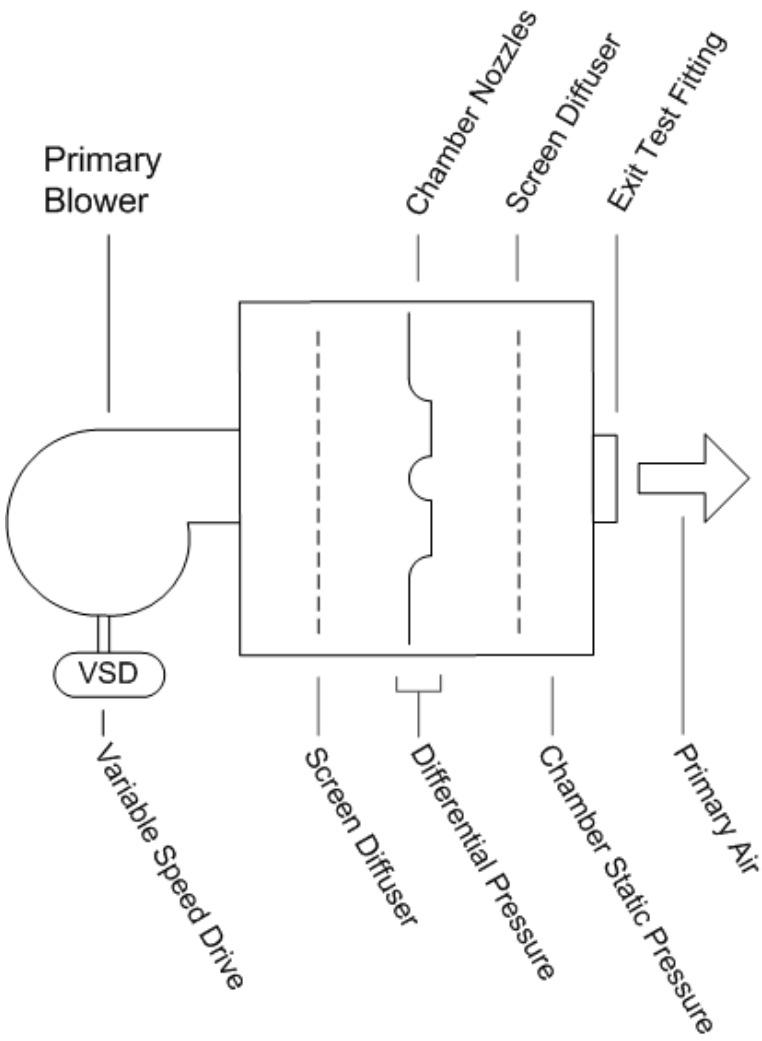

Figure 3-12: "AMCA FIgure 15" flow metering nozzle chamber

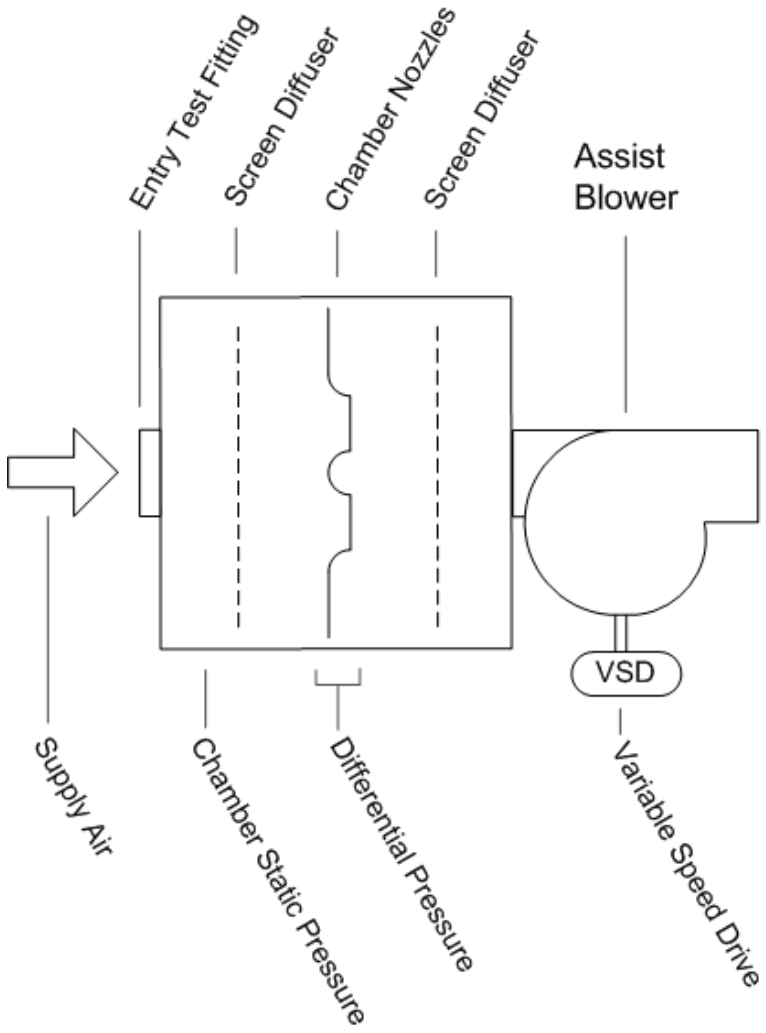

Figure 3-13: "AMCA Figure 12" flow metering chamber

The "AMCA Figure 15" flow chamber had a large capacity primary blower which was dynamically controlled with a variable speed drive (VSD) controller. Air was fed into the chamber with two diffuser screens, which smoothed air entering and exiting an internal wall of selectable pass-through nozzles. Primary airflow was calculated based on cumulative nozzle cross-sectional area, pressure differential across the nozzles and the chamber static pressure. Airflow values were adjusted to standard temperature and pressure conditions to compensate for various environmental changes in the laboratory during the days of data collection. At the outlet of the chamber was an exit test fitting also following the ASHRAE Standard-120 (1999) specification.

The “AMCA Figure 12” air chamber was similar to the “AMCA Figure 15” except that the test fitting was on the entrance and the fan was at the outlet. The assist fan drew test air through the chamber to assist in lowering pressure upstream of the test chamber. The “AMCA Figure 12’” nozzles provided the measurement for cumulative, supply airflow downstream of the FPTU.

The 1st Law of Thermodynamics, Eq. (3.1), was reduced by several assumptions. The airflow measurement points were assumed to be taken at steady-state, with no heat input and zero work performed by the air per Eq. (3.2). The air’s enthalpy, Eq. (3.3), was a function of specific heat and temperature. Uniform unconditioned laboratory air was used for both primary and induced airflow, and temperature rise across the fan was assumed to be negligible. As a result, the enthalpy was assumed constant, Eq. (3.4), and the mass flow rate out was equal to the mass flow rate in. Due to the conservation of mass at similar temperature and pressure, the volumetric output airflow, Eq. (3.5), was also constant.

$$\frac{dE}{dt} = \dot{Q} - \dot{W} + (\dot{m}_{out} h_{out} - \dot{m}_{in} h_{in}) \tag{3.1}$$

$$\dot{m}_{out} h_{out} = \dot{m}_{in} h_{in} \tag{3.2}$$

$$h = cpT \tag{3.3}$$

$$\dot{m}_{out} = \dot{m}_{in} \tag{3.4}$$

$$\sum_{out} \text{airflow} = \sum_{in} \text{airflow} \tag{3.5}$$

Induced airflow, Eq. (3.6), was calculated as the difference of the "AMCA Figure 12" and "AMCA Figure 15" measured flow.

$$Q_{induced} = Q_{supply} - Q_{primary} \tag{3.6}$$

Table 3-2 described the particular chamber characteristics used in the data acquisition test apparatus used in this study. Nozzle combinations differed between each chamber and were selected by the operator. As cumulative nozzle diameter was increased, less pressure was required to attain the same volumetric airflow. See ASHRAE Standard-120 (1999) for complete mathematical techniques used. Each chamber's power, control and motor characteristics are displayed in Table 3-3.

Table 3-2: Flow chamber airflow characteristics

AMCA Chamber	**Maximum Flow** CFM (m3/s)	**Available Nozzles Diameters** inches (cm)					
Figure 15	4,000 (1.89)	1.5 (3.8)	3 (7.6)	5 (12.7)	5 (12.7)	5 (12.7)	5 (12.7)
Figure 12	5,000 (2.36)	1.5 (3.8)	5 (12.7)	5 (12.7)	8 (20.3)		

Table 3-3: Flow chamber power characteristics

AMCA Chamber	**Fan Power** hp (kW)	Controller	Motor
Figure 15	10 (7.5)	VSD	AC Induction
Figure 12	7.5 (5.8)	VSD	AC Induction

The two airflow chambers and FPTU were connected with sheet-metal ductwork. The length of this duct (Figure 3-14) followed the specifications outlined in the ASHRAE Standard-130 (2006). Table 3-4 presents the duct size. The upstream duct diameter was 8 in. (20.3 cm). Downstream was a 16 in. (40.6 cm) x 15 in. (38.1 cm) rectangular outlet duct with an equivalent duct diameter of 17 in. (43.2 cm).

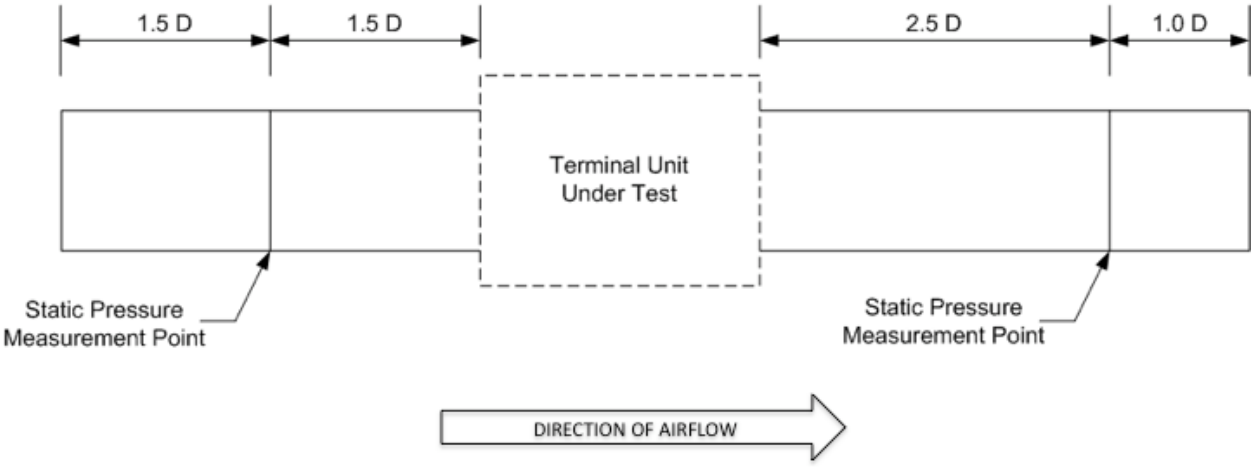

Figure 3-14: Experimental ductwork length

Table 3-4: Experimental ductwork diameters

	D_up	De_down
Diameter	8 in. (20.3 cm)	17 in. (43.2 cm)

ASHRAE Standard-130 (2006) also dictated that the static pressure measurements be located certain distances from the FPTU based on the duct diameter (Figure 3-14). At these duct locations, holes were drilled into the sheet-metal and copper pressure taps with matching hole diameters (Figure 3-15) were applied and sealed directly with adhesive tape. Static pressure was averaged across the respective cross-sections by "daisy chaining" four taps per location with flexible tubing (Figure 3-16).

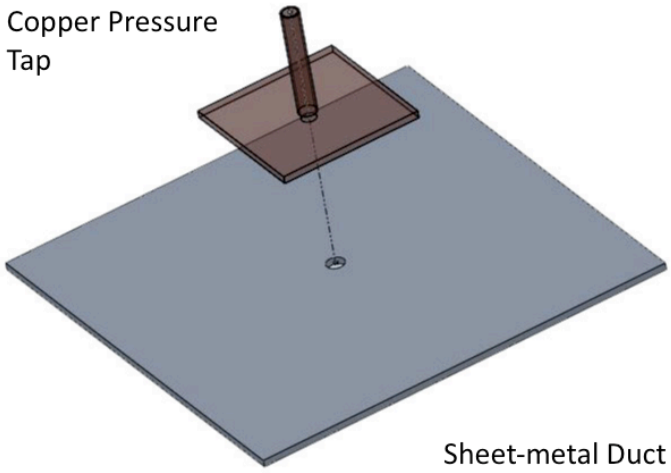

Figure 3-15: Sample pressure tap

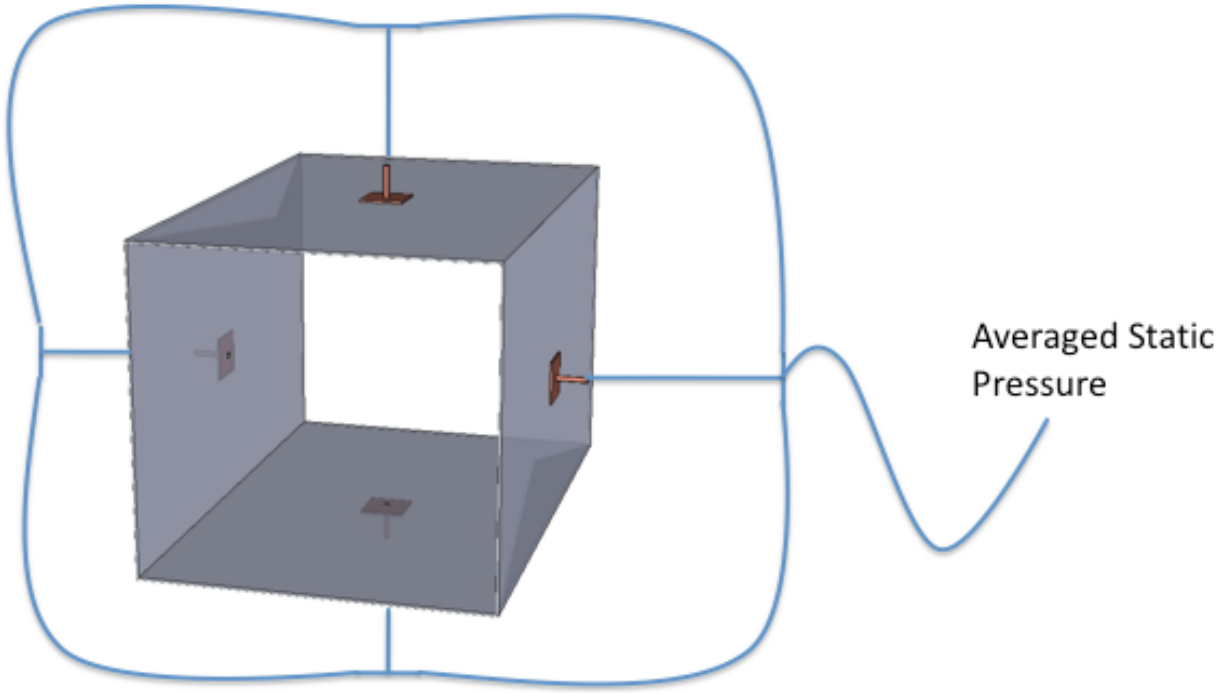

Figure 3-16: "Daisy chained" four point averaged pressure

3.1.3 Data Acquisition. Data points spanning several variable types were acquired for this study. Both static and differential pressure quantities were measured with pressure transducers (Dwyer Series 616C). Physical locations of these pressure measurements followed the ASHRAE Standard-130 (2006). The sizing of the particular pressure transducers can be found on Table 3-5. Each pressure transducer was calibrated with a water manometer to within 0.01 in. w.g. (2.49 Pa) and contained an accuracy of ±0.25% of their full-scale output.

Table 3-5: Pressure transducer sizing

Location	Transducer Size in. w.g. (kPa)
Figure 15 differential pressure	0-6 (0-1.5)
Figure 15 static pressure	0-10 (0-2.5)
Upstream static pressure	0-2 (0-0.5)
Inlet air velocity differential pressure	0-2 (0-0.5)
Downstream static pressure	0-2 (0-0.5)
Figure 12 static pressure	0-10 (0-2.5)
Figure 12 differential pressure	0-6 (0-1.5)

All pressure transducer output was a 4-20 mA current signal which was proportional to the pressure across the device. Terminating resistors converted the output current into a voltage the data acquisition system could measure. However, the resulting voltage from these pressure transducers contained, at times, significant noise. The source of this distortion could be attributed to several sources: pressure pulsation and dirty power. However, regardless of source, the noise effects were compensated for by the application of an inline low-pass filter (Figure 3-17).

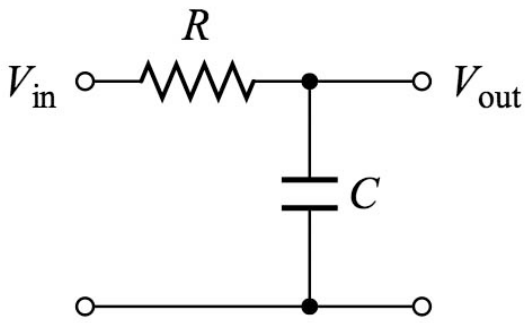

Figure 3-17: Low pass RC circuit

$$|H(f)| = \frac{1}{\sqrt{1+(f/f_b)^2}} \tag{3.7}$$

$$f_b = \frac{1}{2\pi RC} \tag{3.8}$$

The low-pass filter was constructed with a 199 Ω resistor and a 1000 μF capacitor. These values in conjunction with Eq. (3.7) and Eq. (3.8) define the behavior of the filter. In this application, any distortion at 60 Hz will be reduced by 98%. Figure 3-18 provides a visual representation of the filter's affect. In addition to the hardware-based low-pass filter, further signal averaging took place via software by way of a custom visual basic script. Voltage samples were taken at 20 Hz and averaged across a 10 second time interval.

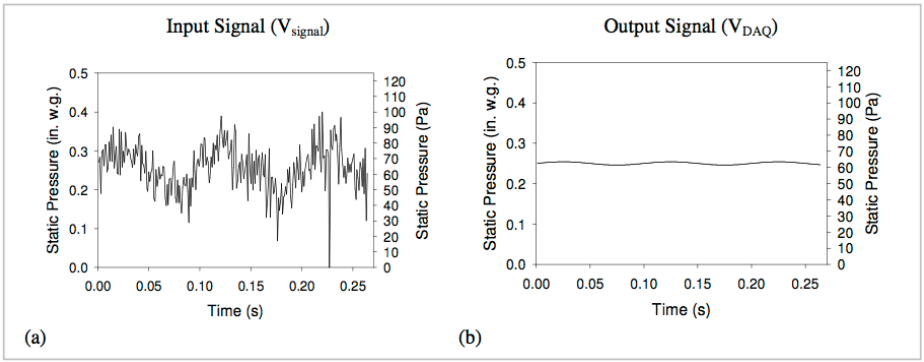

Figure 3-18: Noisy signal (a) before and (b) after low-pass filter

Similar to the pressure measurements, temperature and relative humidity measurements were also taken using transducers with a linear voltage output. Both temperature and relative humidity values were taken with a dual purpose probe (Rotronic L-series). The instrument had a ±0.9 ºF (±0.5 ºC) temperature and ±3% RH accuracy The location of this sensor was near the opening in FPTUs housing but placed so as not to significantly interfere with airflow into the terminal fan (Figure 3-19). However, by being as close to the fan as possible, the sensor was able to best measure the air properties of unconditioned laboratory air used during the test process. A redundant mercury thermometer was also placed near the transducer to allow for quick temperature verification.

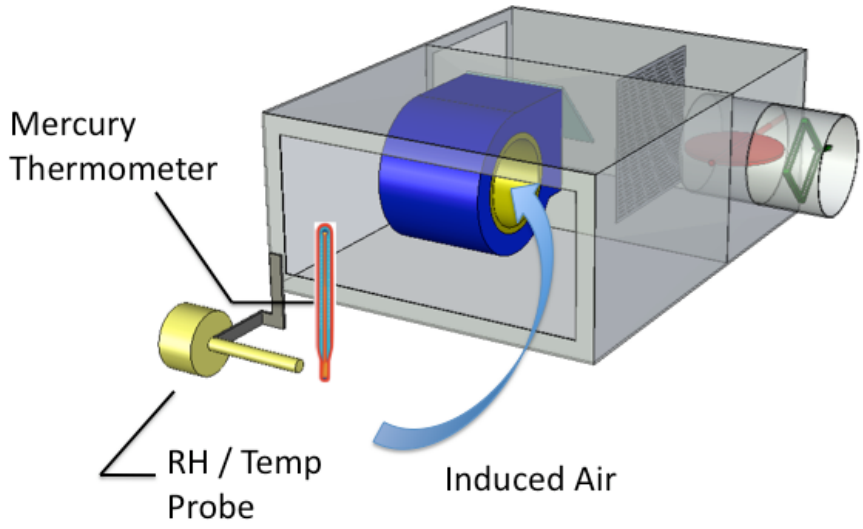

Figure 3-19: Location of the temperature & relative humidity probe

The pressure, temperature and relative humidity voltage signals were collected using a multi-board data acquisition system for a PC. An 8 channel, 16 bit data card (National Instruments SC2040) was used to receive and record half the values, while an 8 channel, 12 bit data card (National Instruments CB 68LP) was used to record the remaining variables as well as control the primary and assist fans via its 0-10 VDC analog outputs. Both external I/O boards were connected to the computer's internal PCI controller cards (National Instruments 6024E and 6034E) via a proprietary serial connection. A custom Visual Basic (1998) computer script provided the user interface. The control system is shown in Figure 3-20 and the device list in Table 3-6.

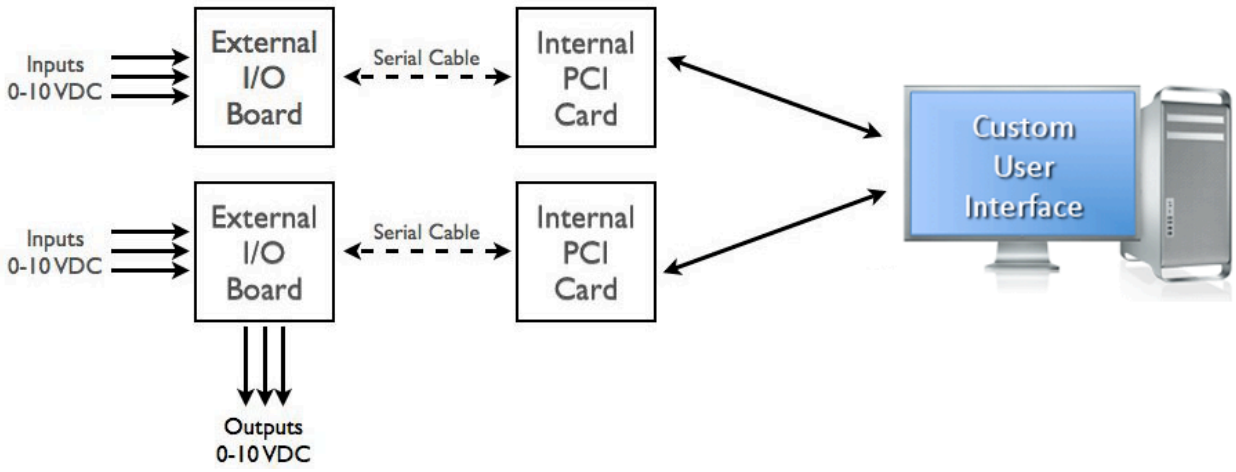

Figure 3-20: Information flow of data acquisition system

Table 3-6: Data acquisition inputs and outputs

	Signal	Device
Inputs	0-10 VDC	Pressure, Temperature, Relative humidity
Outputs	0-10 VDC	Supply blower, Assist blower, Primary air damper, ECM input

3.2 Power Equipment

Electrical performance data were recorded per ASHRAE Standard-130 (2006). A power quality analyzer (Fluke 435) was used to observe the VAV terminal unit's electrical characteristics as measured from the supply line (Figure 3-21). Current probes rated for 0-5A (Fluke i5S) were selected and had a 1% accuracy. The current clamps were applied to both the power and neutral wires of the single phase 277 VAC input as seen in Figures 3-20 and aligned per Figure 3-22. The simultaneously measured and recorded data included, but was not limited to: real and apparent power, RMS voltage (V_{RMS}) and current (I_{RMS}), associated harmonics and total harmonic distortion. The inclusive data files were cached in the power quality analyzer's internal memory then transfered to a computer by means of a USB interface cable.

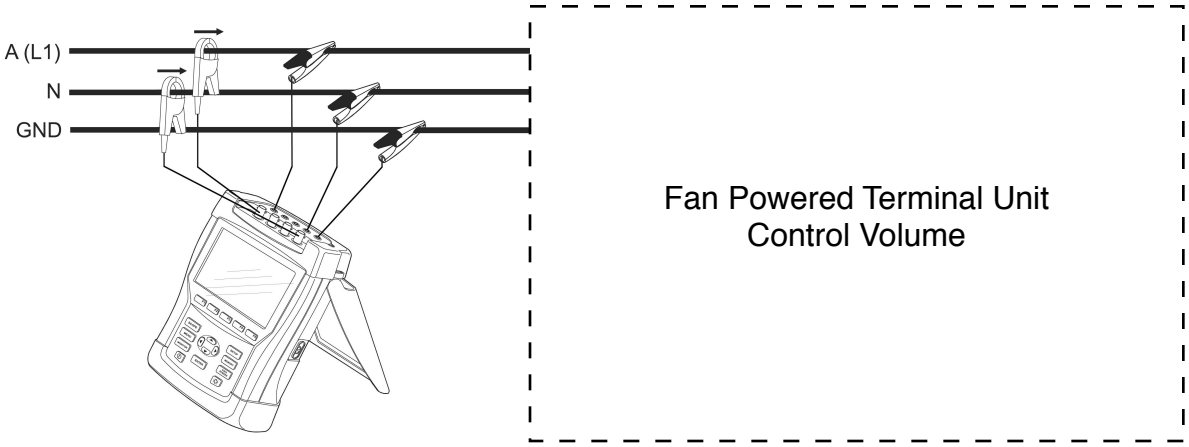

Figure 3-21: Electrical acquisition

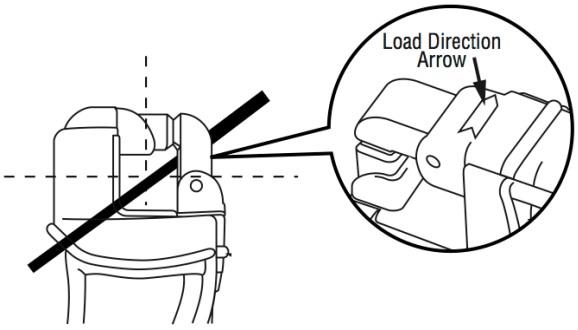

Figure 3-22: Current clamp application

CHAPTER IV

EXPERIMENTAL PROCEDURE

Empirical data were obtained for two ECM controlled fan powered terminal units to quantify and characterize their behavior. Both airflow and power measurements were recorded using the equipment outlined in the previous chapter. This chapter describes the scientific reasoning, the physical data acquisition process and the subsequent statistical analysis techniques used on the raw data.

4.1 Method of Experimentation

A factorial test matrix spanning several independent variables was established for both series and parallel fan powered terminal unit designs to adequately simulate the expected range of operation in the field. Each independent variable's value is statistically known as a "level." The interrelated variables listed in Tables 4-1 and 4-2 outline the various input levels used to set the conditions for the study.

Table 4-1: Series terminal unit test levels

Independent Variable	Test Points	Value Range
D, damper position	4	100%, 75%, 50%, 25% open
V_{fan}, fan input voltage	4	100%, 75%, 50%, 25% full scale
P_{up}, upstream static	6	0.0 - 2.0 in. w.g. (0 - 498 Pa)
P_{down}, downstream static	1	0.25 in. w.g. (62 Pa)

Table 4-2: Parallel terminal unit test levels

Independent Variable	Test Points	Value Range
D, damper position	4	100%, 75%, 50%, 25% open
V_{fan}, fan input voltage	5	100%, 75%, 50%, 25%, 0% full scale
P_{up}, upstream static	5	0.0 - 2.0 in. w.g. (0 - 498 Pa)
P_{down}, downstream static	3	0.1 - 0.5 in. w.g. (25 - 125 Pa)

The damper position, D, varied for the respective FPTU designs. Orientation was controlled using a damper actuator with a 0-10 VDC input that could vary the damper position between 100% fully open (0º) and fully closed. Parallel units containing a butterfly damper had a 90º range of damper rotation between full open (0º) and full closed position (90º). Therefore, 0º, 22.5º, 45º and 67.5º were chosen as full scale, equally spaced damper settings. Series units with opposing-blade dampers had a 45º range of operation, therefore, the four damper test points were 0º, 11.25º, 22.5º and 33.75º. The fully closed condition was not included in either test matrix because this damper position would have produced redundant results for all upstream pressure settings due to the factorial nature of the test matrix. With the damper fully closed, there would be no primary airflow regardless of upstream pressure. Such a condition was recorded however, during a supplemental “Fan Only” test performed at the conclusion of the test matrix. The “Fan Only” test involved running the terminal fan exclusively without the primary “AMCA Figure 15” blower’s operation.

The VAV terminal's internal fan was controlled with a 0-10 VDC input signal, V_{fan}. This input voltage fed a logic circuit which controlled the speed of the ECM. The calibration of input signal versus fan RPM was programable and unique for each application. Because fan speed was not available as a control input, voltage input was used exclusively. Four equally spaced 0-10 VDC input voltage levels were used to represent fan speed in the respective test matrixes. The inputs were 2.5, 5.0, 7.5 and 10 VDC. For series test units, a 0.0 VDC condition was impractical due to the inline nature of the design. The fan must always be on. However, for parallel units, the 0.0 VDC condition did represent a meaningful "full cool" condition. When the internal fan turned off, induced airflow was eliminated. During "full cool" operation, only conditioned primary air was delivered as supply air.

In a real building, both upstream static pressure, P_{up}, and downstream static pressure, P_{down}, depend on conditions in the building. These variables were also included in the test matrix. Pressure adjustments were made by use of the variable speed drives (VSD) controlling the assist blowers on the upstream and downstream airflow chambers. The data acquisition system allowed the user to manually adjust the VSD controlled blowers as needed to achieve the desired test pressures. Tests were performed with upstream static pressure reaching as high as 2.0 in. w.g. (498 Pa) for both series and parallel designed FPTUs. However, downstream pressure differed based on unit design. Unlike series test units, parallel FPTUs must have their upstream static pressure higher than the downstream. If this were not the case, air would flow upstream. Therefore, the parallel test matrix consisted of only of test conditions were the upstream pressure exceeded the downstream. Thus, the respective terminal designs required two unique test matrixes with respect to upstream and downstream static pressures.

4.2 Environmental Considerations

Experimental data were collected at the Riverside Campus facility of the Energy Systems Laboratory at Texas A&M University. The test environment was located in an open, high-bay lab where the space temperature varied between 60 ºF (15.5 ºC) to 80 ºF (26.7 ºC). Much of the FPTU testing was performed during seasonably mild temperatures which allowed for the lab to operate without external heating or cooling. The relative humidity varied between 40% and 70%.

Typical HVAC systems supply conditioned 55 ºF (12.8 ºC) primary air to the terminal unit. For this study, unconditioned laboratory air was used because the research was primarily concerned with FPTU airflow and power consumption. Both air temperature and relative humidity were assumed to be uniform throughout the process. Temperature across the FPTU could be as high as 2 ºF (1.2 ºC) higher due to heat gains through the terminal fan. This temperature difference had minimal affect on air density. For example, using a psychometric chart, the density of air at 70°F (21°C) & 60 %RH is 0.0738 lb/ft3 (1.18 kg/m3). The density of air at 75°F (24°C) & 50 %RH is 0.0731 lb/ft3 (1.17 kg/m3). This 5 °F (2.8°C) temperature difference results in a density difference of less than 1%. Therefore, the effects of temperature rise per test were ignored.

Temperature, relative humidity and pressure measurements were used to calculate the airflow per the ASHRAE Standard 120-99 (1999) specification. Because there could be significant air density changes due to temperature and relative humidity differences across the various test days, all volumetric airflow was adjusted to a standardized airflow with a reference air density of 0.075 lb/ft^3 (1.20 kg/m^3).

4.3 Method of Statistical Analysis

For the statistical analysis, SPSS software (2008) was used. The aim of the analysis was to obtain accurate, yet simple and intuitive, mathematical models regarding the respective FPTUs and their behavior; specifically fan airflow and power.

Models were developed using similar techniques based on previous fan powered terminal unit research performed at Texas A&M University (Furr et al. 2007). Both linear and non-linear airflow and power regressions were based on temperature, upstream and downstream static pressure, inlet air velocity pressure, damper position and FPTU fain input voltage. However, care was taken not to include interdependent variables, which if used would have created unnecessary redundancy. The regression assumptions were: an appropriate linear relationship between the response variable and predictors, errors were independent and random, and the error had constant variance (Montgomery et al. 2001).

The accuracy of the mathematical model to the data set was based on the corresponding R^2 value. The R^2 statistic is a value between 0 and 1 used to represent how well the model explains the variance in the data. An R^2 value of 1 meant that the model fits the data set perfectly (Montgomery et al. 2001).

Due to the fundamental differences between the two, separate analysis were performed for both series and parallel terminal units. However, the basic form of the mathematical models was generally consistent. Thus, while maintaining acceptably high R^2 value, common expressions were used with the only difference being coefficient values. By using previously established expressions, it was possible to directly compare the results from the ECM controlled units versus the SCR controlled results (Furr et al. 2007).

CHAPTER V

SERIES TERMINAL UNIT RESULTS

Experimental data were collected for ECM controlled VAV terminal unit using the equipment discussed in Chapter III. Airflow and power models were developed as a function of variables that significantly influenced the performance of the terminal unit. A separate section is provided for both airflow and power analysis. Each section presents a brief summary of the method used, the resulting ECM controlled FPTU results, a comparison with previous SCR controlled FPTU data and discussion regarding each.

5.1 Series Terminal Unit Airflow

The distinguishing feature of the series VAV fan powered terminal unit (Figure 5-1) is the inline centrifugal fan. The fan, which must operate continuously, lowers the internal terminal unit chamber pressure which draws additional unconditioned induced air from the surrounding and mixes it with conditioned primary air supplied upstream of the unit.

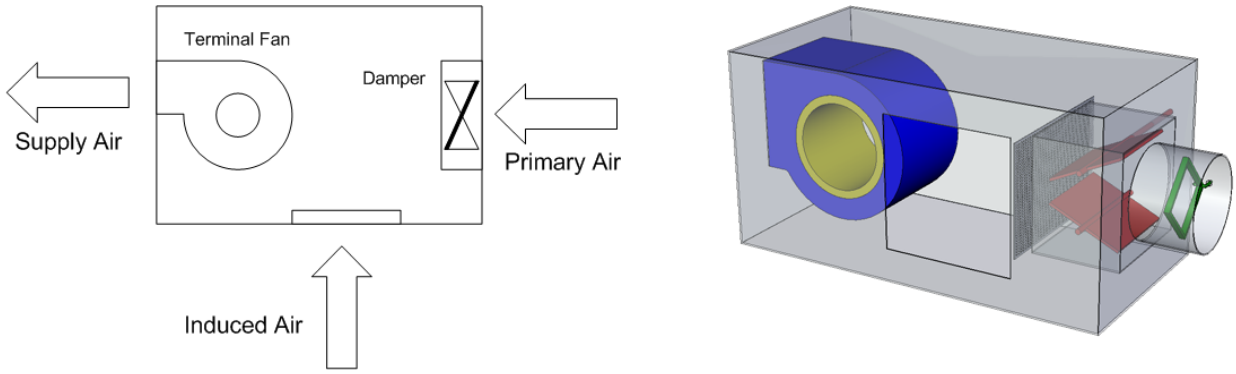

Figure 5-1: Typical series VAV fan powered terminal unit

The desired airflow model needed to quantify both the induced and supply air delivered by the ECM controlled series FPTU. The primary interface to the terminal unit was a 0-10 VDC user controlled input. The voltage was typically selected based on the unit's published fan calibration table (Appendix C). ECM controlled FPTUs employ application-specific programmable logic routines which allow the controller's internal microprocessor to dynamically adjust fan motor RPM and torque with the purpose of delivering constant airflow over a range of external conditions.

The generic relationship between input voltage and fan speed is not directly proportional due to the inherent dynamic operation of the ECM controller, it's programmable logic and the ability to alter torque "on the fly" based on external loads. Figure 5-2 was generated using an optical tachometer. For this reference plot, 0.25 in. w.g. (62 Pa) was used for both upstream and downstream static pressure.

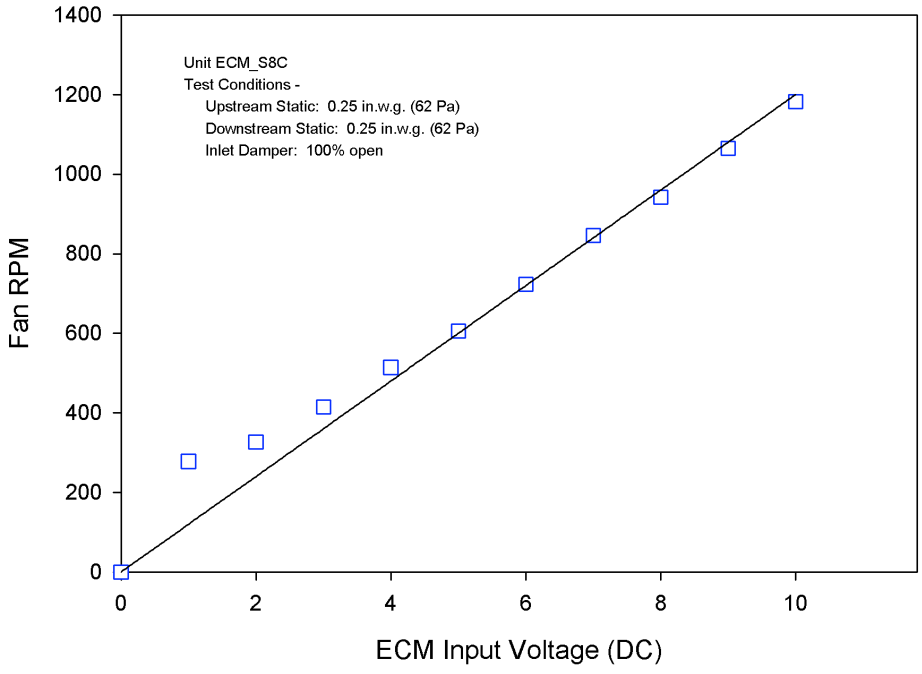

Figure 5-2: Measured ECM series FPTU fan speed

The ECM series fan RPM curve appeared approximately linear throughout the entire 0-10 VDC input range. Test matrix in Chapter IV specified four equally spaced test voltage levels: 2.5, 5.0, 7.5 and 10.0 VDC. These cover then entire range of the fan controller.

Previous research of series designed FPTUs used a SCR controller which allowed a reduction of the full scale 277 AC input voltage. The SCR chopped the voltage sine wave twice every period (Figure 5-3) and slowed the motor speed. The amount of voltage chop is determined by a setscrew located on the SCR. The rotation of the setscrew fixed the minimum voltage due to mechanical restriction.

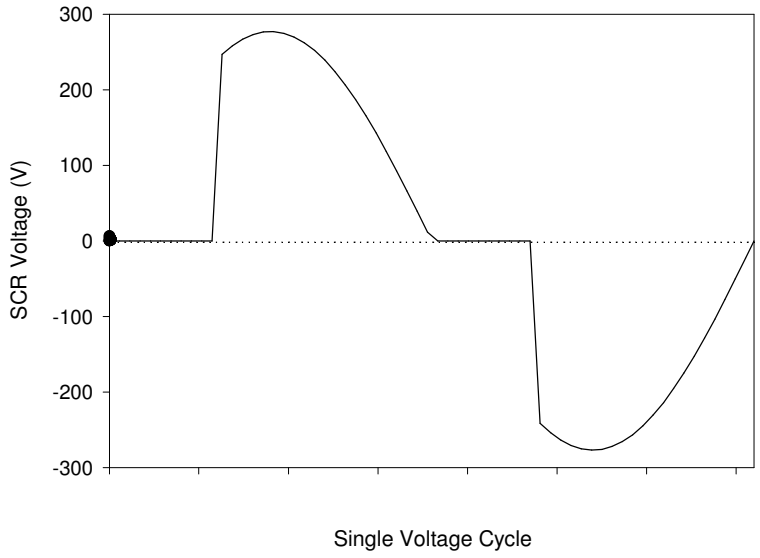

Figure 5-3: Idealized voltage sine wave resulting from SCR operation

Figure 5-4 was created using an optical tachometer on the SCR controlled series terminal unit provided by the same supplier as the ECM controlled unit. The fan speed curve for the SCR controlled unit was linear when measured against the SCR output. The upper and lower limits of voltage input for each control type are displayed in Table 5-1.

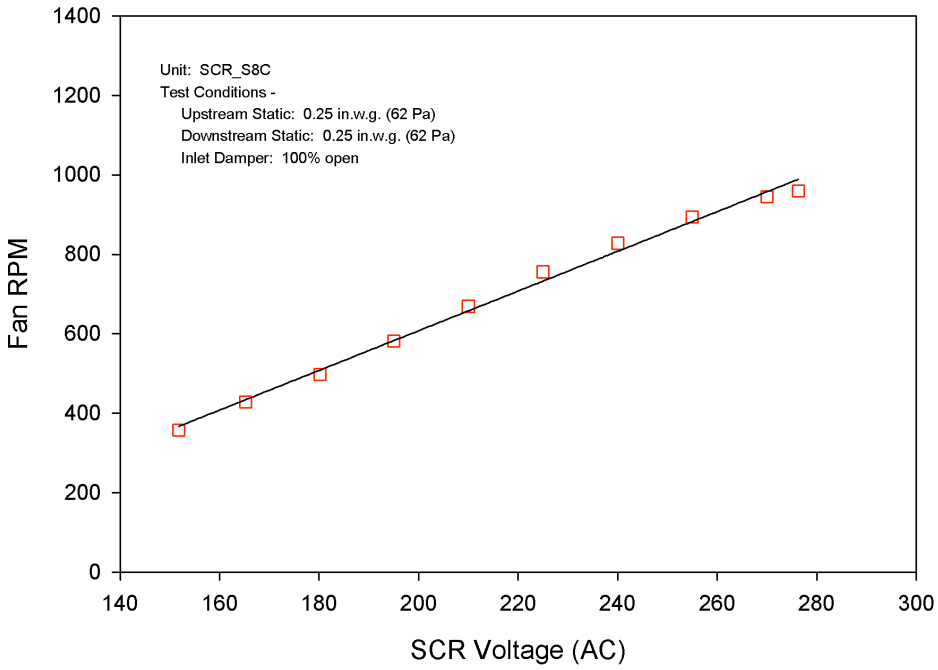

Figure 5-4: Measured SCR series FPTU fan speed

Table 5-1: Series FPTU range of operational control

Control	Min	Max
ECM (VDC)	0	10
SCR (VAC)	160	277

Throughout this chapter, results of fan power terminal units with ECM control were contrasted with similar SCR controlled units from the same manufacturer. Fan input voltage was often used as the primary variable. While the particular FPTU fans conformed to their appropriate fan laws (ASHRAE 2001), the respective input controls differed in scope and calibration. The various controller input levels were not chosen to match fan speeds, but were selected to provide uniform coverage of the respective input voltage range. Therefore, comparisons between ECM and SCR controlled test levels should be made with their RPM differences in mind. The approximate fan speed relationship for common input voltages reported throughout this chapter are provided in Table 5-2.

Table 5-2: Approximate fan speed

	ECM		SCR		
Level	**Input Volt (DC)**	**Fan RPM***	**Input Volt (AC)**	**Fan RPM***	**ΔRPM***
1	2.5	370	160	390	20
2	5.0	600	200	625	25
3	7.5	895	235	825	70
4	10	1180	277	960	220

*all RPM measurements are approximate and are intended for reference only

5.1.1 Fan Airflow Analysis and Model. The variable with the greatest influence on fan airflow was fan speed. However, the relationship between voltage input and RPM was unique to each FPTU tested. As a consequence, the applicability of the results found in this section will need to be evaluated with more data to determine if they are applicable to a broad range of FPTU designs from different manufacturers. Furthermore, the dynamic operation of the ECM controller dictates that fan speed be removed from the performance model's input. In combination with the calibration in Figure 5-2, voltage input was used as the primary independent variable for both its intuitive property as well as its steady-state value. As a contrast to previous research (Furr 2006), the ECM controlled motors with their 0-10 VDC input was compared against the SCR controlled units using a 160-277 VAC input range.

For developing an airflow performance model, fan curves and fan laws explain that for a given fan geometry, the only other significant variable is the pressure across the fan (ASHRAE 2001). Figure 5-5 illustrates the principle pressure locations of a series VAV fan powered terminal unit.

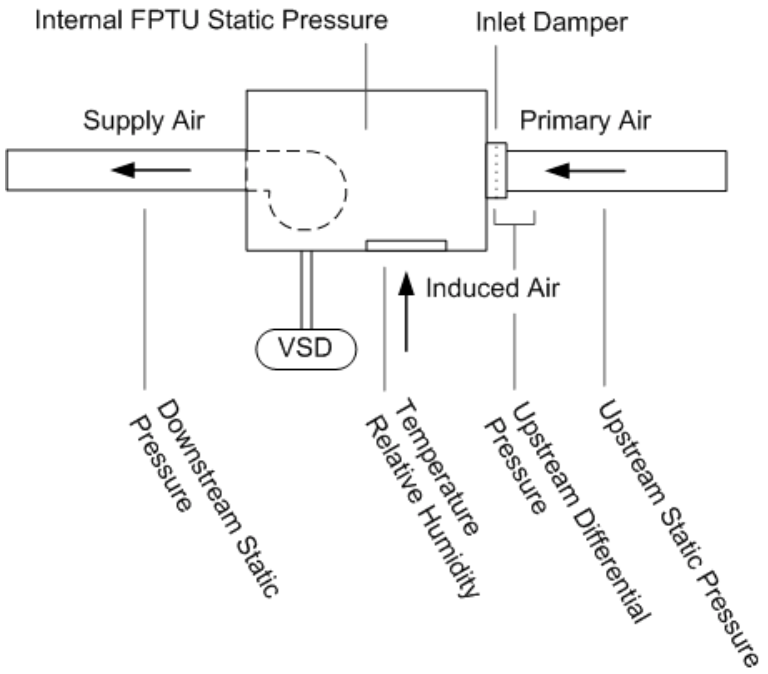

Figure 5-5: Typical series VAV fan powered terminal unit pressures

For all experimental levels tested, the fan's downstream static pressure was maintained constant at 0.25 in. w.g. (62 Pa), and it was eliminated as a primary explanatory variable. The pressure upstream of the internal fan is the internal static pressure of the FPTU chamber. However, this value was not directly recorded because not only would it be difficult to quantify, it is not a measured variable in the field, nor is it a value predicted in building energy simulation programs.

During normal operation, the chamber static pressure was less than atmospheric pressure. The pressure differential with the outside ambient air is what drew additional induced air. While the FPTU fan lowered its internal chamber pressure, the upstream primary airflow raised it. However, upstream static pressure was an unreliable descriptive variable due to its heavy dependence on the terminal unit's inlet damper orientation. The most convenient upstream pressure measurement was then determined to be the inlet air velocity pressure, P_{iav}, which is found at the inlet manifold of every VAV terminal unit.

Figures 5-6 and 5-7 show the results of the respective VAV fan outputs as a function of inlet air velocity pressure. The nearly horizontal slopes of the trend airflow suggested minimal dependency on inlet air velocity pressure. The plot supported previous research (Alexander and Int-Hout 1998, Furr 2006) which stated variations of upstream duct pressure, primary flow and damper position have little effect on the fan's airflow performance. The series VAV terminal unit was thus quite stable in providing uniform airflow despite changes in the upstream condition.

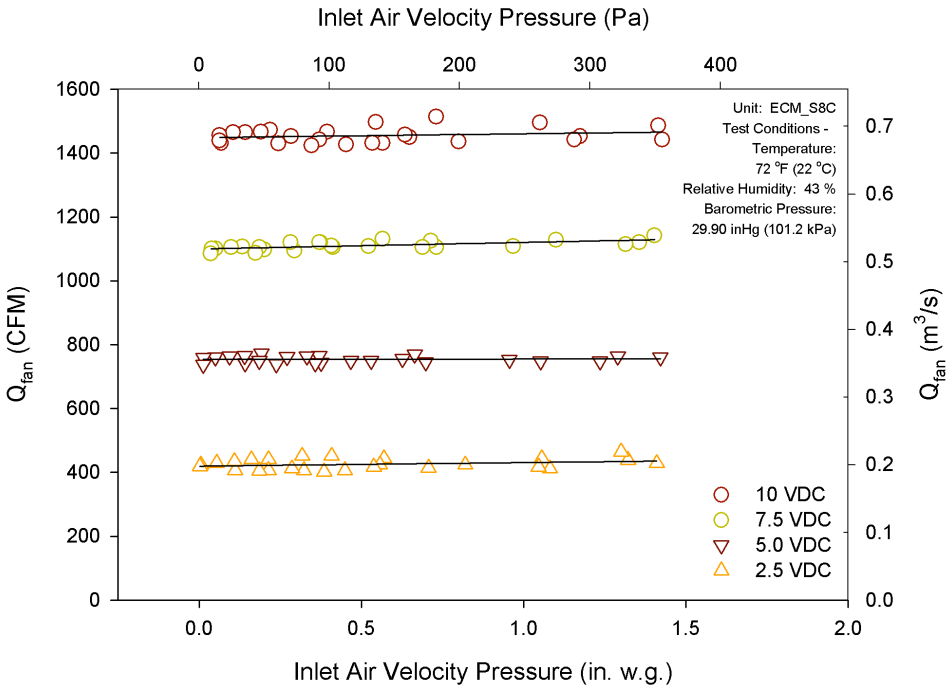

Figure 5-6: Fan airflow for ECM series terminal unit

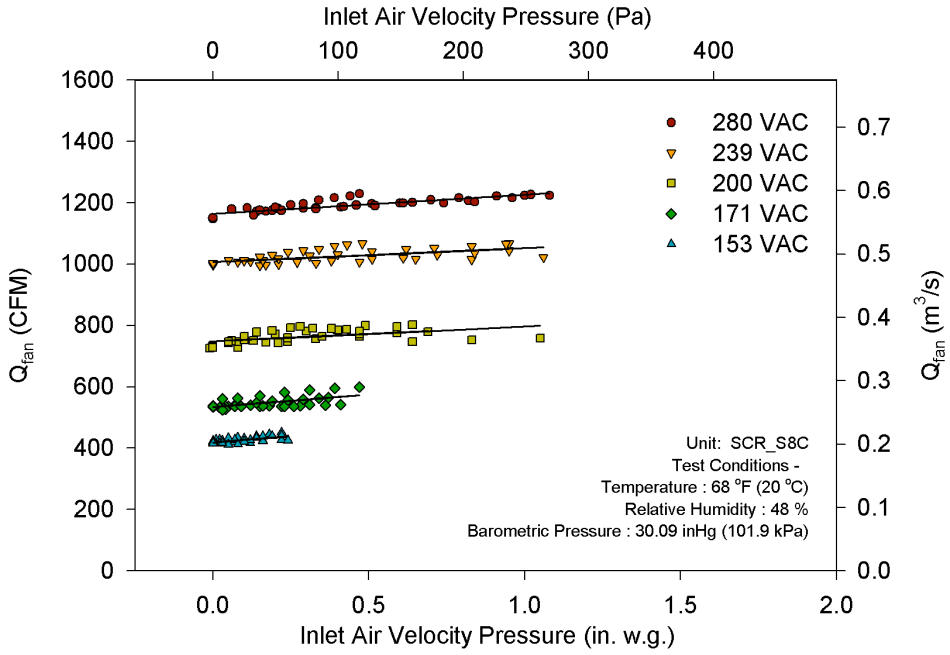

Figure 5-7: Fan airflow for SCR series terminal unit

The fan airflow model used for the series ECM fan powered terminal unit is shown in Eq. (5.1) and is the same expression used for SCR controlled FPTUs (Furr et al. 2007). Coefficients for the same manufacturers' 8 in (20.3 cm) series FPTUs are presented in Table 5-3.

$$Q_{fan} = C_1 + C_2 V + C_3 V^2 + C_4 P_{iav} \tag{5.1}$$

Table 5-3: Model coefficients for fan airflow in series terminal units

Control	**C_1 [CFM]**	**C_2 [CFM/V]**	**C_3 [CFM/V^2]**	**C_4 [CFM/in. w.g.]**	**R^2**
ECM (VDC)	108.301	122.977	1.130	12.441	0.997
SCR (VAC)	-1310	6.918	0.0091	0.0394	0.997

The high R^2 value indicates that the model correlates to the empirical data set very closely. It should be noted however, that the voltage scales for ECM and SCR are different. ECM controls employ a 0-10 VDC input while the SCR uses a mechanical 160-277 VAC turn screw to achieve voltage regulation. If a universal model with generic coefficients were desired, a dimensionless normalized input would be needed in place of the respective VDC and VAC values.

5.1.2 Primary Airflow Analysis and Model. Primary airflow as a function of differential pressure (DP) across the terminal units was also quantified. Figures 5-8 and 5-9 present primary terminal unit airflow as a set of parabolic curves based on inlet damper position. Both ECM and SCR terminal series FPTU used opposing blade inlet dampers which had a 45º range of operation. The damper setting of 0º represented full open, while the damper setting of 45º represented the fully closed position.

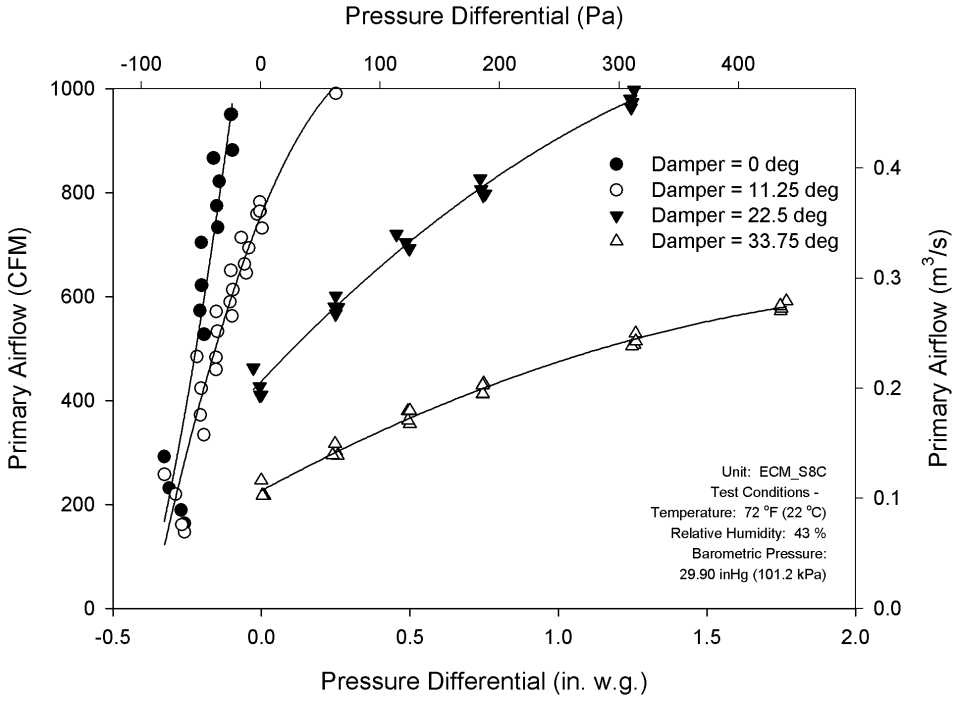

Figure 5-8: Primary airflow for ECM series terminal unit

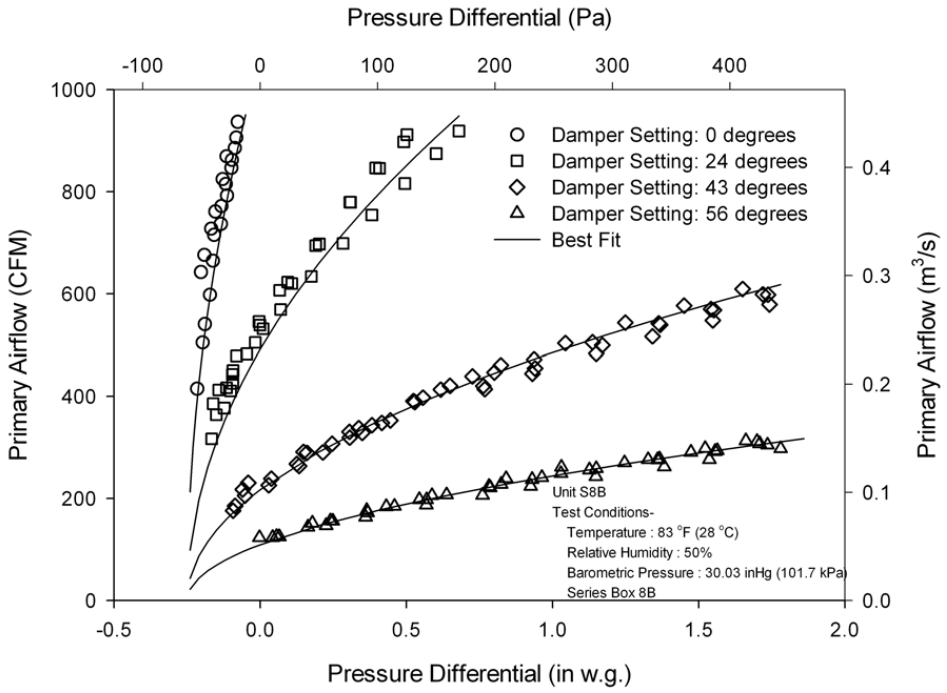

Figure 5-9: Primary airflow for SCR series terminal unit

Eq. (5.2) was borrowed from previous SCR research (Furr et al. 2007) and states the primary airflow of the terminal unit was proportional to the square root of the pressure differential across the terminal unit for a given damper setting. The primary airflow curves approached zero as pressure differential across the internal FPTU fan approached zero. The model's 0.27 in. w.g. differential offset pressure was slightly greater than the downstream static pressure set-point because it better fit the empirical data and achieved a higher R^2 value (Furr et al 2007). The ECM data also supported the additional offset achieving a R^2 of .977. The primary airflow model was irrespective of fan input voltage, and thus the ECM model coefficients were very similar to those of the SCR controlled model (Table 5-4).

$$Q_{primary} = C_1(1 + C_2S + C_3S^2)\sqrt{(DP + 0.27)} \quad (5.2)$$

Table 5-4: Model coefficients for primary airflow in series terminal units

Control	**C_1 [CFM/(in.w.g)$^{0.5}$]**	**C_2 [CFM/deg]**	**C_3 [CFM/deg^2]**	**R^2**
ECM	2344.0	-0.0384	4.15 E-04	0.977
SCR	2136.9	-0.0317	2.82 E-04	0.920

The high R^2 value indicated that the model correlated to the empirical data set very closely.

5.2 Series Terminal Unit Power

The series VAV fan powered terminal units required continuous operation of the internal fan. The behavior of the fan was expected to closely follow the fan curves for a centrifugal, solid width scroll fan (ASHRAE 2001). Power consumption performance with ECM control was specially of interest due to historical bias against this configuration.

5.2.1 Power Consumption Analysis and Model. The ECM controlled fan power consumption as a function of airflow is best approximated by a 2nd order curve as seen in Figure 5-10. This is in contrast to a similarly configured, SCR controlled series terminal units in Figure 5-11 which displayed a linear relationship. Due to the ECM control's specific calibration and the brushless DC motor's high efficiency at low RPM, the power consumption was much lower than the SCR controlled AC induction motor at low RPM.

Figures 5-12 and 5-13 display power consumption per airflow over the range of fan output. These plots represent the efficiency of the controller/motor combination at a given flow output. The ECM controlled units displayed better power-to-airflow ratios at lower volumetric flow while for SCR controlled units better ratios were obtained at high volumetric flow. The SCR controlled units demonstrated higher relative efficiency when the SCR output voltage approached the ideal 277 VAC input signal. The controller was much more efficient when it wasn't required to do work and distort the input sine wave. Thus, the negatively sloped SCR trends.

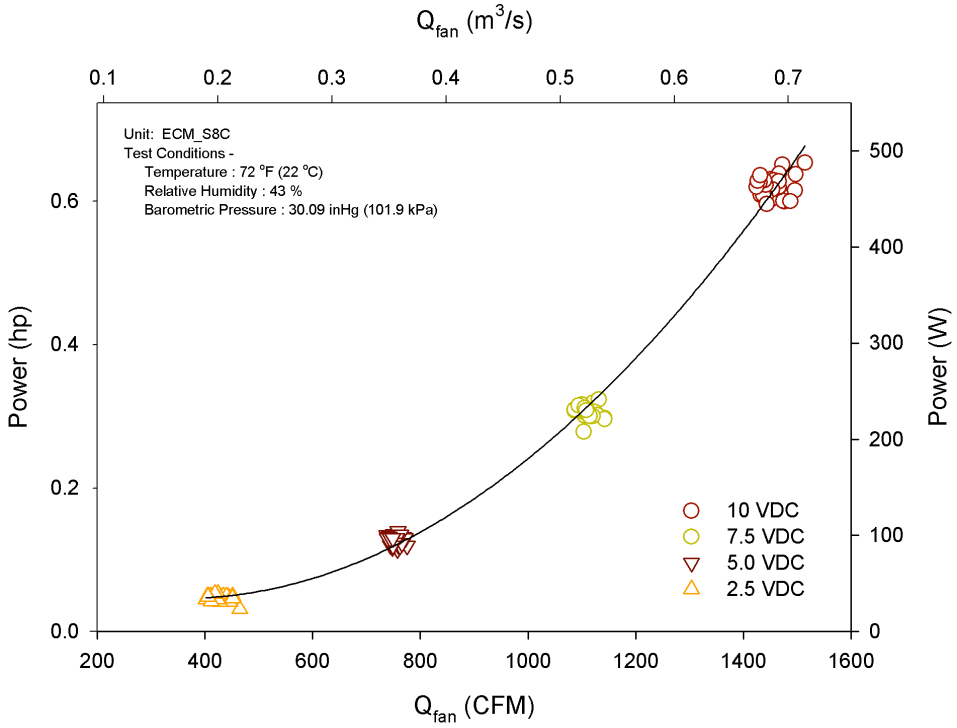

Figure 5-10: Power consumption for ECM series terminal unit

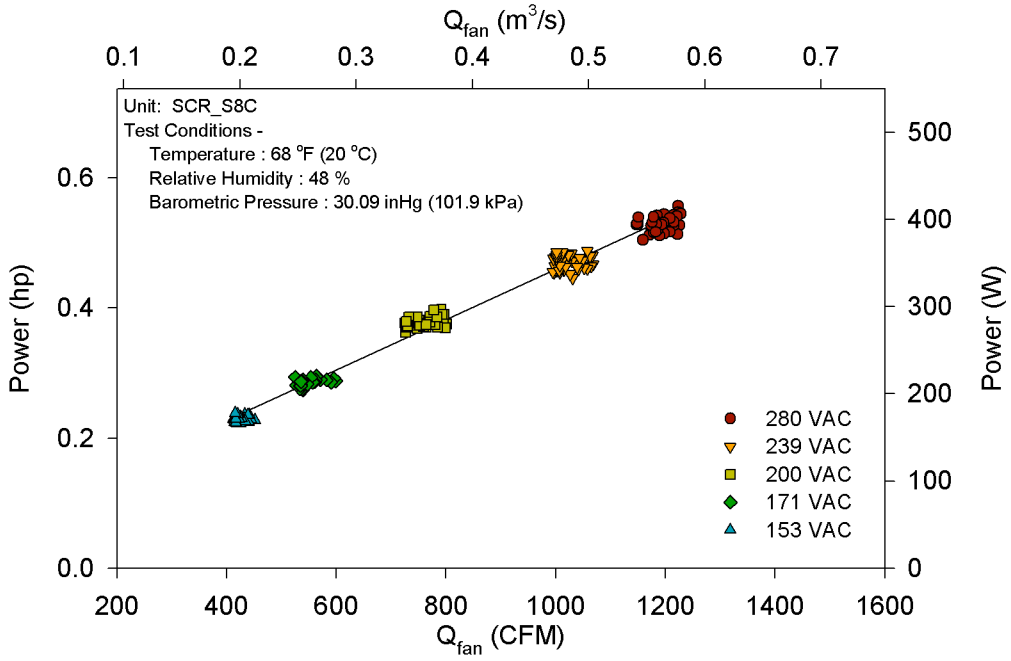

Figure 5-11: Power consumption for SCR series terminal unit

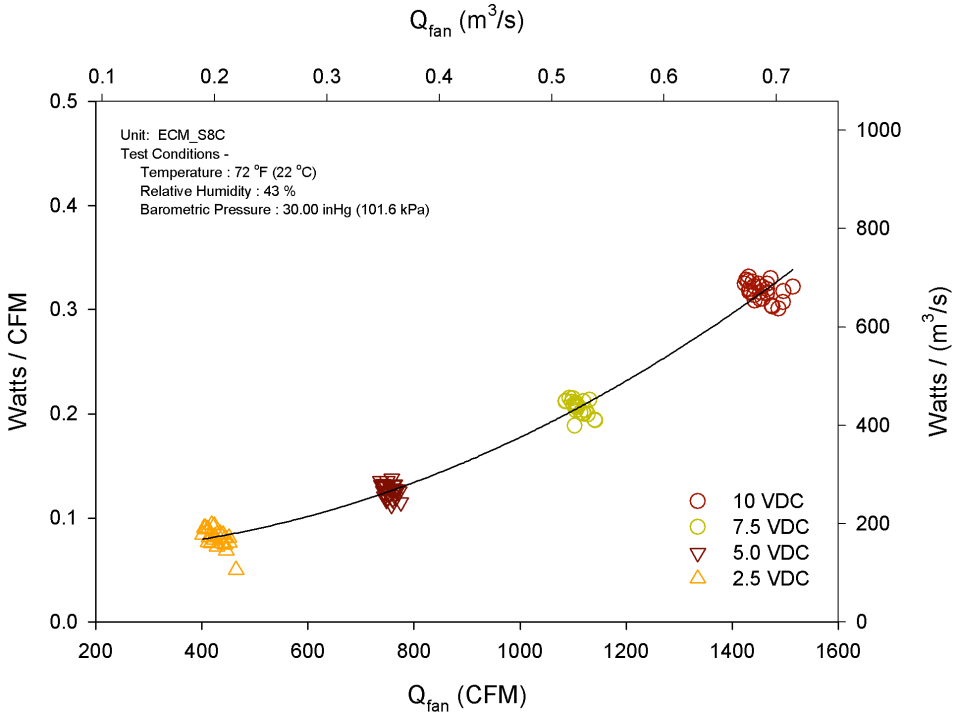

Figure 5-12: ECM series terminal unit watt per CFM vs. CFM

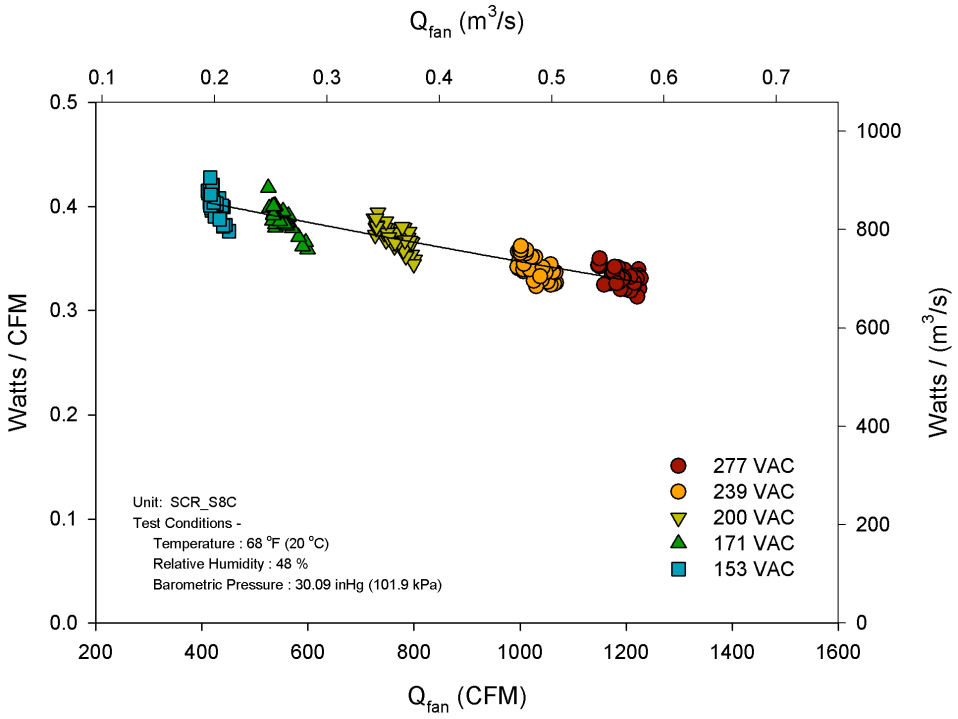

Figure 5-13: SCR series terminal unit watt per CFM vs. CFM

Using the mathematical expression developed in previous research (Furr et al. 2007), the model for fan power consumption is expressed in Eq. (5.3). The model is based on both input voltage and inlet air velocity pressure. The coefficients for the respective control types are listed in Table 5-5.

$$\text{Power}_{\text{fan}} = C_1 + C_2 V + C_3 V^2 + C_4 P_{\text{iav}} \tag{5.3}$$

Table 5-5: Model coefficients for power consumption in series terminal units

Control	**C_1 [W]**	**C_2 [W/V]**	**C_3 [W/V^2]**	**C_4 [W/in. w.g.]**	**R^2**
ECM (VDC)	78.998	-31.497	7.045	-12.993	0.998
SCR (VAC)	-455.5	5.32	-0.00817	1.91	0.994

The high R^2 value indicated that the model correlated to the empirical data set very closely. It should be noted however, that the voltage scales for ECM and SCR were different. ECM controls employed a 0-10 VDC input while the SCR used a mechanical 160-277 VAC set-screw to achieve voltage regulation.

5.2.2. Power Quality Analysis. The power quality analysis of the series VAV terminal unit focuses on power factor and total harmonic distortion. Power quality is often represented using a power triangle (Figure 1-3) and power factor Eq. (1.2).

In addition to real power consumption (watts), apparent power (VA) was also deemed an important variable. Figures 5-14 and 5-15 illustrate the significant difference in ECM versus SCR operation with regards to power factor. Never exceeding 0.45 and maintaining a fairly horizontal trend versus input voltage, the ECM power factor was much lower than the SCR control. This was due to the ECM controller's built in inverter and microprocessor. However, the SCR controlled unit's PF approached unity. This was due to the nature of the SCR control which distorts the input sine wave as needed to reduce pass-though voltage. At the full setting the 277 VAC signal was passed without modification, the controller did very little work and the PF was nearly equal to 1.

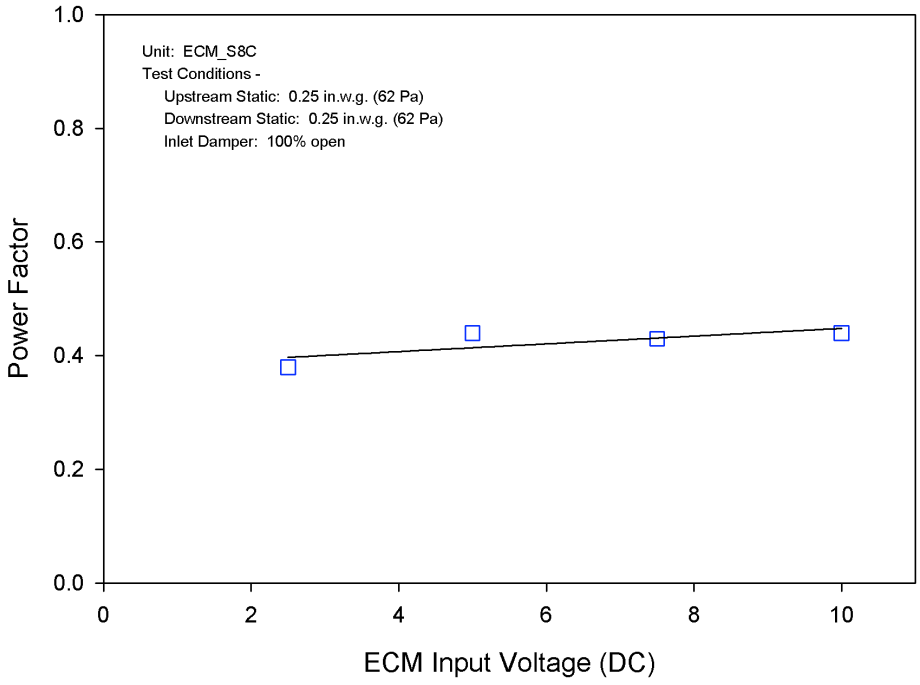

Figure 5-14: Power factor for ECM series terminal units

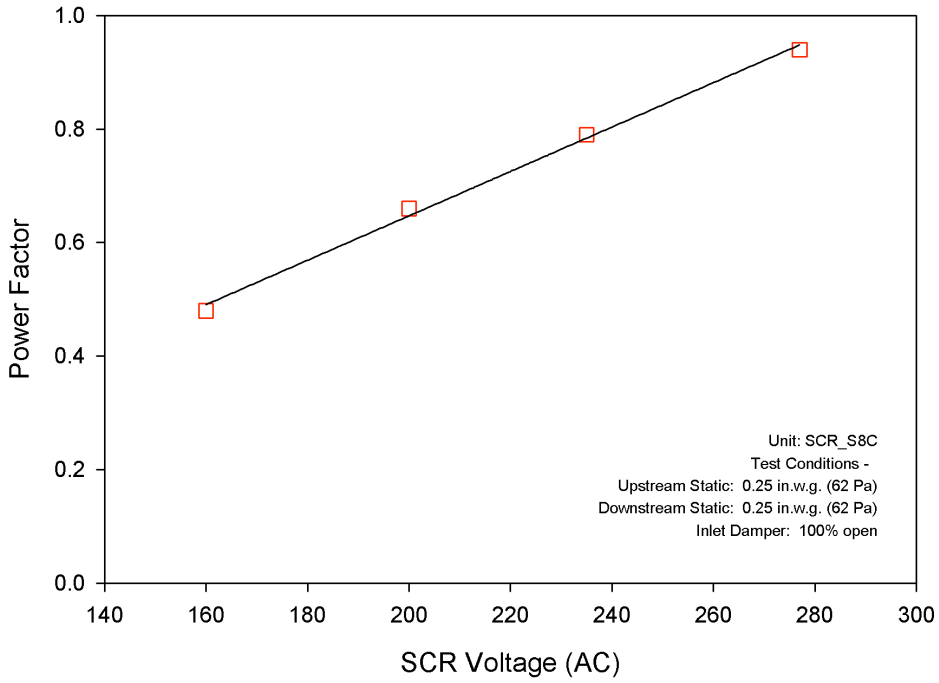

Figure 5-15: Power factor for SCR series terminal units

A comparison of real power consumption for both ECM and SCR controlled VAV terminal units was made in Figure 5-16. Across all flow rates, the power consumption of the ECM controlled unit was less than that of the SCR controlled unit. Specifically at lower flows, the power consumption advantage was significant. However as fan speed increased, the performance gap began to close. Only at extreme flow rates beyond the advertised output did the ECM unit power consumption exceed that of the SCR controlled unit.

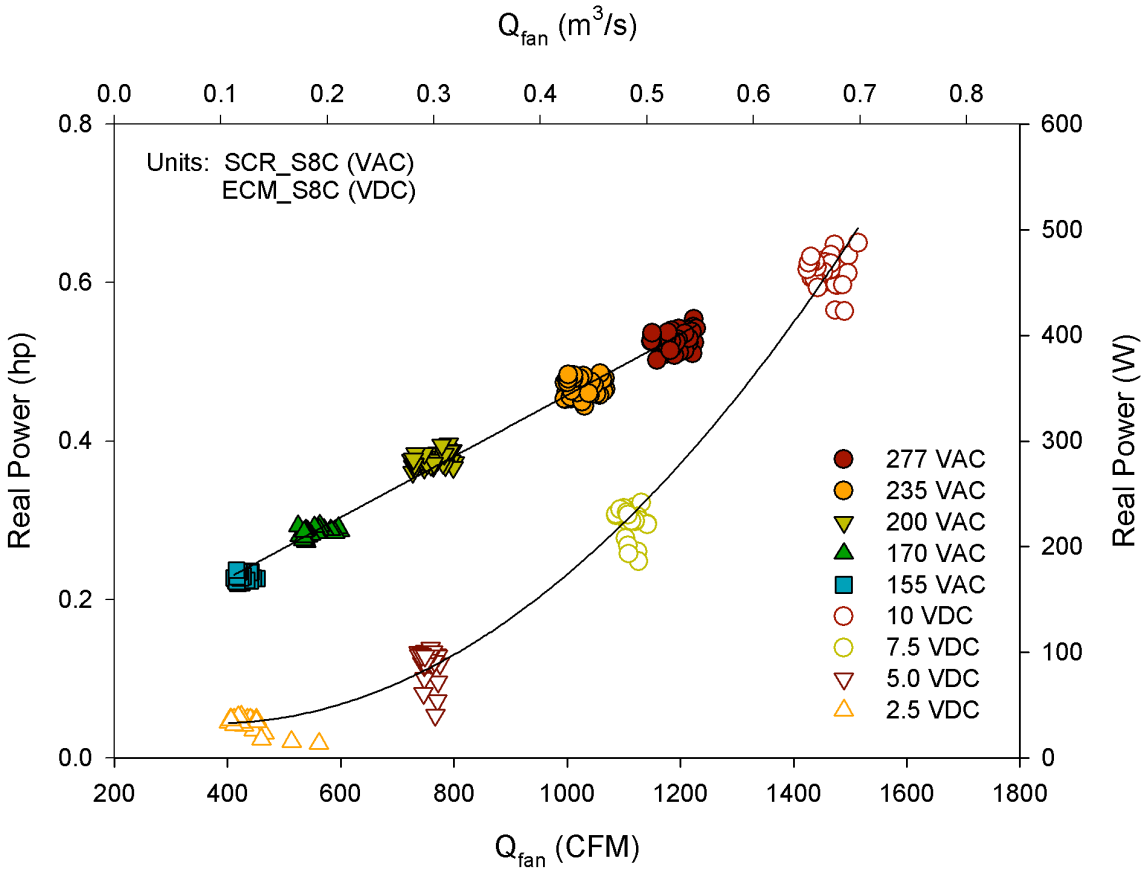

Figure 5-16: Series FPTU real power comparison

Figure 5-17 compared apparent power of the two series units. The SCR apparent power curve was fairly horizontal due to it's power factor approaching unit at high fan speed. The ECM power factor was nearly constant and thus, its apparent power trend closely matched the real power trend. The apparent power sampling favored the ECM controlled unit until approximately 1050 CFM (0.496 m^3/s). Towards the upper limit of fan flow, the apparent power advantaged shifted to the SCR control due largely to the poor ECM power factor.

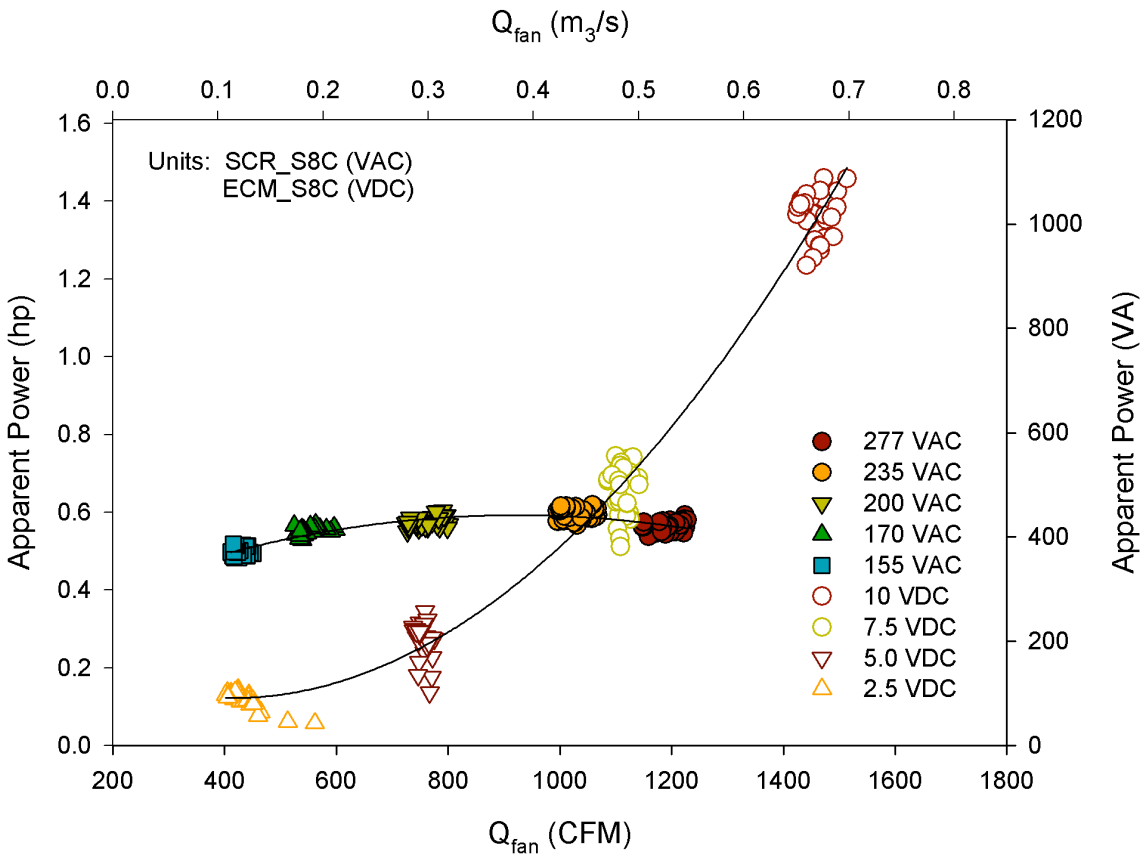

Figure 5-17: Series FPTU apparent power comparison

The harmonic frequencies of voltage, amperage and real power were also recorded. These values represent the amount of distortion to the power grid caused by the VAV fan motor and accompanied electronics. The complete set of harmonic values are reported in Appendix A.

Figures 5-18 and 5-19 present the ECM and SCR controlled current harmonics for the typical test condition of 0.25 in. w.g. (62 Pa) both upstream and downstream of the FPTU. The harmonics are much more pronounced for the ECM control. The ECM control displayed more harmonic relative distortion at high speed while the SCR control displayed more at low speed. Figures 5-20 and 5-21 present the triplen current harmonics for both control types. These particular harmonics which are odd, multiples of the 3rd harmonic are especially of interest in regards to power quality. Due to the internal logic and signal processing, the ECM controlled units displayed a much larger presence of triplen harmonics than the SCR controlled units. At high input voltage, the SCR controller did little work and therefore had minimal triplen harmonic presence. However, even at low input voltage, the SCR current harmonics were far less than the ECM.

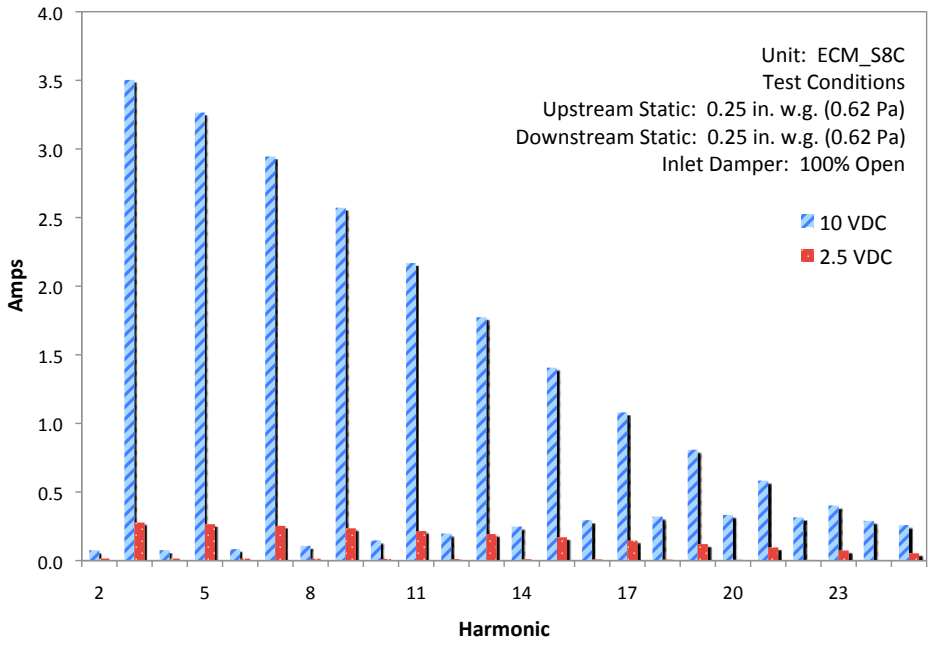

Figure 5-18: ECM series current harmonics

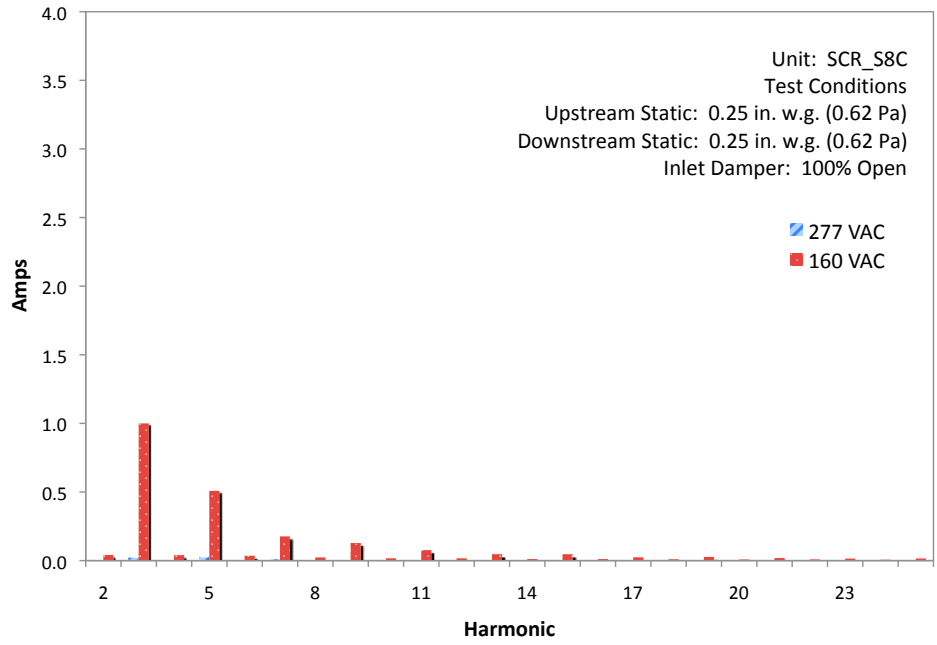

Figure 5-19: SCR series current harmonics

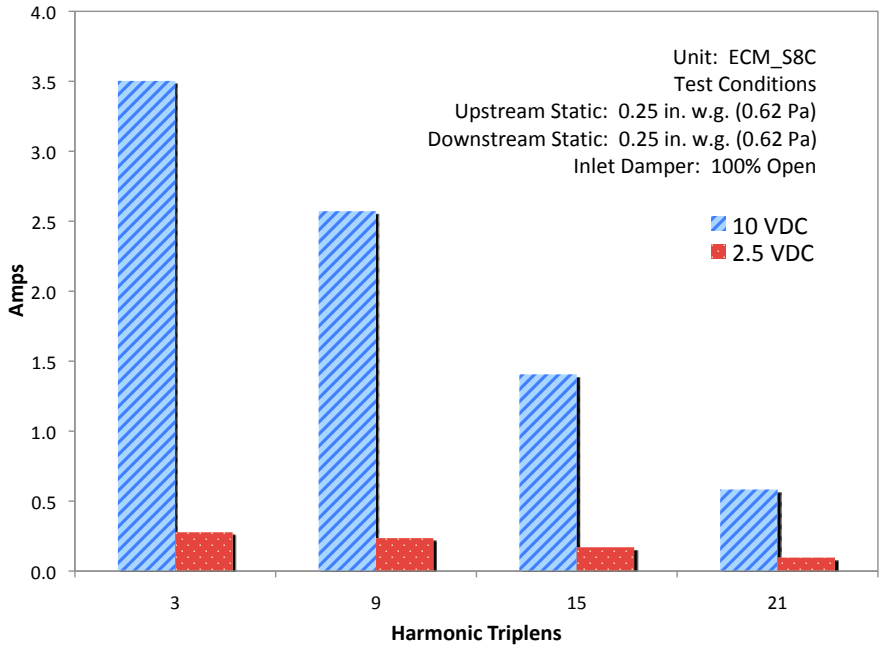

Figure 5-20: ECM series triplen current harmonics

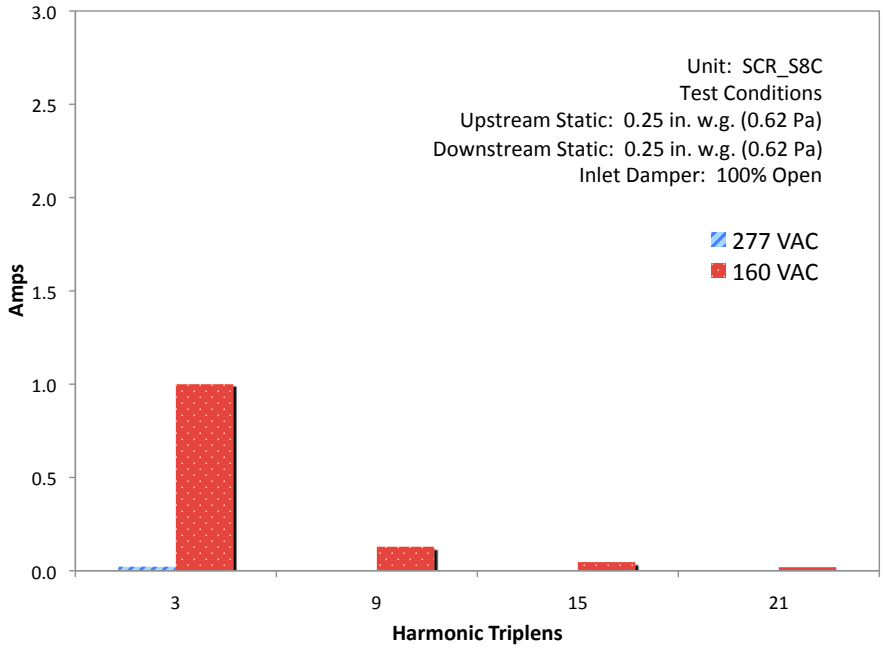

Figure 5-21: SCR series triplen current harmonics

Figures 5-22 and 5-23 present the voltage harmonics for the same typical test condition of 0.25 in. w.g. (62 Pa) for both upstream and downstream static pressures. The voltage harmonics were much closer in magnitude than the current harmonics and represented only a small fraction of the 277 VAC supply voltage.

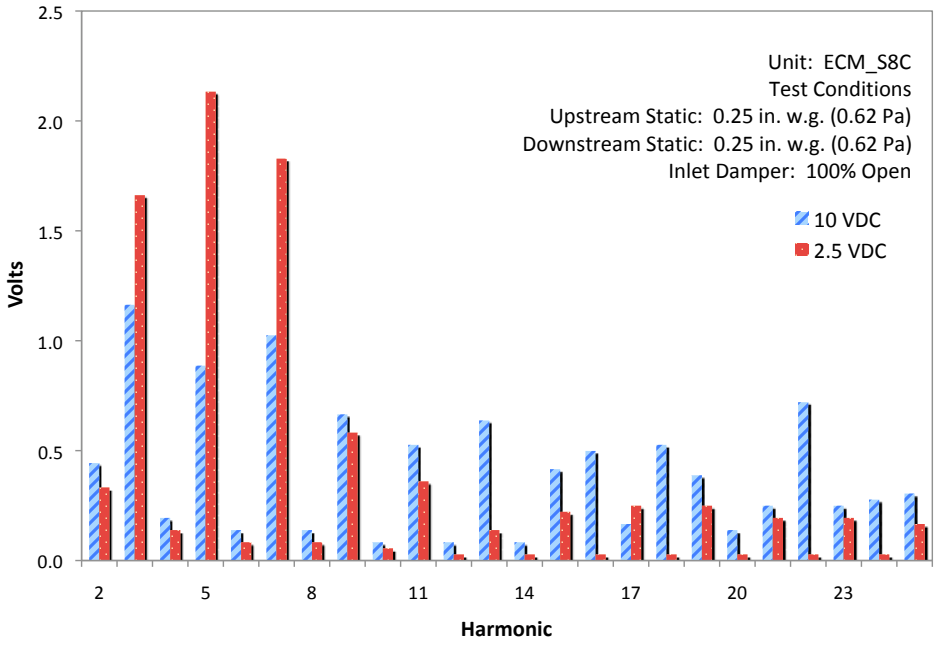

Figure 5-22: ECM series voltage harmonics

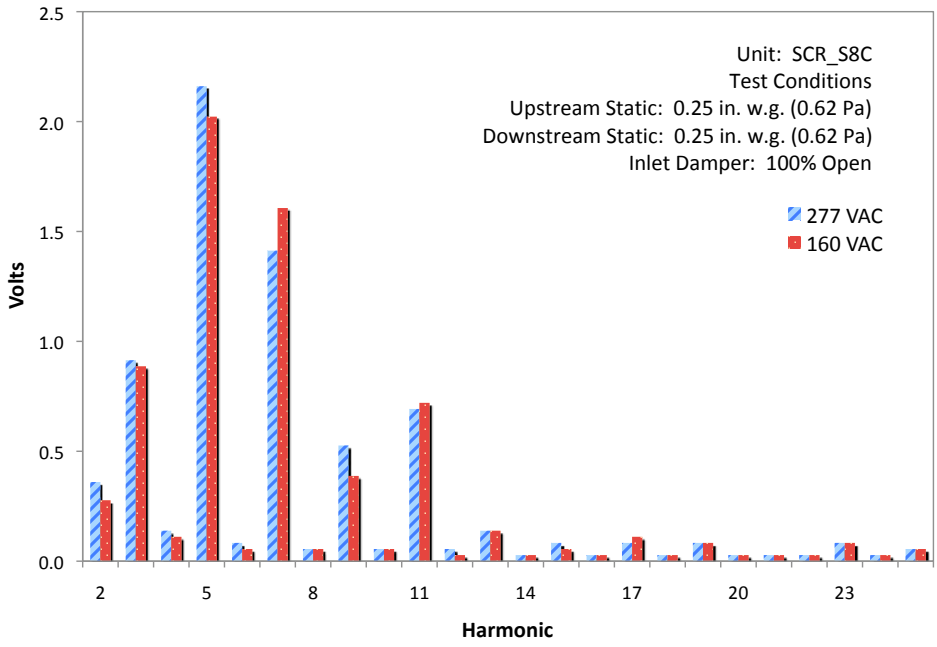

Figure 5-23: SCR series voltage harmonics

Figures 5-24 and 5-25 present the respective control's real power harmonics under the same upstream and downstream conditions. Similar to the voltage harmonics, the watt harmonics were relatively small in magnitude and represented only a small fraction of the real power consumed. The negative harmonic values were attributed to that part of the cycle where energy is actually transferred from the inductor (load) back into the voltage source.

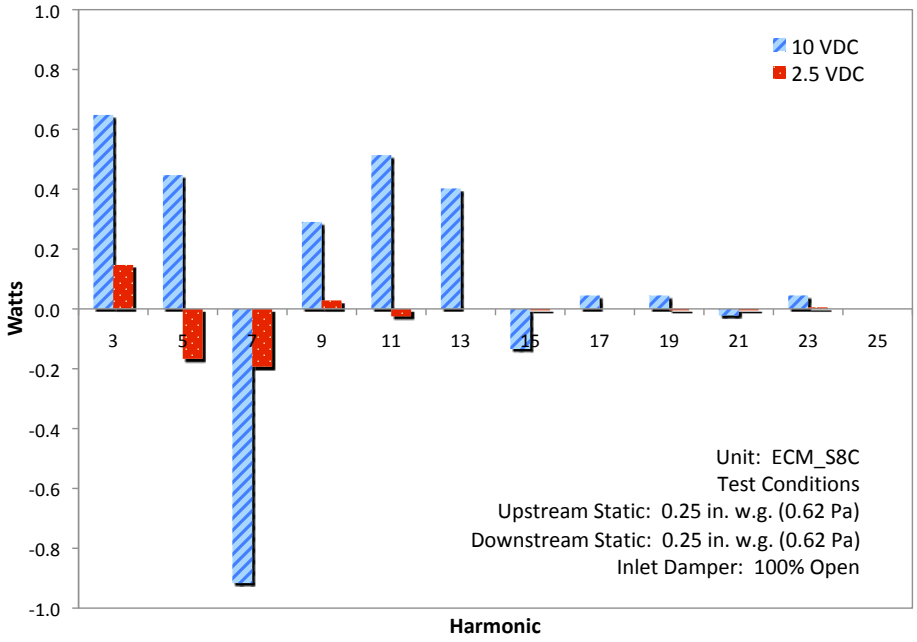

Figure 5-24: ECM series real power harmonics

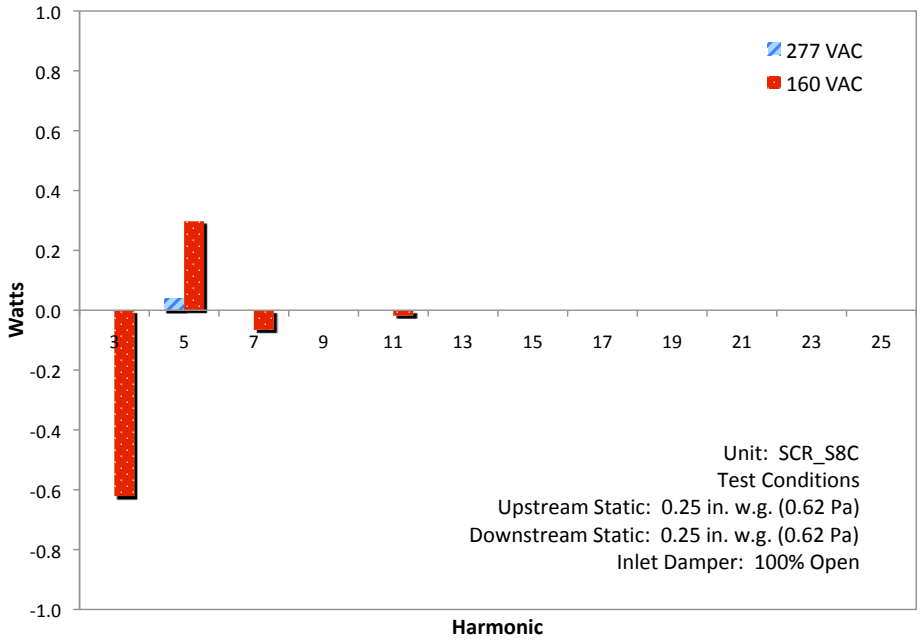

Figure 5-25: SCR series real power harmonics

For both ECM and SCR control, current, voltage and real power harmonics (as a percentage) grew with reduced control voltage (see Appendix A). This was especially true for the SCR. Harmonics represent distortion and the AC motor achieves variable operational speed by distorting the ideal VAC input sine wave. However, at full 277 VAC SCR control, the harmonics became almost negligible due to the SCR not performing any significant work. The ECM control however, utilized a DC motor which required significant work throughout the operation window. However, as input voltage increased, so did the nominal amperage. Thus, in the case of the ECM controlled units, total harmonic distortion was greater at higher fan airflow.

Observing harmonic frequencies required looking at a set of values, rather than a singular variable. Thus they could be difficult to analyze en masse. Total harmonic distortion (THD) was a convenient cumulative value to plot and analyze. THD, as defined in Eq. (1.3), was the ratio of harmonic frequencies over the fundamental 60Hz frequency. Power THD is a common value used in industry and is most widely used in it's percentage form.

Figures 5-26 and 5-27 present both ECM and SCR control's real power THD over the their respective control input ranges. Similar to power factor the SCR displayed an advantage as fan speed was increased via input voltage. The SCR approached 0% total harmonic distortion while the ECM controlled FPTU never dropped below 0.8%. For current and voltage THD data, see Appendix A.

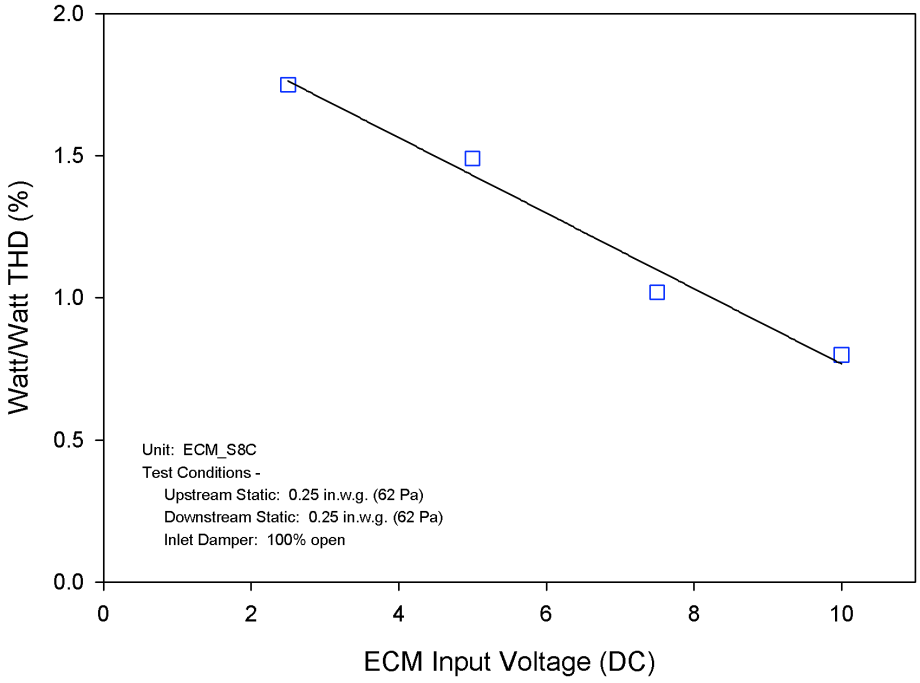

Figure 5-26: Real power THD for ECM series terminal units

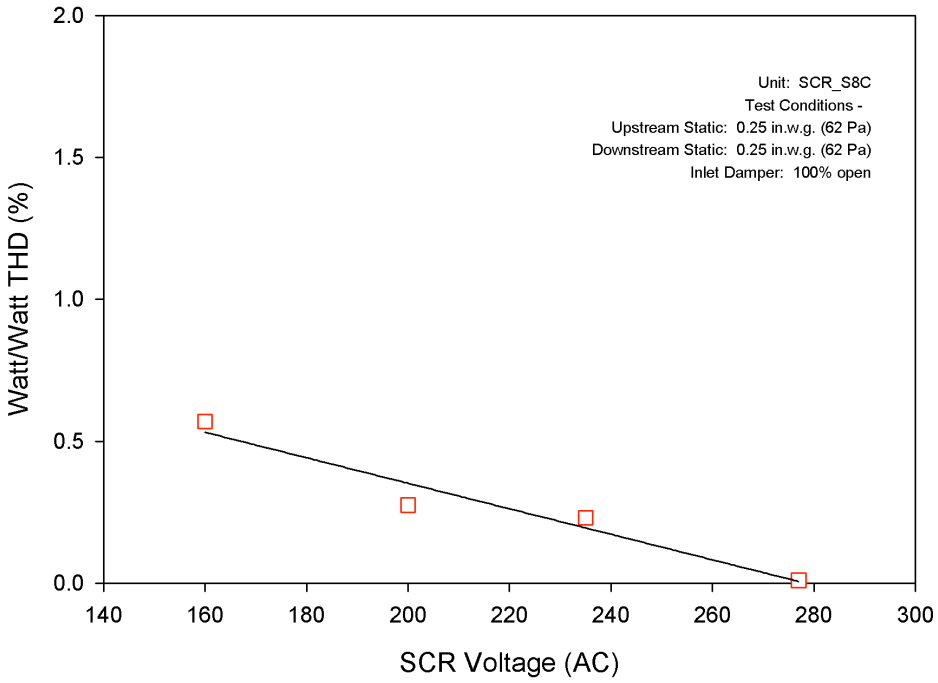

Figure 5-27: Real power THD for SCR series terminal units

CHAPTER VI

PARALLEL TERMINAL UNIT RESULTS

Experimental data were collected for ECM controlled VAV terminal unit using the equipment discussed in Chapter III. Airflow and power models were developed as a function of variables that significantly influenced the performance of the terminal unit. A separate section is provided for both airflow and power analysis. Each section presents a brief summary of the method used, the resulting ECM controlled FPTU results, a comparison with previous SCR controlled FPTU data and discussion regarding each.

6.1 Parallel Terminal Unit Airflow

The distinguishing feature of the parallel VAV fan powered terminal unit (Figure 6-1) is the perpendicular terminal fan providing induced airflow parallel to the primary air stream. Unlike the series FPTU the parallel fan's operation is optional. Unconditioned induced airflow was only present when the fan was engaged, mixing the optional induced air with the conditioned primary air delivered upstream.

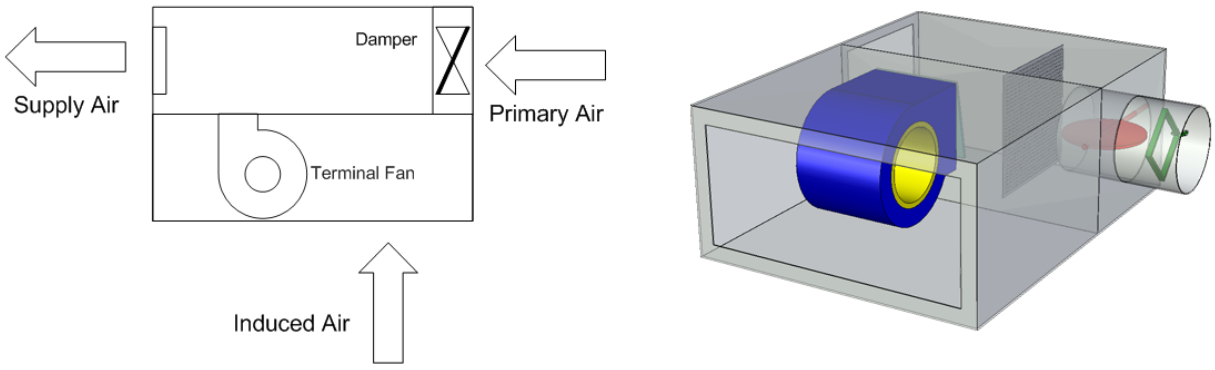

Figure 6-1: Typical parallel VAV fan powered terminal unit

The desired airflow model quantifies induced air delivered by the ECM controlled parallel FPTU. Similar to the ECM controlled series VAV terminal unit, the parallel FPTU was operated via a 0-10 VDC input signal which was custom calibrated to a specific CFM output table. The generic relationship between input voltage and fan speed was not directly due to the ECM's programmable logic and the ability to alter RPM and torque "on the fly" based on external loads. Figure 6-2 was generated for the parallel VAV terminal unit's fan using an optical tachometer.

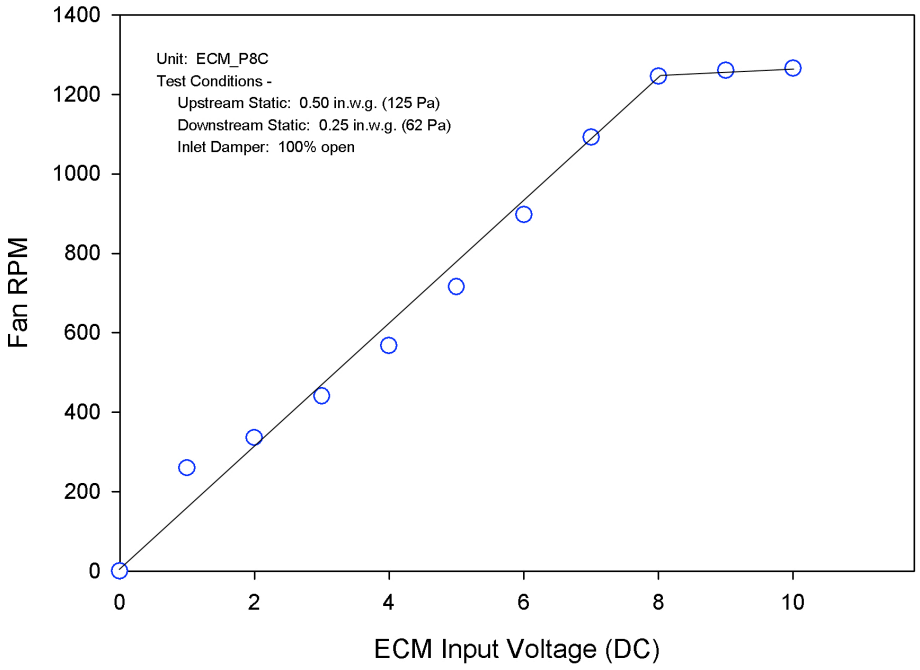

Figure 6-2: Measured ECM parallel FPTU fan speed

Contrary to the approximately linear calibration of the ECM controlled series terminal unit, the parallel controller tested was programmed to plateau at approximately 1250 CFM (0.590 m^3/s). Instead the RPM data was better described using two linear segments. Per the test matrix outlined in Chapter IV equally spaced input voltages of 2.5, 5.0, 7.5 and 10.0 were used. However, as seen in Figure 6-2, there was little difference between the 7.5 and 10.0 settings.

Similar to the series analysis, ECM controlled fan power terminal unit data in this chapter was compared against similar units from the same manufacturer with SCR control. Fan input voltage was used as the primary variable of distinction. Figure 6-3 was created using an optical tachometer and displays the SCR controlled fan speed at the same conditions used for the ECM reference curve. Table 6-1 presents the range or respective controller input voltages. Table 6-2 lists the four test points and their approximate RPM relationship as measured during the tests.

The average speed differential per test level was much higher for the parallel comparison versus the series comparison. The dissimilar fan speed values should discourage direct comparison of numerical test levels between ECM and SCR.

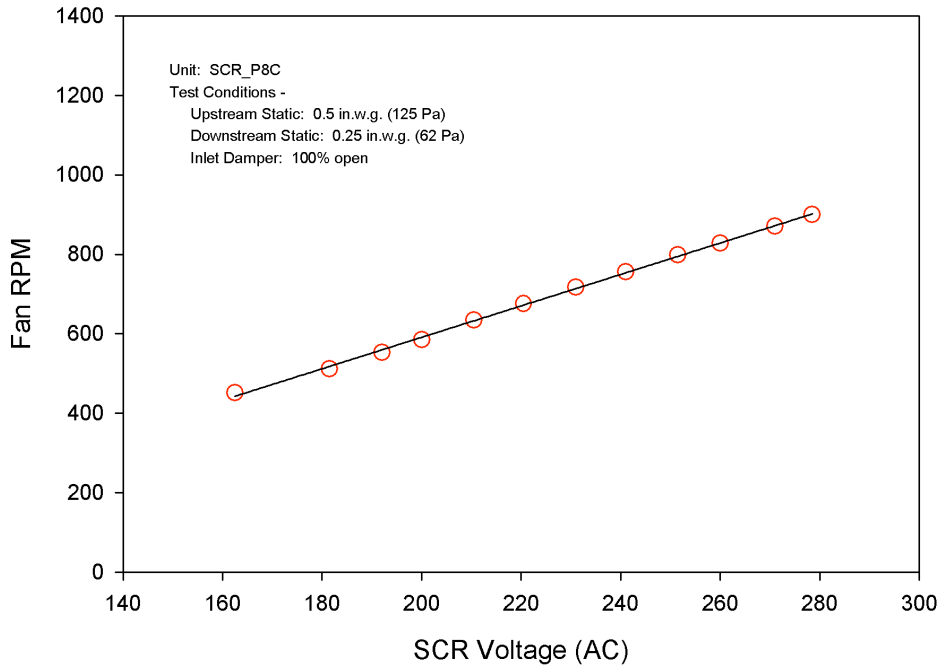

Figure 6-3: Measured SCR parallel FPTU fan speed

Table 6-1: Parallel FPTU range of operational control

Control	Min	Max
ECM (VDC)	0	10
SCR (VAC)	160	277

Table 6-2: Approximate fan speed comparison

	ECM		SCR		
Level	Input Volt (DC)	Fan RPM*	Input Volt (AC)	Fan RPM*	ΔRPM*
1	2.5	400	160	450	50
2	5.0	700	200	585	115
3	7.5	1150	235	725	425
4	10	1250	277	900	350

*all RPM measurements are approximate and are intended for reference only

6.1.1 Fan Airflow Data Analysis and Model. The variable with the greatest influence on fan airflow was fan speed. However, the relationship between voltage input and RPM was unique to each FPTU tested. As a consequence, the applicability of the results found in this section will need to be evaluated with more data to determine if they are applicable to generic simulation. Furthermore, the dynamic operation of the ECM controller dictates that fan speed be removed from the performance model's input. However, in combination with the calibration in Figure 6-2, voltage input was used as the primary independent variable for both its intuitive property as well as its steady-state value. As a contrast to previous research (Furr 2006), the ECM controlled motors with their 0-10 VDC input was compared against the SCR controlled units using a 160-277 VAC input range.

For developing an airflow performance model, fan curves and fan laws explain that for a given fan geometry the only other significant variable is the pressure across the fan (ASHRAE 2001). Figure 6-4 illustrates the principle pressure locations of a series VAV fan powered terminal unit.

The fan inlet of the parallel FPTU design was held approximately constant at atmospheric pressure. The fan output pressure was the FPTUs internal chamber pressure, which was not measured. Instead, the fan output pressure was approximated to be equal to the measured downstream static pressure. Thus downstream static pressure was used in addition to fan input voltage as a primary influence on airflow performance. Fan airflow as a result of input control voltage and downstream pressure are shown in Figure 6-5. The previous SCR controlled data are shown in Figure 6-6.

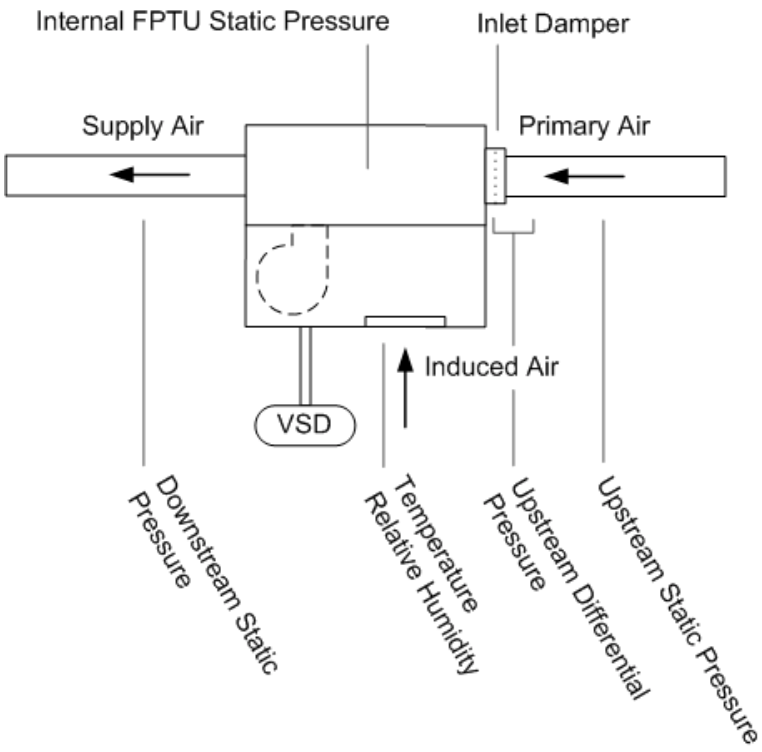

Figure 6-4: Typical parallel VAV fan powered terminal unit pressures

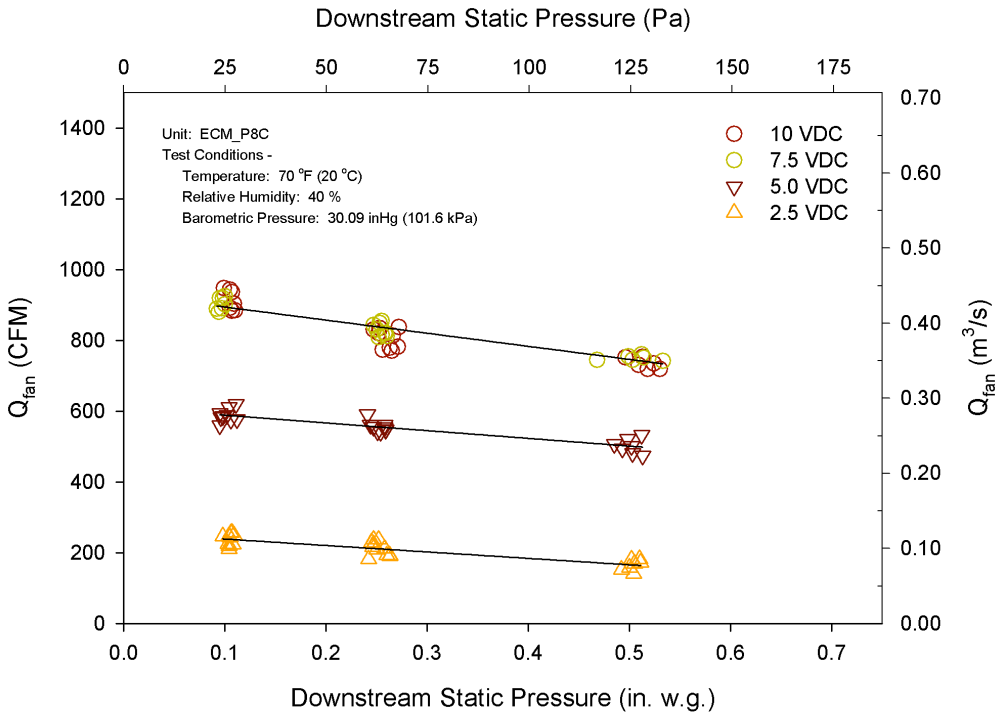

Figure 6-5: Fan airflow for ECM parallel terminal unit

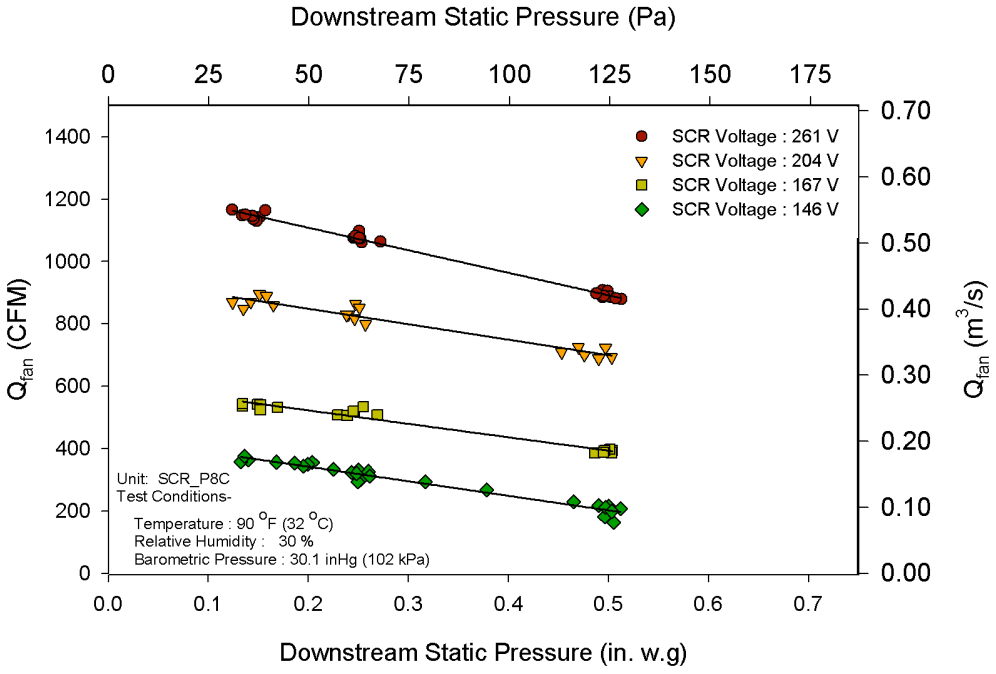

Figure 6-6: Fan airflow for SCR parallel terminal unit

The fan airflow for the ECM controlled parallel FPTU compares similarly to that of the SCR controlled unit, with negatively slopping lines grouped for each fan input voltage. The fan airflow model used for the parallel ECM fan powered terminal unit is shown in Eq. (6.1) and is the same expression used for SCR controlled FPTUs (Furr et al. 2007). Coefficients for the same manufacturers' 8 in (20.3 cm) parallel FPTUs are presented in Table 6-3.

$$Q_{fan} = C_1 + C_2 V + C_3 V^2 + C_4 P_{down} \tag{6.1}$$

Table 6-3: Model coefficients for fan airflow in parallel terminal units

Control	**C_1 [CFM]**	**C_2 [CFM/V]**	**C_3 [CFM/V^2]**	**C_4 [CFM/in. w.g.]**	**R^2**
ECM (VDC)	-282.267	257.991	-13.841	-290.917	0.982
SCR (VAC)	-1725	19.79	-0.0328	-564.4	0.991

The high R^2 value indicates that the model correlates to the empirical data set very closely. It should be noted however, that the voltage scales for ECM and SCR are different. ECM controls employ a 0-10 VDC input while the SCR uses a mechanical 160-277 VAC turn screw to achieve voltage regulation. If a universal model with generic coefficients were desired, a dimensionless normalized input would be needed in place of the respective VDC and VAC values.

6.1.2 Airflow Leakage Analysis and Model. The induced fan airflow was not directly measured. The 1st law of Thermodynamic derivation used in Chapter III concluded that, with the given assumptions:

$$\sum_{out} \text{airflow} = \sum_{in} \text{airflow} \tag{3.5}$$

where induced airflow was measured as the difference of the downstream "AMCA Figure 12" supply airflow and the upstream "AMCA Figure 15" primary airflow.

$$Q_{induced} = Q_{supply} - Q_{primary} \tag{3.6}$$

The calculation assumed that all airflow was captured by the three quantities: primary air, induced air and supply air. That assumption was valid for series terminal units but not for parallel designed FPTUs. Series FPTUs have a lower than atmospheric internal FPTU chamber static pressure. Therefore, any potential leakage was into the FPTU chamber which was simply absorbed and added into induced airflow quantity. However, the internal chamber static pressure of a parallel FPTU was always greater than atmospheric, thus, unaccounted air leakage leaked out of the FPTU chamber and added a fourth term to the volumetric airflow balance, Eq. (6.2).

$$Q_{induced} = \left(Q_{supply} - Q_{primary}\right) + Q_{leakage} \tag{6.2}$$

Air leakage occurred at either the terminal unit's sheet metal seams or along the edges of the backdraft damper (Figure 6-7). During full cooling mode the parallel terminal fan was turned off. At this time the backdraft damper was to fully seal preventing air from escaping backwards through the fan. In this mode of operation the supply airflow downstream should equal the primary airflow upstream. However, this was not the case.

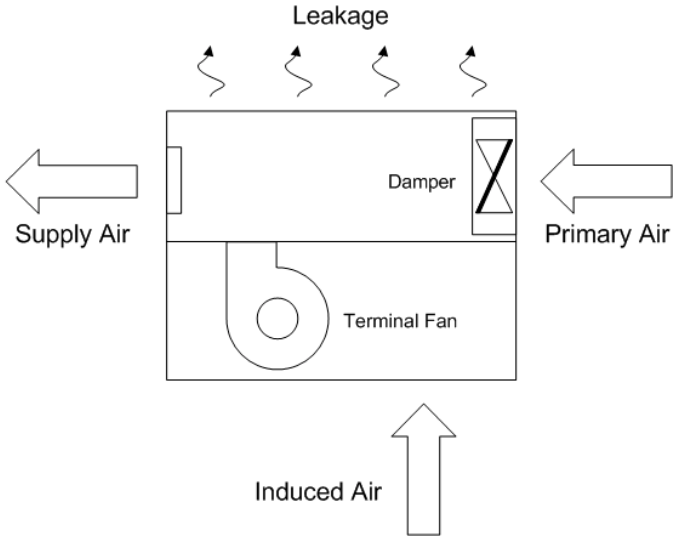

Figure 6-7: Terminal unit leakage for parallel FPTUs

A leakage model was created to quantify the amount of leakage for the terminal units. The primary variable influencing air leakage was the internal FPTU static pressure (see Figure 6-4). However, this value was not measured. Therefore, an assumption was made that the internal FPTU static pressure was closely approximated by the downstream static pressure. Thus the downstream static pressure was used as a proxy for the pressure inside the terminal unit chamber and was expected to be the most significant variable in the leakage model.

The leakage at the seems was almost entirely a function of internal FPTU static pressure. However, the analysis of the backdraft damper leakage was more complex. In addition to internal static pressure, airflow velocity on and around the backdraft damper was expected to have an influence. This would certainly be the case for terminal units incorporating an air-operated backdraft damper (Figure 3-10), although with lesser effect on gravity operated dampers (Figure 3-11). The models tested in this study used a gravity backdraft damper, however, primary airflow was still assumed to have some influence.

Leakage tests were run using the concept of a full cooling mode where the internal fan was turned off. This allowed a direct comparison of measured air between the upstream "AMCA Figure 15" and the downstream "AMCA Figure 12" airflow chambers. The airflow differential would be near zero if there were no leaks (See Appendix C for chamber calibration), however this was not the case. Using the fan off test levels from the test matrix (Chapter IV), Figures 6-8 through 6-10 were generated.

The leakage exhibited a much stronger correlation to downstream static pressure (Figure 6-8) versus inlet air velocity pressure (Figure 6-9). Inlet air velocity pressure appears to have little effect, per the nearly horizontal trend line. However, for high downstream static pressure, there was some evidence of influence. This supported the theory that for gravity operated backdraft dampers the effect of primary airspeed was minimal. However the model included the velocity term to maintain robustness for future application with FPTUs with an air-operated backdraft damper. The ECM leakage data closely matched the results of the SCR leakage shown in Figure 6-10. This was to be expected as fan control and operation were not included in the leakage test. Terminal unit geometry and construction were the primary factors regarding leakage, and for this study, both units were from the same manufacturer.

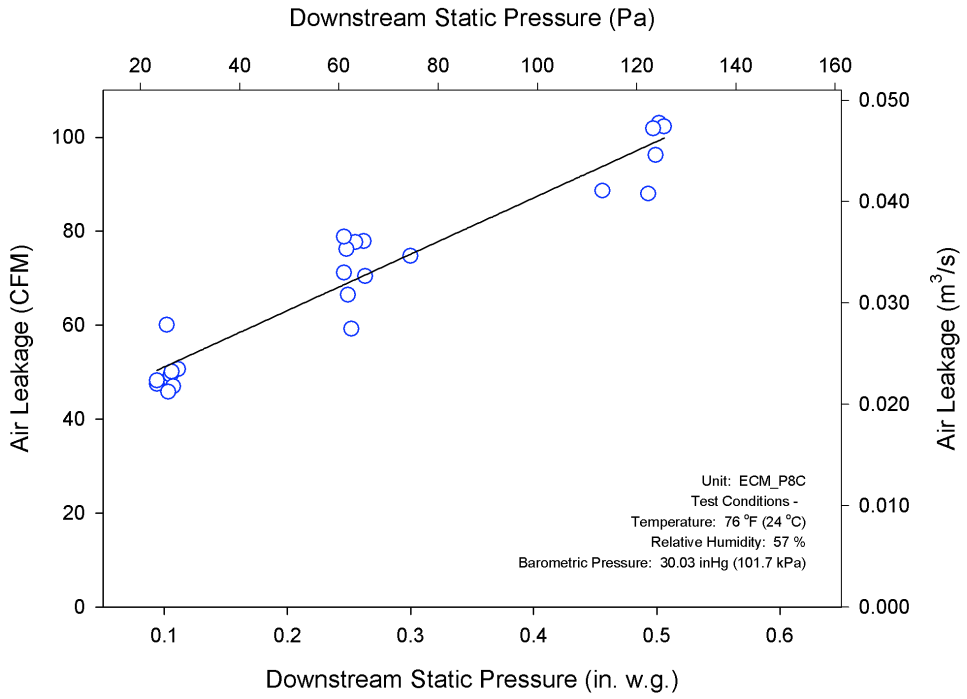

Figure 6-8: ECM parallel FPTU air leakage vs. downstream static pressure

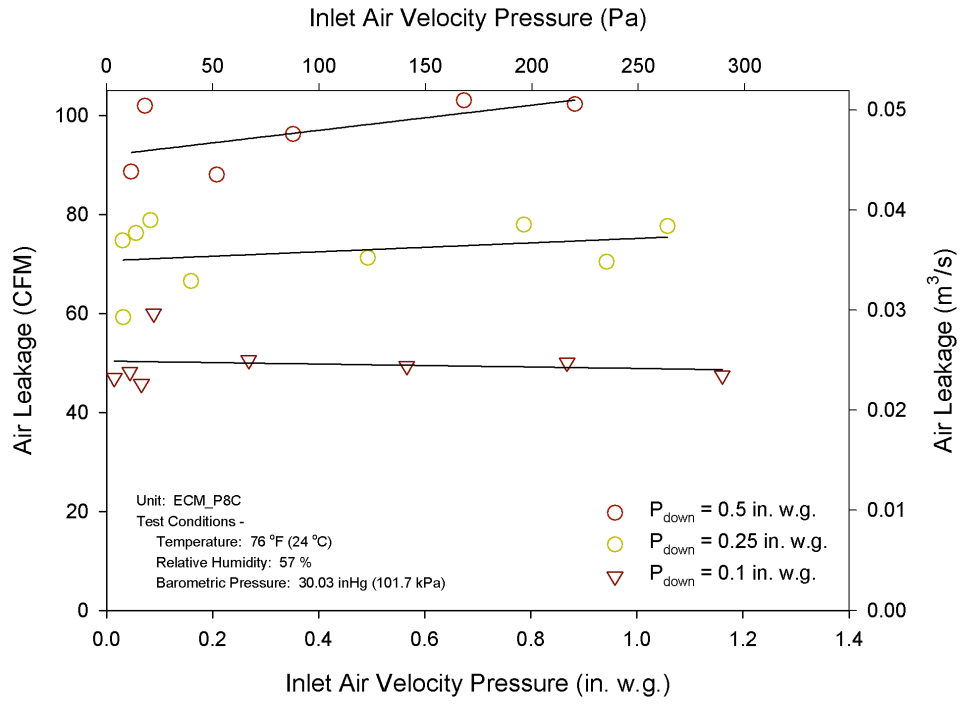

Figure 6-9: ECM parallel FPTU air leakage vs. inlet air velocity pressure

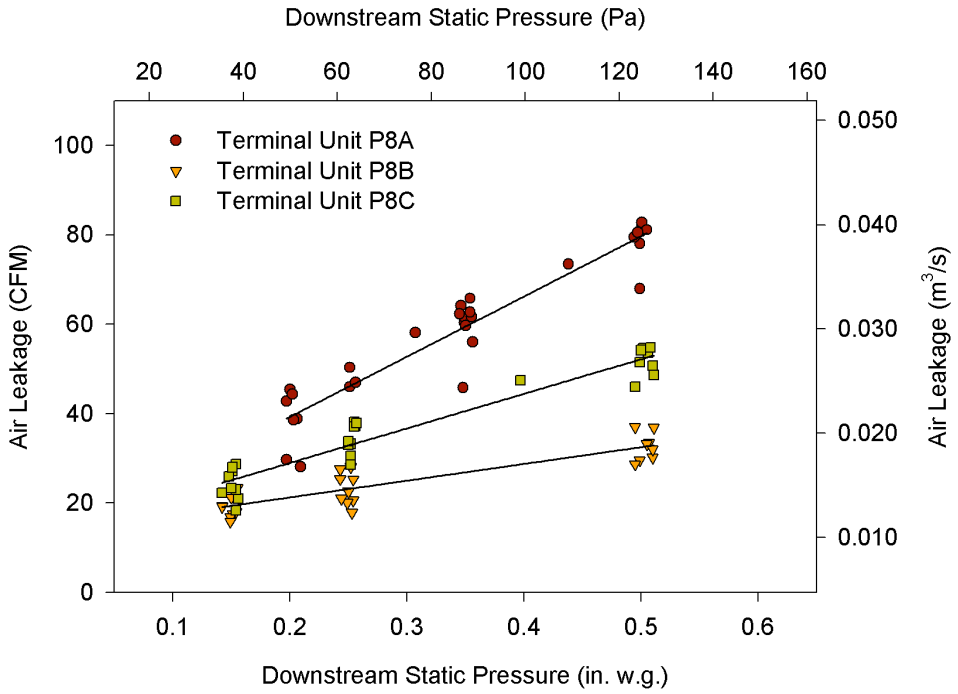

Figure 6-10: SCR parallel FPTU air leakage vs. downstream static pressure

Eq. (6.3) was the model used to express the amount of air leakage in the parallel configured fan power terminal unit (Furr et al. 2007). In this model the P_{down} term accounted for the effect of internal FPTU chamber pressure on leakage, while P_{iav} represented any effects of primary air velocity on the backdraft damper. The coefficients for both the ECM and SCR controlled terminal units are shown in Table 6-4.

$$Q_{leakage} = C_1 + C_2 P_{down} + C_3 P_{iav} \tag{6.3}$$

Table 6-4: Model coefficients for leakage airflow in parallel terminal units

FPTU	**C_1 [CFM]**	**C_2 [CFM/in.w.g.]**	**C_3 [CFM/in.w.g.]**	**R^2**
ECM	37.87	119.98	3.213	0.918
SCR	16.86	77.55	-10.76	0.970

The R^2 value was above 90% for both and the coefficients are within the same order of magnitude. This implied the leakage model provided a good description of of leakage behavior given upstream and downstream pressure conditions. However, this model was developed while the FPTU's fan was disengaged; which was done to eliminate the induced air variable and to allow direct differential airflow measurement. However, it is hypothesized that leakage during this "full cool" test included leakage not only at the sheet metal seams but also at the backdraft damper. Thus, this leakage model should not be considered valid for situations when the FPTU fan was engaged. When the internal fan was on, it was assumed that most leakage previously found at the backdraft damper was eliminated due to the fan discharge pressure.

6.1.3 Primary Airflow Analysis and Model. Primary airflow model as a function of differential pressure across the terminal units was investigated. Figures 6-11 and 6-12 present primary terminal unit airflow as a set of parabolic curves based on inlet damper position. Both ECM and SCR terminal parallel FPTU used circular butterfly inlet dampers which had a 90º range of operation. The damper setting of 0º represented full open, while the damper setting of 90º represented the fully closed position.

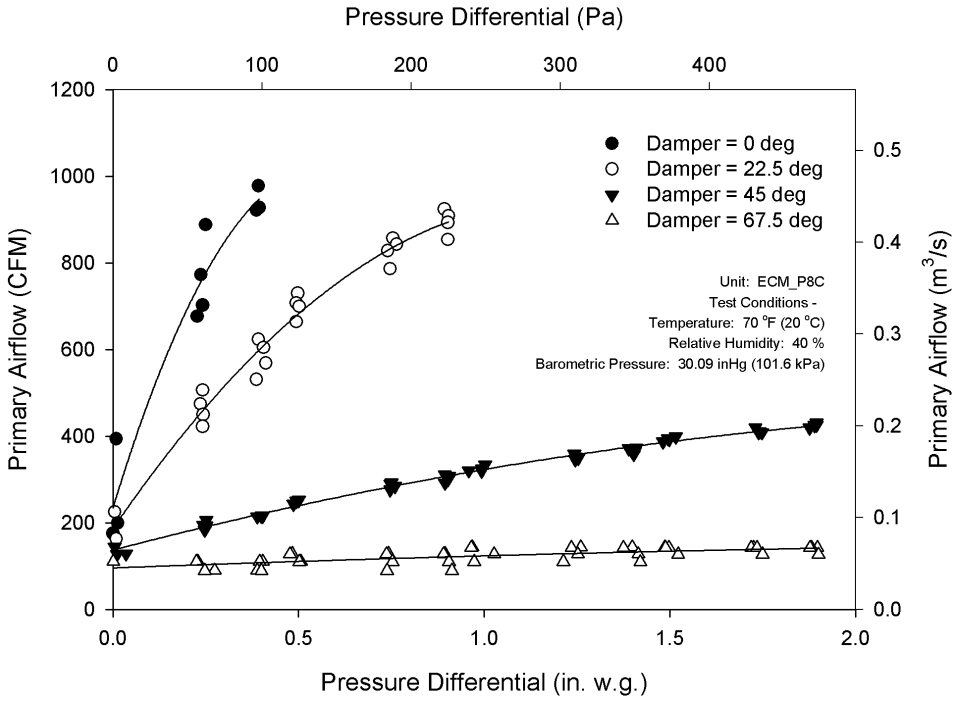

Figure 6-11: Primary airflow for ECM parallel terminal unit

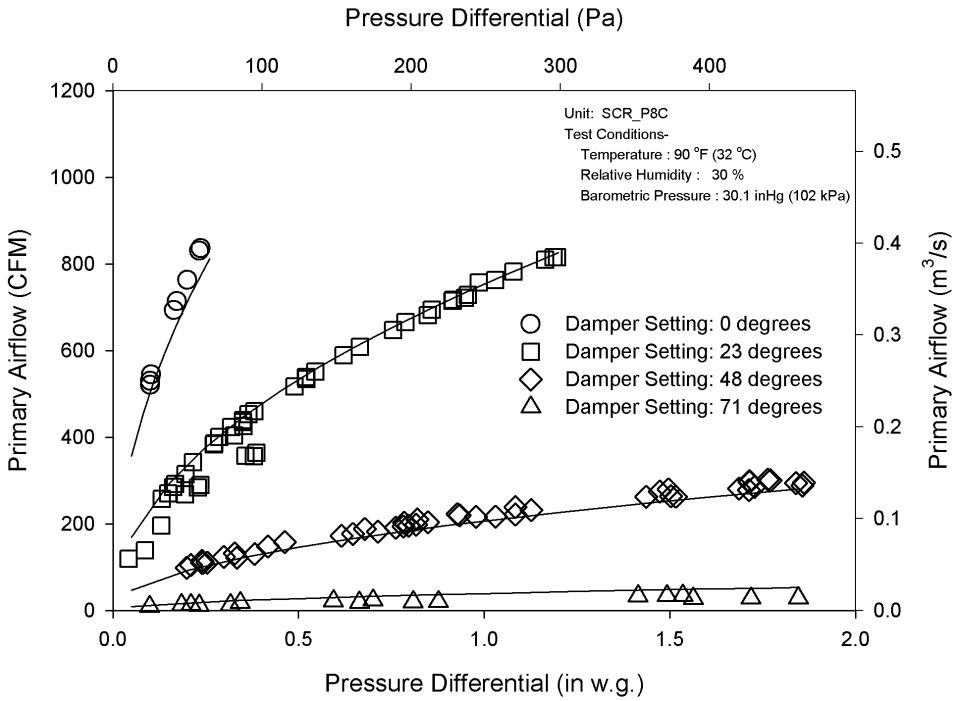

Figure 6-12: Primary airflow for SCR parallel terminal unit

Similar to the series model, Eq. (6.4) was reused from previous SCR research (Furr et al. 2007). The model defines primary FPTU airflow as proportional to the square root of the pressure differential across the terminal unit for a given damper setting. Unlike the series unit, a differential offset pressure was not needed. Differential pressure across the VAV terminal unit is required for airflow in the parallel design, thus when differential pressure reached zero, so did primary flow. Akin to the series data, the parallel model was irrespective of fan input voltage. Again the ECM model coefficients were very similar to those of the SCR controlled model (Table 6-5).

$$Q_{primary} = C_1(1 + C_2S + C_3S^2)\sqrt{DP} \quad (6.4)$$

Table 6-5: Model coefficients for primary airflow in parallel terminal units

Control	**C_1 [CFM/(in.w.g)$^{0.5}$]**	**C_2 [CFM/deg]**	**C_3 [CFM/deg^2]**	**R^2**
ECM	1671.3	-0.0253	1.71 E-04	0.978
SCR	1593.8	-0.0273	1.91 E-04	0.981

The high R^2 value indicated that the model correlated to the empirical data set very closely.

6.2 Parallel Terminal Unit Power

The power analysis of this study can be broken down into two divisions: power consumption and power quality. The techniques and methodology used for the parallel FPTU ECM motor is much the same as the series FPTU found in the previous chapter.

6.2.1 Power Consumption Analysis and Model. The ECM controlled fan power consumption as a function of airflow is best approximated by an 3rd order curve as seen in Figure 6-13. This is in contrast to a similarly configured, SCR controlled series terminal units in Figure 6-14.

Figures 6-15 and 6-16 display power consumption per airflow over the range of fan output. ECM controlled units displayed the best power-to-airflow ratio at lower volumetric flow while for SCR controlled units it was the opposite. SCR control has better power-to-airflow ratios at high volumetric flow. However, unlike the smooth general trend of the SCR data, the ECM Watts/CFM data were clearly segregated by input voltage.

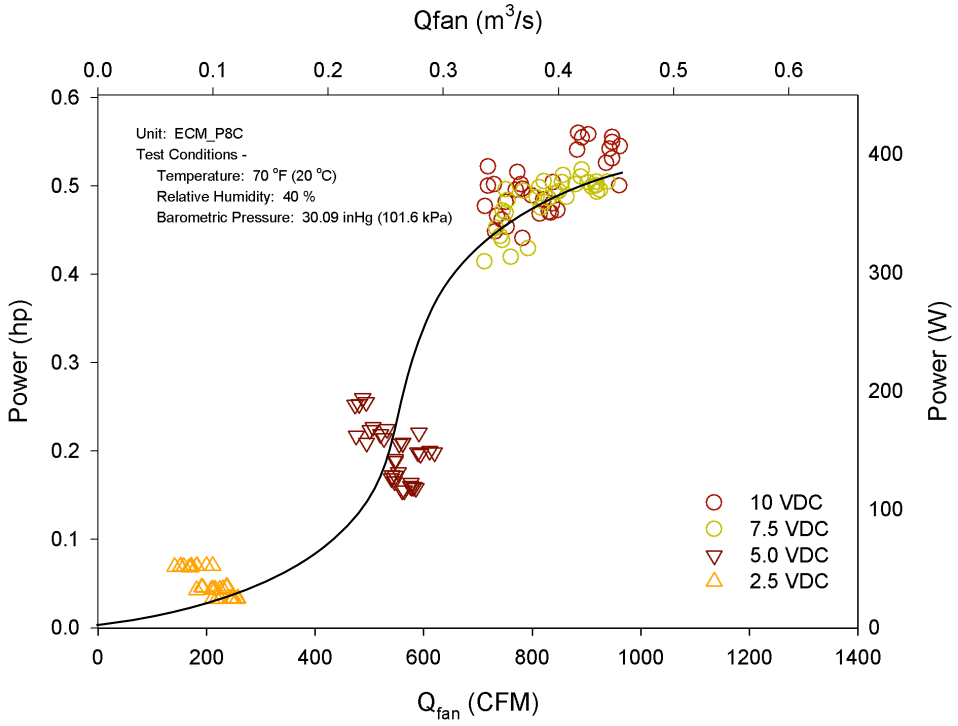

Figure 6-13: Power consumption for ECM parallel terminal unit

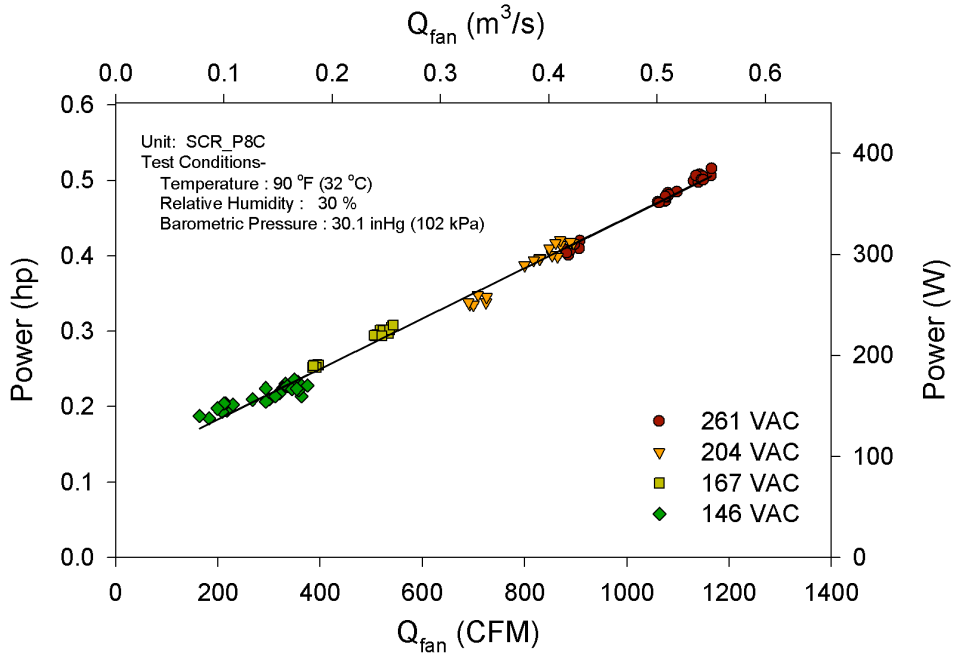

Figure 6-14: Power consumption for SCR parallel terminal unit

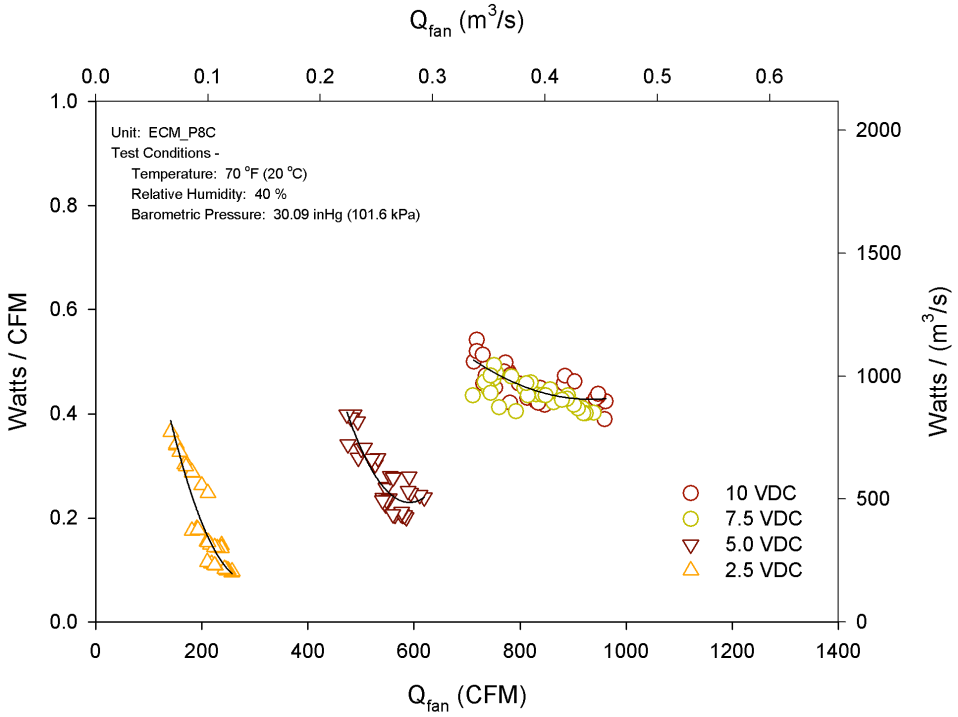

Figure 6-15: ECM parallel terminal unit watt per CFM vs. CFM

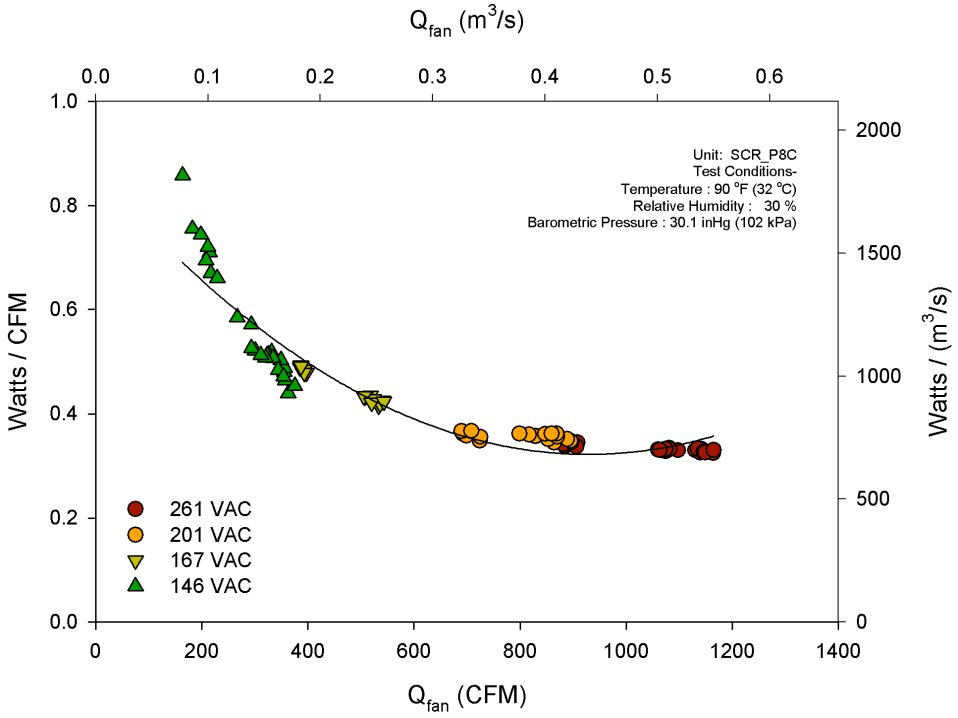

Figure 6-16: SCR parallel terminal unit watt per CFM vs. CFM

Using the mathematical expression developed in previous research (Furr et al. 2007), the model for fan power consumption is expressed in Eq. (6.5). An additional coefficient was added however, due to the logistic flow curve found in Figure 6-13. The model is based on both input voltage and downstream static pressure. The coefficients for the respective control types are listed in Table 6-6.

$$\text{Power}_{fan} = C_1 + C_2 V + C_3 V^2 + C_4 P_{down} \quad (6.5)$$

Table 6-6: Model coefficients for power consumption in parallel terminal units

Control	C_1 [CFM]	C_2 [CFM/V]	C_3 [CFM/V^2]	C_4 [CFM/V^3]	C_5 [CFM/in. w.g.]	R^2
ECM (VDC)	100.652	12.141	30.690	-2.390	-290.407	0.990
SCR (VAC)	-363	5.18	-0.0088	0	-145	0.990

The high R^2 value indicated that the model matches the empirical data set very closely. The additional 3rd order C4 coefficient allowed the ECM model to achieve a 99%. It should be noted however, that the voltage scales for ECM and SCR are different. ECM controls employed a 0-10 VDC input while the SCR used a mechanical 160-277 VAC turn screw to achieve voltage regulation.

6.2.2. Power Quality Analysis. The power quality assessment of the parallel VAV terminal unit focuses on power factor and harmonic distortion similar to the series unit. In addition to the real power consumption (watts) reported in section 6.2.2, apparent power (VA) was also considered. Figures 6-17 and 6-18 illustrate the significant difference in ECM versus SCR operation in regards to power efficiency.

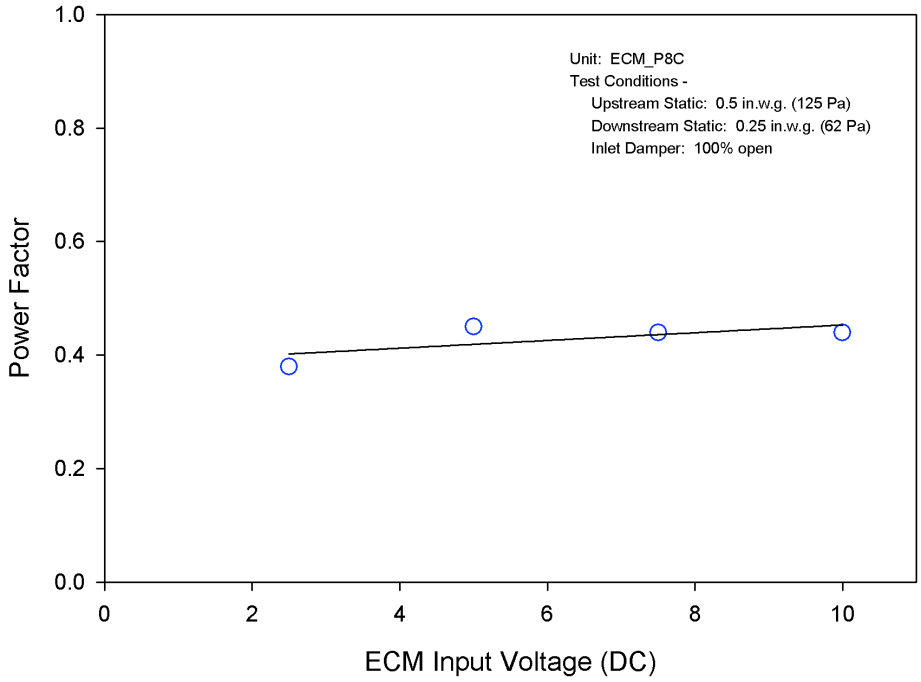

Figure 6-17: Power factor for ECM parallel terminal units

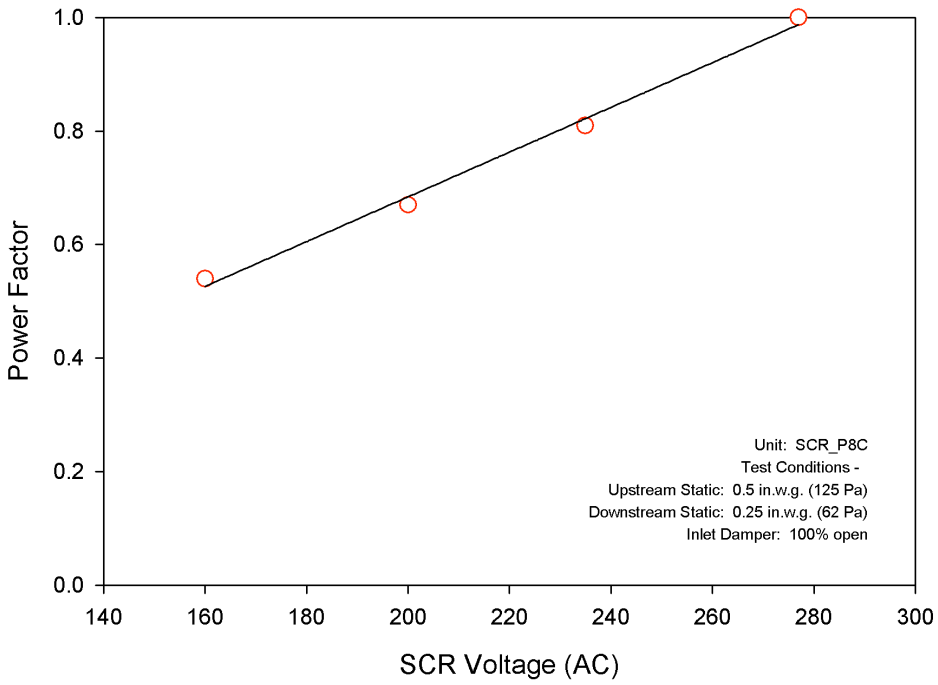

Figure 6-18: Power factor for SCR parallel terminal units

A comparison of real power consumption for both ECM and SCR controlled VAV terminal units was made in Figure 6-19. Across lower flow rates, the power consumption of the ECM controlled unit was less than that of the SCR controlled unit. Specifically at minimum flows, the power consumption advantage was significant. However as fan speed increased, the performance gap began to close. At flow rates above approximately 550 CFM (0.26 m^3/s) the real power consumption was less for the SCR controlled units.

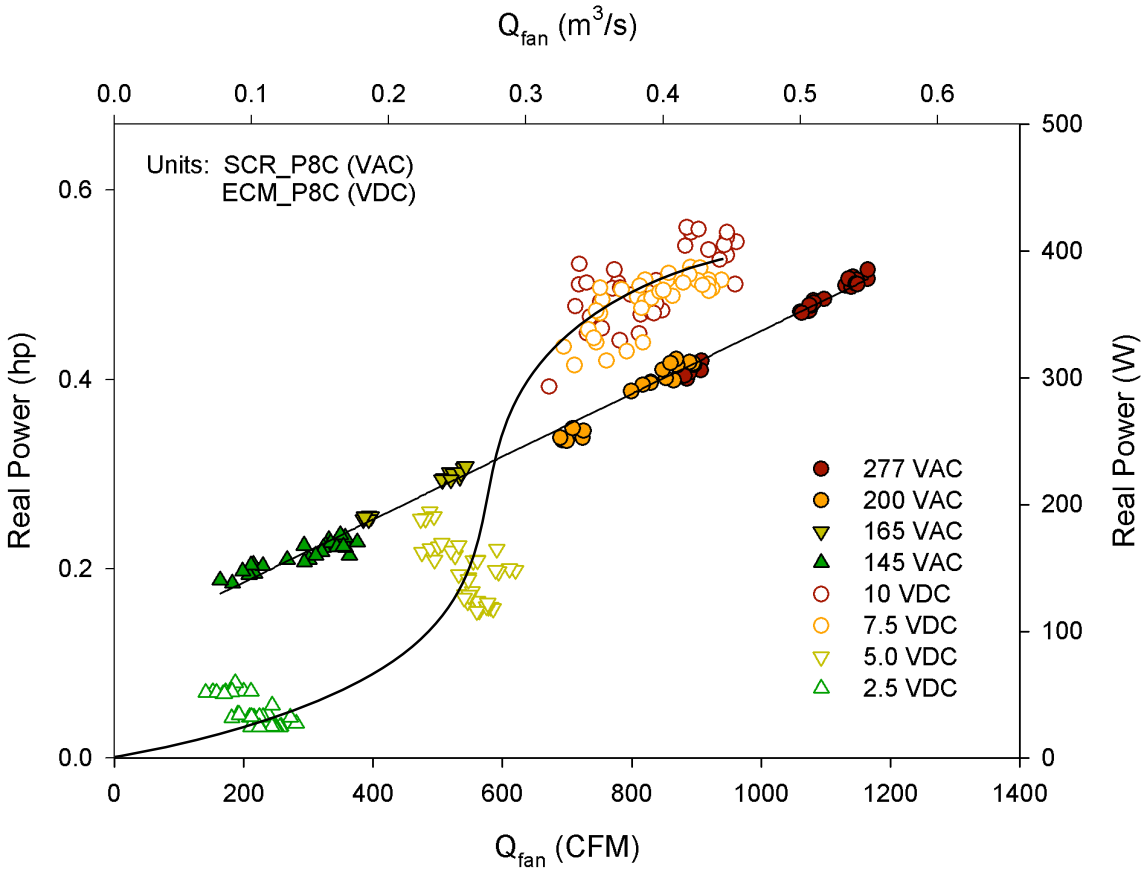

Figure 6-19: Parallel FPTU real power sampling

Figure 6-20 compared apparent power of the two series units. The SCR apparent power curve was fairly horizontal due to it's power factor approaching unit at high fan speed. The ECM power factor was nearly constant and thus, its apparent power trend closely matched the real power trend. The apparent power sampling favored the ECM controlled unit until approximately 500 CFM (0.236 m^3/s). For moderate to high fan airflows, the apparent power advantaged shifted to the SCR control due largely to the poor ECM power factor.

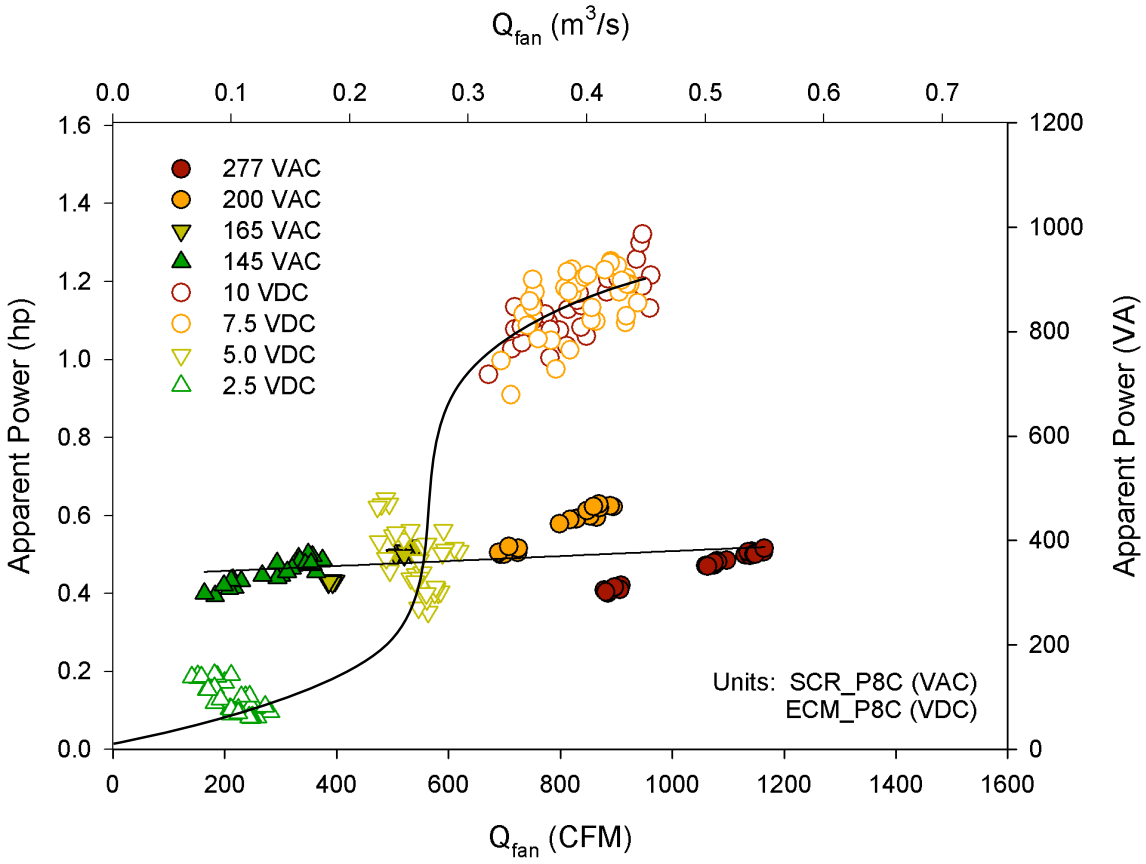

Figure 6-20: Parallel FPTU apparent power sampling

The harmonic frequencies of voltage, amperage and real power were also recorded. These values represent the amount of distortion to the power grid caused by the VAV fan motor and accompanied electronics. The complete set of harmonic values are reported in Appendix A.

Figures 6-21 and 6-22 present the ECM and SCR controlled current harmonics for the typical test condition of 0.5 in. w.g. (125 Pa) upstream of the FPTU and 0.25 in. w.g. (62 Pa) downstream. The harmonics are much more pronounced for the ECM control. The ECM control displayed more harmonic relative distortion at high speed while the SCR control displayed more at low speed. Figures 6-23 and 6-24 present the triplen current harmonics for both control types. These particular harmonics which are odd, multiples of the 3rd harmonic are especially of interest in regards to power quality. Due to the internal logic and signal processing, the ECM controlled units displayed a much larger presence of triplen harmonics than the SCR controlled units. At high input voltage, the SCR controller did little work and therefore had minimal triplen harmonic presence. However, even at low input voltage, the SCR current harmonics were far less than the ECM.

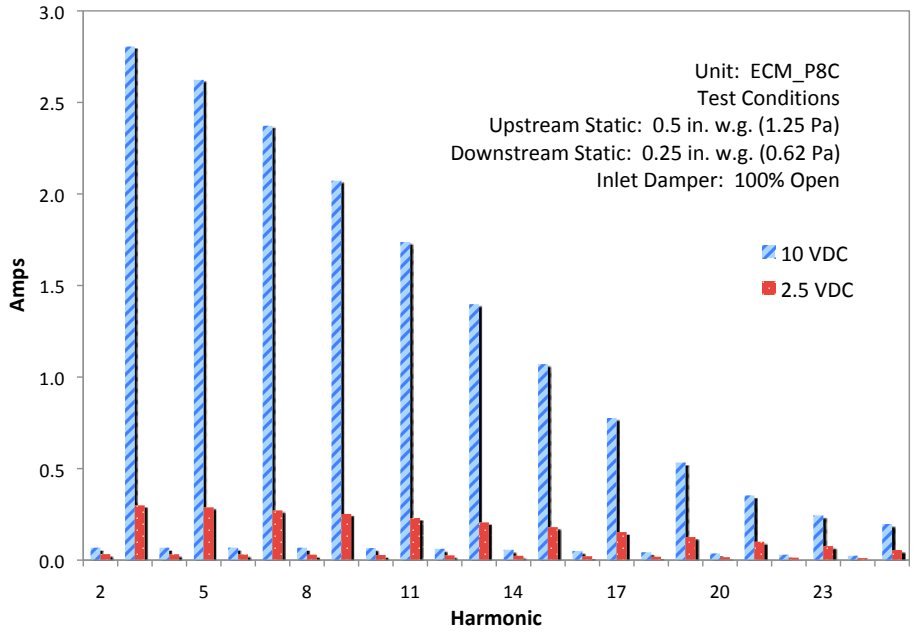

Figure 6-21: ECM parallel current harmonics

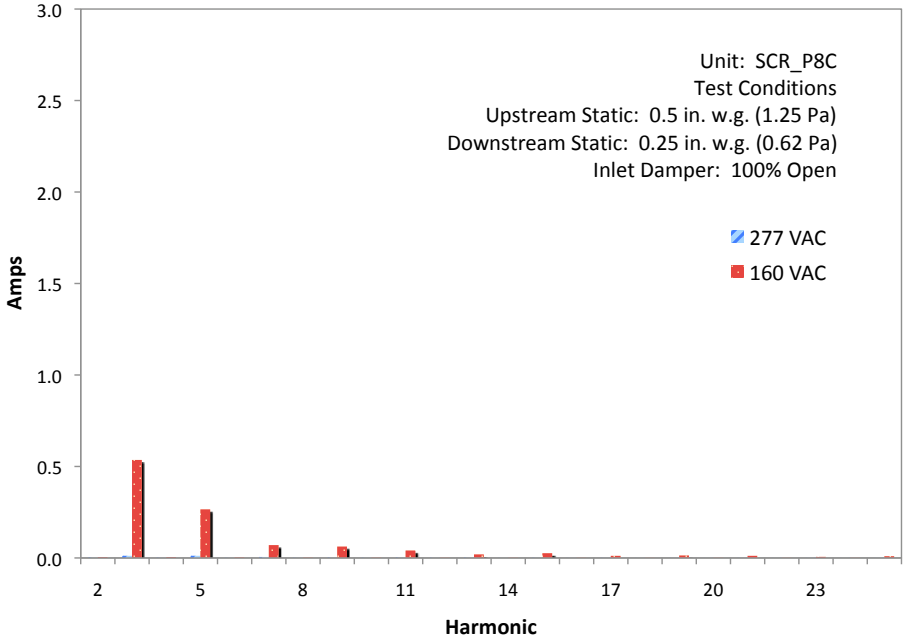

Figure 6-22: SCR parallel current harmonics

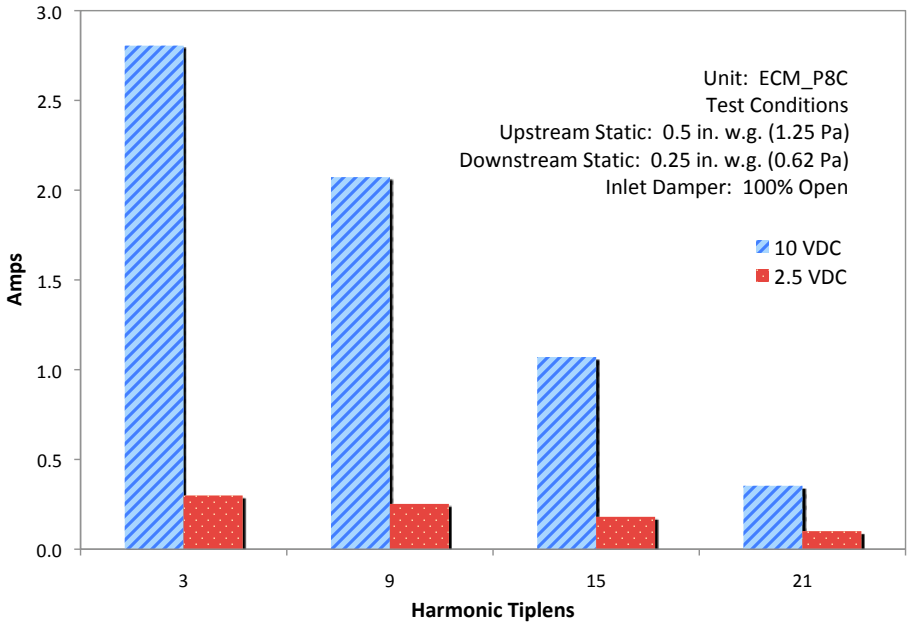

Figure 6-23: ECM parallel triplen current harmonics

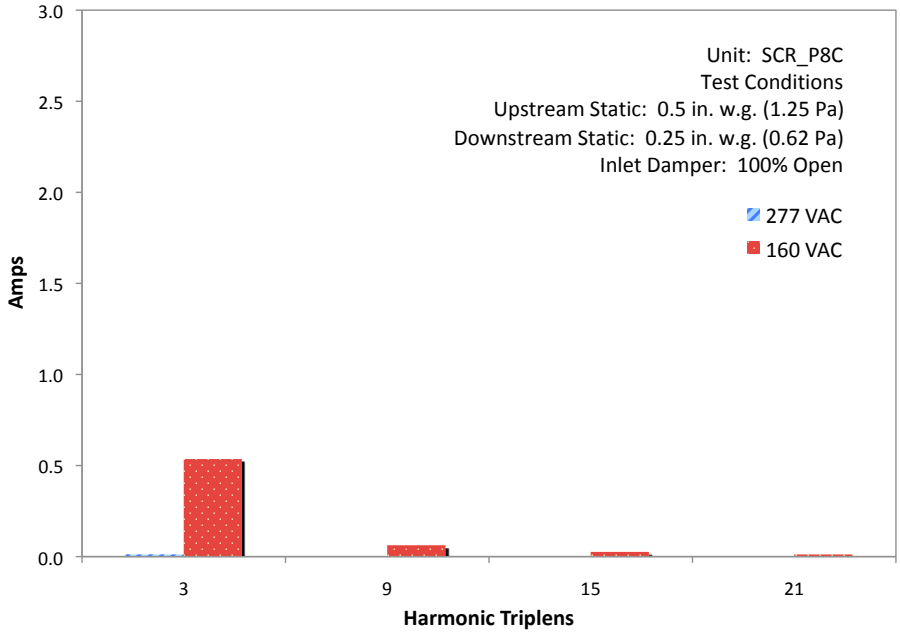

Figure 6-24: SCR parallel triplen current harmonics

Figures 6-25 and 6-26 present the voltage harmonics for the same typical test condition of 0.5 in. w.g. (125 Pa) of upstream static pressure and 0.25 in. w.g. (62 Pa) downstream static. The voltage harmonics were much closer in magnitude than the current harmonics and represented only a small fraction of the 277 VAC supply voltage.

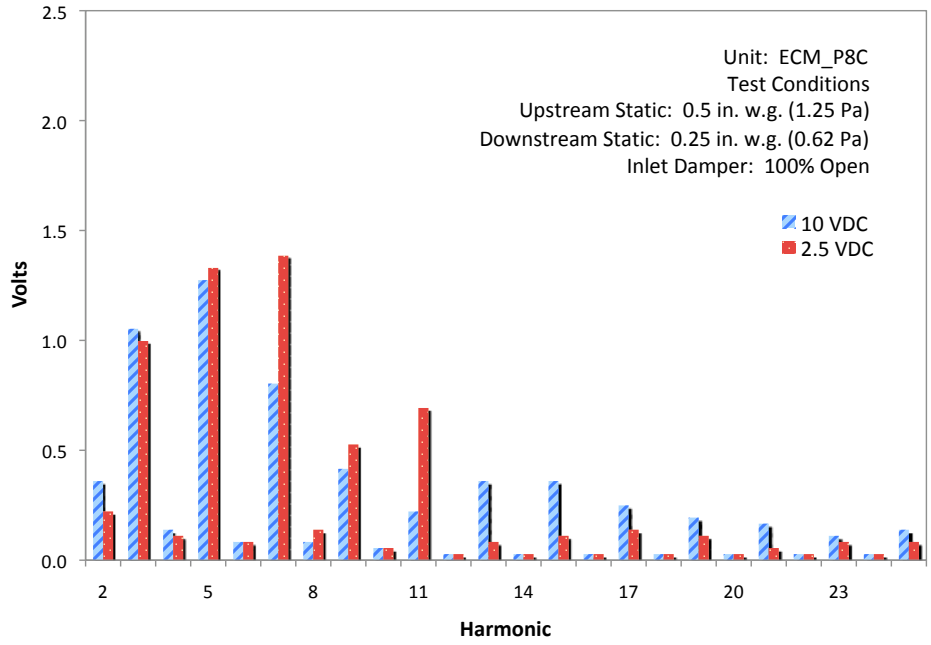

Figure 6-25: ECM parallel voltage harmonics

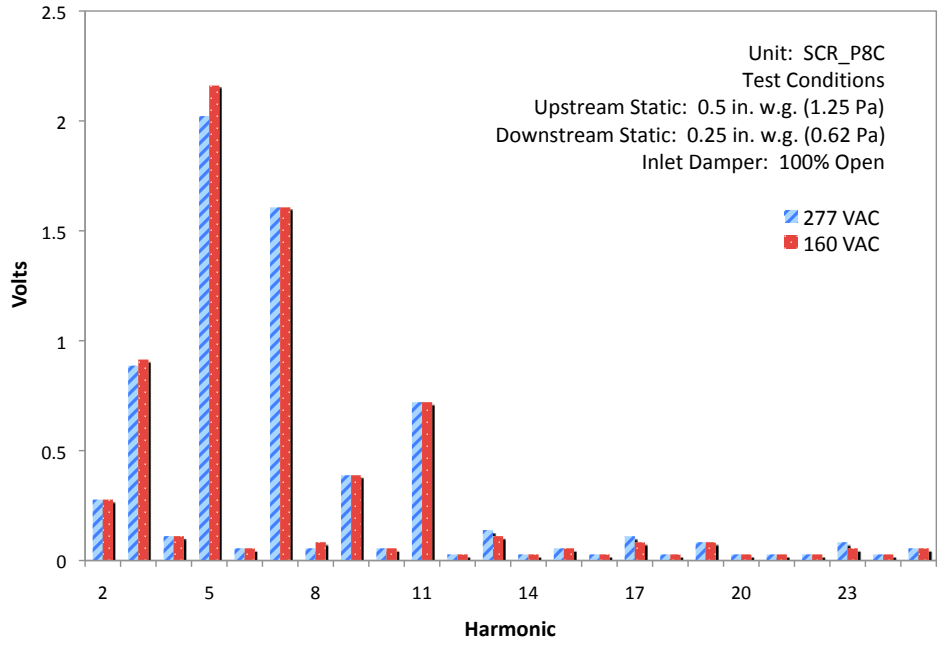

Figure 6-26: SCR parallel voltage harmonics

Figures 6-27 and 6-28 present the respective control's real power harmonics under the same upstream and downstream conditions. Similar to the voltage harmonics, the watt harmonics were relatively small in magnitude and represented only a small fraction of the real power consumed. The negative harmonic values were attributed to that part of the cycle where energy is actually transferred from the inductor (load) back into the voltage source.

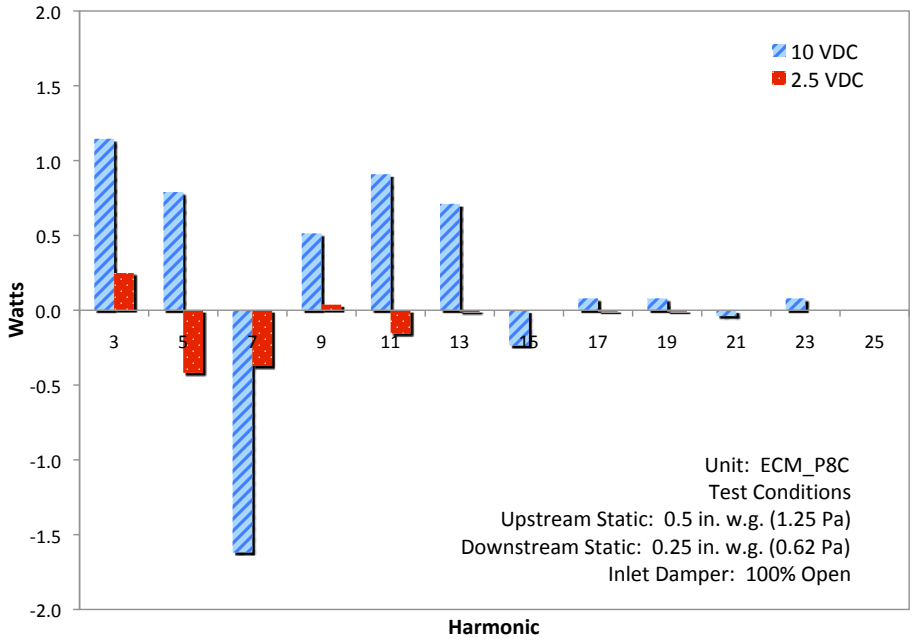

Figure 6-27: ECM parallel real power harmonics

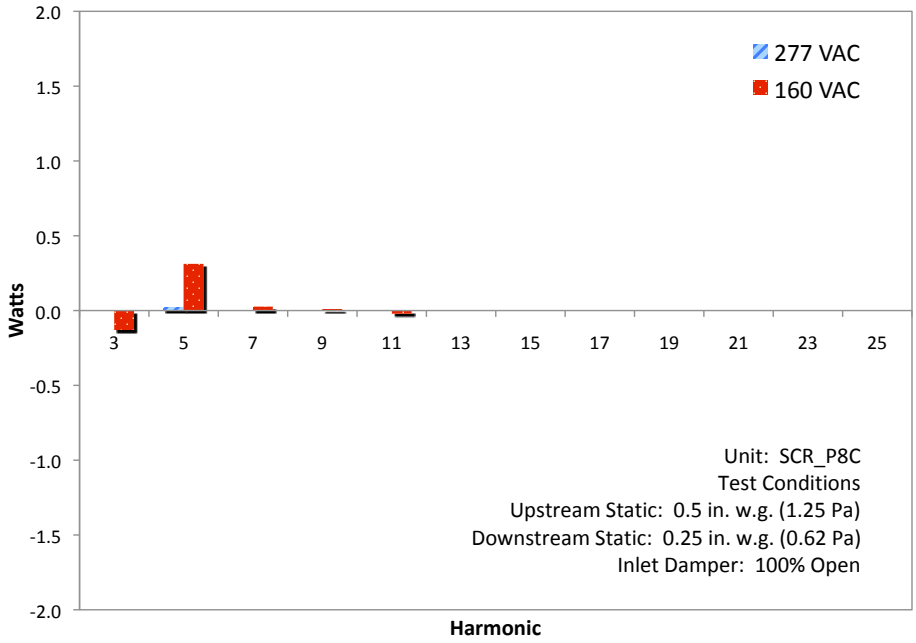

Figure 6-28: SCR parallel real power harmonics

For both ECM and SCR control, current, voltage and real power harmonics (as a percentage) grew with reduced control voltage (see Appendix B). This was especially true for the SCR. Harmonics represent distortion and the AC motor achieves variable operational speed by distorting the ideal VAC input sine wave. However, at full 277 VAC SCR control, the harmonics became almost negligible due to the SCR not performing any significant work. The ECM control however, utilized a DC motor which required significant work throughout the operation window. However, as input voltage increased, so did the nominal amperage. Thus, in the case of the ECM controlled units, total harmonic distortion was greater at higher fan airflow.

Observing harmonic frequencies required looking at a set of values, rather than a singular variable. Thus they could be difficult to analyze en masse. Total harmonic distortion (THD) was a convenient cumulative value to plot and analyze. THD, as defined in Eq. (1.3), was the ratio of harmonic frequencies over the fundamental 60Hz frequency. Power THD is a common value used in industry and is most widely used in it's percentage form.

Figures 6-29 and 6-30 present both ECM and SCR control's real power THD over the their respective control input ranges. Similar to power factor the SCR displayed an advantage as fan speed was increased via input voltage. The SCR approached 0% total harmonic distortion while the ECM controlled FPTU never dropped below 0.5%. For current and voltage THD data, see Appendix B.

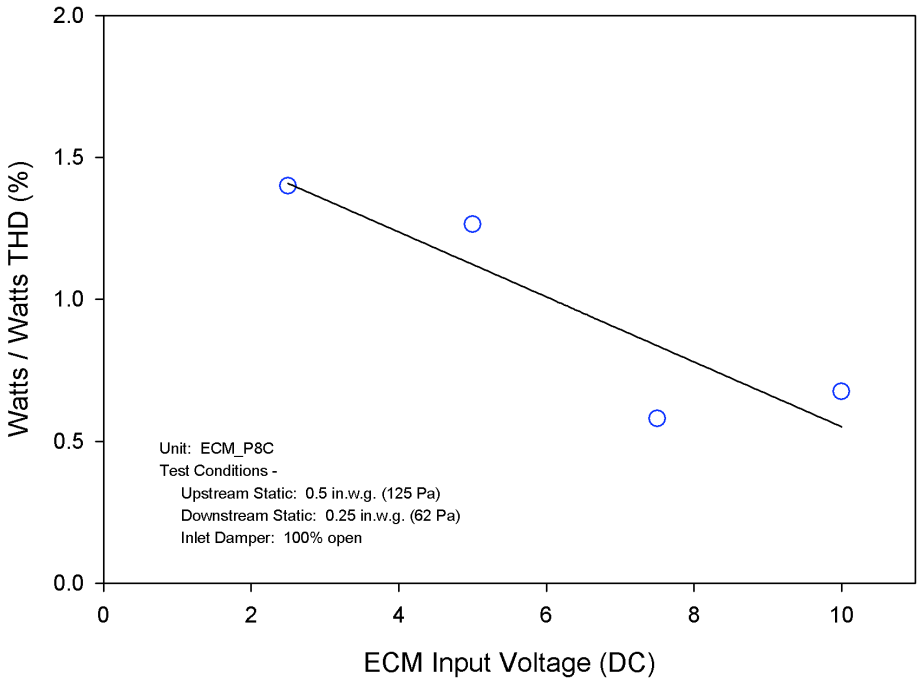

Figure 6-29: Real power THD for ECM series terminal units

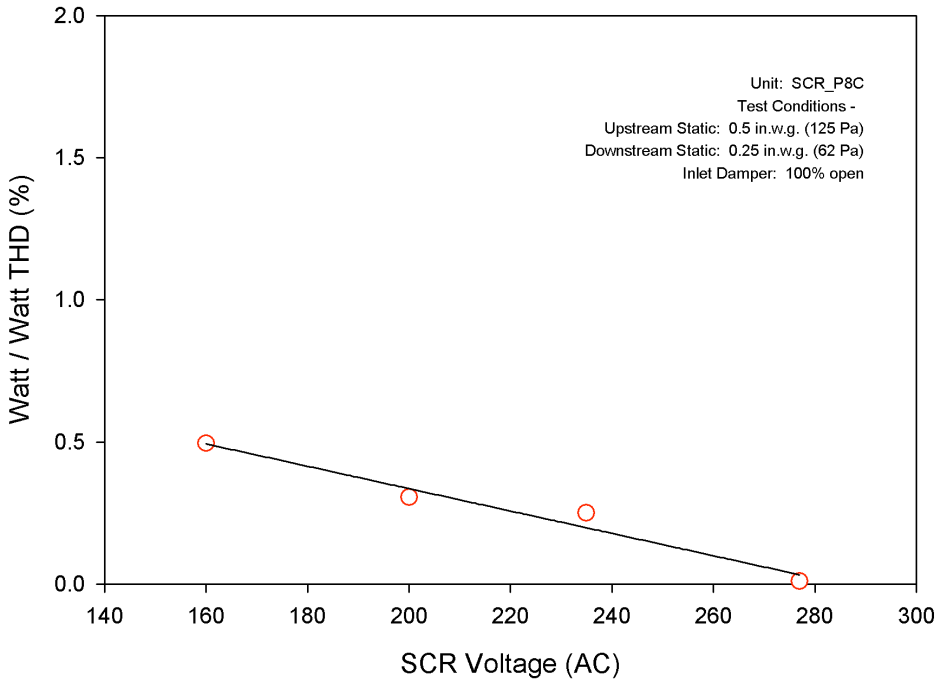

Figure 6-30: Real power THD for SCR series terminal units

CHAPTER VII

SUMMARY AND CONCLUSIONS

Variable air volume terminal units are a historically proven, effective solution for air distribution systems of commercial buildings. Fan powered terminal units can be configured in either a series or parallel design. Series FPTUs require that the internal fan be in continual operation, which means that induced air is always present. However, Parallel FPTUs have the ability to go into a condition known as "full cool" where the fan is turned off and there is no additional induced air added to the upstream primary air stream.

Traditionally fan powered terminal units include AC induction fan motors controlled by silicon rectified controllers (SCR). However, VAV terminals can also be equipped with high efficiency brushless DC motors controlled by electronically commutated motor (ECM) controls. The ECM combination allows for much higher efficiency at lower fan speed, lower acoustical noise and programable application-specific control.

The purpose of this research was to create performance models for both airflow and power consumption of ECM equipped variable air volume series and parallel fan powered terminal units. Empirical models were borrowed from previous research (Furr et al. 2007) and modified as need. However, an attempt was made to quantify the ECM control in a way that it could be compared with that of SCR controlled terminal units. Additionally power quality variables such as: power factor, harmonics and total harmonic distortion were obtained and presented for both ECM and SCR applications.

An experimental setup and test procedure were created in order to test the terminal units at typical design pressures and airflows. Each terminal unit observed in this study used an 8 in (20.3 cm) primary air inlet. Data were collected for fan power and airflow as a function of several independent variables: the upstream and downstream static pressures, the controller input value, the position of the primary airflow damper, and the amount of primary airflow as measured by an inlet air velocity pressure. The models were derived from the experimental data. The statistical analysis yielded a single expression for each performance variable where terminal units were distinguished by unique coefficients.

Three models were employed for the series terminal units. The first empirical model characterized the airflow of the terminal fan, which also expresses the entire FPTUs downstream supply airflow. The R^2 statistics indicated that the model coefficients could accommodate 99.7% of the variation for both ECM and SCR controlled terminal units. The second model was for primary airflow into the FPTU. A function independent of fan voltage, the R^2 value was 97.7% for ECM control and 92% for SCR controlled units. The power consumption model used coefficients producing an R^2 statistic accounting for 99.8% of ECM data and 99.4% of SCR data.

Real power consumption for the series ECM controlled FPTU outperformed the SCR counterpoint for nearly all test conditions. With static upstream and downstream pressure set to 0.25 in. w.g. (62 Pa) the ECM terminal unit provided a 66% power consumption (watts) advantage at 800 cfm (0.377 m^3/s) and a 37.5% advantage at 1200 cfm (0.57 m^3/s). However, in addition to real power consumption, power quality was also observed. At the same test conditions, but considering apparent power, the ECM controller only had a 52% advantage at 800 cfm and actually required 50% more volt-amps at 1200 cfm. It was quite clear that the SCR had a power factor advantage which was quite pronounced at maximum input levels. It is at low fan speed where the ECM controller truly excels.

However, at low fan speed is where total harmonic distortion is at its highest. In regards to harmonic distortion, the ECM is clearly the largest offender. Although maintaining values below 2% THD, the best ECM distortion value (found at maximum fan speed) could not exceed the worst SCR distortion (found at minimum fan speed).

Four models were developed for the parallel VAV terminal units. Unique to the parallel construction due to its pressurized static FPTU chamber pressure was a leakage model. This model characterized the leakage found along the seams of the sheet-metal construction as well as any leakage that may occur along the parallel fan's backdraft damper. This model was derived for conditions where the internal fan was turned off. The R^2 value for the leakage model indicated that 92% of the variance was accounted for both ECM and SCR controlled units. The primary influence on leakage was downstream static pressure, which was used in the model because it best approximated the internal chamber pressure of the FPTU. As downstream static increased, so did leakage.

Like the series analysis, the parallel FPTU also included fan airflow, primary airflow and power consumption models. The R^2 value associated with the fan airflow coefficients explained 99% of the variance for both ECM and SCR control. Primary airflow coefficients yielded an R^2 value approximately 98% for both ECM and SCR controlled units. Lastly for the real power consumption model, all parallel units analyzed achieved an R^2 value of 99%.

The power quality analysis of the parallel terminal units further strengthened the argument that SCR control provides less distortion to the power grid, especially at high fan speed. Using typical pressure set points of 0.5 in. w.g. (125 Pa) upstream static pressure and 0.25 in. w.g. (62 Pa) downstream static pressure the ECM control only demonstrated an advantage at mid-operation. At 500 cfm (0.236 m^3/s) airflow, the ECM control presented a 29% power consumption advantage versus SCR. However, at this condition it required 3% more volt-amps of apparent power. At the control approached maximum fan speed the advantage completely went to the SCR controlled unit. At 1000 cfm (0.472 m^3/s) of fan airflow the ECM had a 15% disadvantage in real power consumption and a 127% disadvantage in apparent power. Power factor and total harmonic distortion also displayed similar trends to that of the series model, which is to say the SCR model enjoyed less distortion at all speeds but particularly at maximum fan speed conditions.

Where as the SCR control is directly proportional to fan speed, the ECM control's programmable calibration creates an unknown variable when performing research such as this. The power consumption and power quality of the ECM motor combination appears to be heavily dependent on the unique programming of the unit in question. The series and parallel ECM terminal unit contain a nearly identical controller and motor combination, however, their calibration curves are completely unique. As such, they enjoy different benefits and suffer different consequences in the operational range.

Future research is necessary to properly encapsulate ECM behavior. While there may be an infinite number of programmable calibration curves, adequate modeling should include a variable dictating whether the input-CFM calibration is 1st order, 2nd order or in the case of the parallel unit tested, 3rd order. Although the R^2 values obtained in this research are quite high, they are only valid for the particular units and combinations tested. The inclusion of generic calibration variables would allow a more comprehensive and applicable simulation model.

Additional research is also required for the parallel leakage model. The model used in this study is only valid during "full cool" mode but should be incorporated into all periods of fan operation. That said, the airflow models currently used do enjoy a high R^2 value without the inclusion of the leakage term at all. However, integration of the leakage model may well prove advantageous when modeling the entire air distribution system as a whole.

REFERENCES

AMCA. 1999. *ANSI/AMCA Standard 210-99. Laboratory Methods of Testing Fans for Aerodynamic Performance Rating*. Arlington Heights, IL: Air Movement and Control Association

Alexander, J. and D. Int-Hout. 1998. Assuring zone IAQ. White paper. http://www.titus-hvac.com/tech_papers.asp.

Ardehali, M.M. and T.F. Smith. 1996. Evaluation of variable volume and temperature HVAC system for commercial and residential buildings. *Energy Conversion Management* 37(9): 1469-1479.

ASHRAE. 1999. *ANSI/ASHRAE Standard 120-1999, Method of Testing to Determine Flow Resistance of HVAC Ducts and Fittings*. Atlanta: American Society of Heating, Refrigerating and Air-Conditioning Engineers, Inc.

ASHRAE. 2001. *2001 ASHRAE Handbook-Fundamentals*. Atlanta: American Society of Heating, Refrigerating and Air-Conditioning Engineers, Inc.

ASHRAE. 2004. *ANSI/ASHRAE Standard 90.1-2004, Energy Standard for Buildings Except Low-Rise Residential Buildings*. Atlanta: American Society of Heating, Refrigerating and Air-Conditioning Engineers, Inc.

ASHRAE. 2006. *ANSI/ASHRAE Standard 130-1996 (RA 2006), Methods of Testing for Rating Ducted Air Terminal Units*. Atlanta: American Society of Heating, Refrigerating and Air-Conditioning Engineers, Inc.

BLAST Support Office. 1992. *BLAST 3.0 Users Manual*. Urbana- Champaign, Illinois: BLAST Support Office, Department of Mechanical and Industrial Engineering, University of Illinois, Urbana-Champaign.

Chen, S.Y.S., and S.J. Demster. 1996. *Variable Air Volume Systems for Environmental Quality*. New York: McGraw-Hill.

Crawley, D., Lawrie, L., Peterson, C. and Winkelmann, F. 2000. EnergyPlus: Energy Simulation Program. *ASHRAE Online Journal* 42(4): 49-56.

DOE-2. 1998. *DOE-2 Users Manual, Version 2.2*. Lawrence Berkeley National Laboratory, Berkeley, CA.

Elleson, J.S. 1993. Energy use of fan-powered mixing boxes with cold air distribution. *ASHRAE Transactions* 99(1):1349-1358.

EnergyIdeas Clearinghouse. 2003. *Reducing Power Factor Cost*. Washington State University Cooperative Extension Energy Program and Northwest Energy Efficieny Alliance. WSUCEEP02_140.

Engdahl, F. and Johannson, D. 2003. *Optimal Supply Air Temperature with Respect to Energy Use in a Variable Air Volume System*. Lund University. Lund, Sweden.

Furr, J. 2006. Development of models for series and parallel fan variable air volume terminal units. M.S. Thesis, Texas A&M University, College Station.

Furr, J, O'Neal, D., Davis, M., Bryant, J., Cramlet, A. 2007. *ASHRAE Project 1292-RP, Phase I Final Report*. Energy Systems Laboratory, Texas A&M University, College Station, TX.

GE. 2000. Presenting the GE ECM 2.3 Series Motor. GET-8068 GE Industrial Systems. Markham, ON, Canada.

Gosbell, V. J. 2000. Technical Note No.3. *Power Quality Centre*. University of Wollongong, NSW Australia.

HASP/ACLD. 1971. Perimeter Annual Load for Air Conditioning. *HASP/ACLD 7101*. Japan Building Mechanical Engineers Association.

Hydeman, M., Taylor, S., and Stein, J. 2003. *Advanced Variable Air Volume System Design Guide*. *Integrated Energy Systems: Productivity and Building Science*. San Francisco: CA: Energy Commission.

Inoue, U. and T. Matsumoto. 1979. A study on energy savings with variable air volume systems by simulation and field measurement. *Energy and Buildings* 2:27-36.

Johnson, G. A., 1984. Variable air volume implementation. *ASHRAE Transactions*. 90(2B), 201.

Kennedy, B. W. 2000. *Power Quality Primer*. Dubuque, IA. McGraw-Hill Professional.

Khoo, I., G.J. Levermore, and K.M. Letherman. 1998. Variable-air-volume terminal units I: steady state models. *Building Services Engineering Research & Technology* 19(3): 155-162.

Kolderup, E., Hong, T., Hydeman, M., Taylor, S., and Stein, J. 2003. *Integrated energy systems: productivity and building science*. San Francisco: California Energy Commission, San Francisco, CA

Kreider, J., Curtiss, P., and Rabl, A. 2002. *Heating and Cooling of Buildings*. Dubuque, IA. McGraw-Hill.

Microsoft. 1998. *Microsoft Visual Studio 6*. Microsoft, Redmond, CA

Montgomery, D.C., E.A. Peck, G.G. Vining. 2001. *Introduction to Linear Regression Analysis*. 3rd Ed. New York: John Wiley & Sons, Inc.

Nailor Industries. 2003. *The ECM Motor Story*. Nailor Industries Inc. Houston, TX.

Sankaran, C. 2002. *Power Quality*. Boca Raton, FL. CRC Press LLC.

Sekhar, S.C. 1997. A critical evaluation of variable air volume system in hot and humid climates. *Energy and Buildings* 26: 223-232.

SEEP. 2006. Energy Efficiency Measures. *Southwest Energy Efficiency Project* http://www.utahefficiencyguide.com/measures/commercial/hvac.htm

SPSS. 2008. *SPSS for Windows 15*. *SPSS 16 for Macintosh*. SPSS Inc., Chicago, IL.

TRACE 600: Load Design and Economics Simulation Program. 1993. La Cross, WI: The Trane Company, American Standard Company.

U.S. Department of Energy. 1982. *DOE-2 Engineers Manual, v 2.1A*. Washington, DC. U.S Department of Energy.

Wendes, H. 1994. *Variable Air Volume Manual*. Lilburn, GA: The Fairmont Press, Inc.

APPENDIX A

SERIES DATA

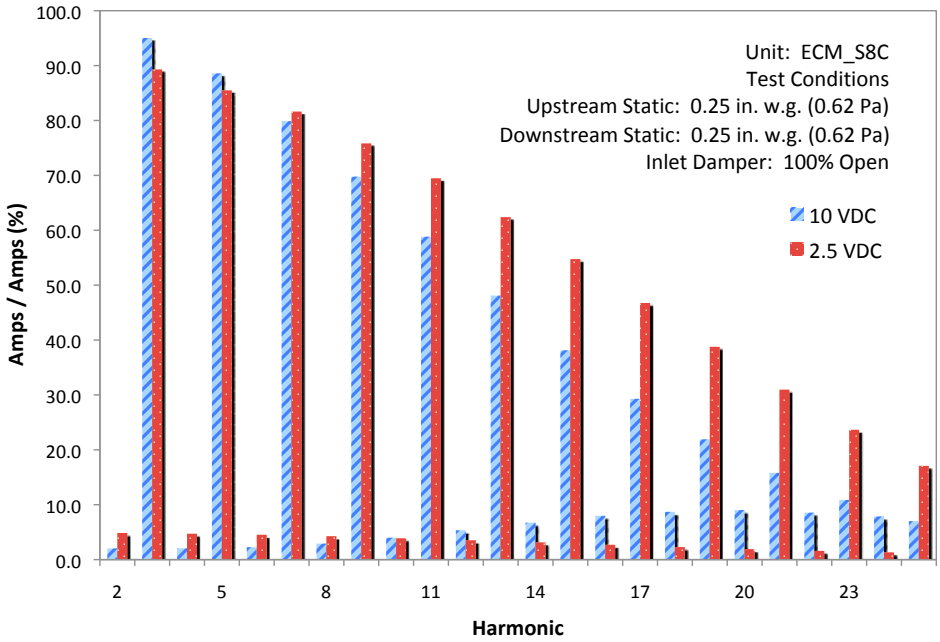

Figure A-1: ECM series percent current harmonics

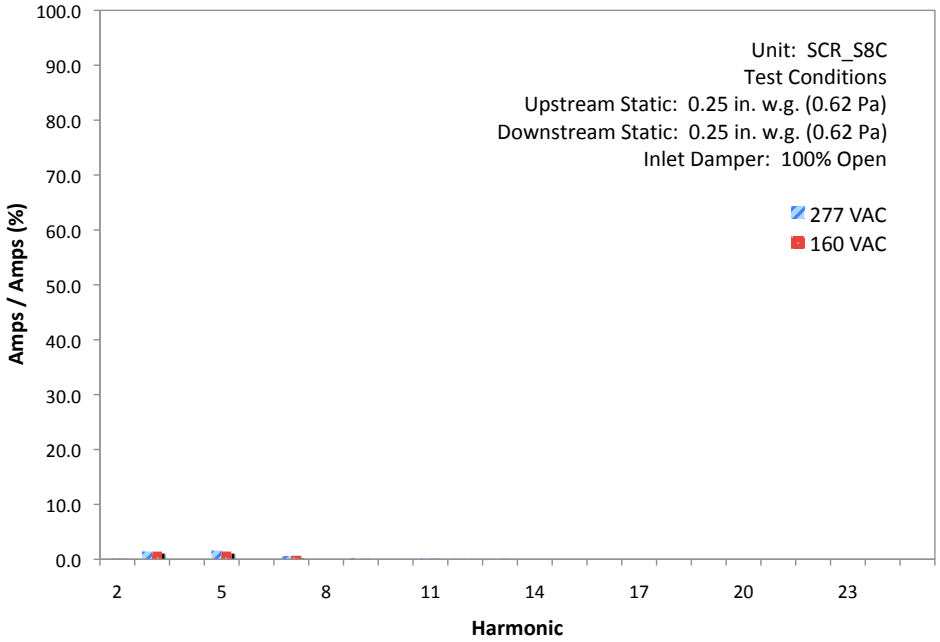

Figure A-2: SCR series percent current harmonics

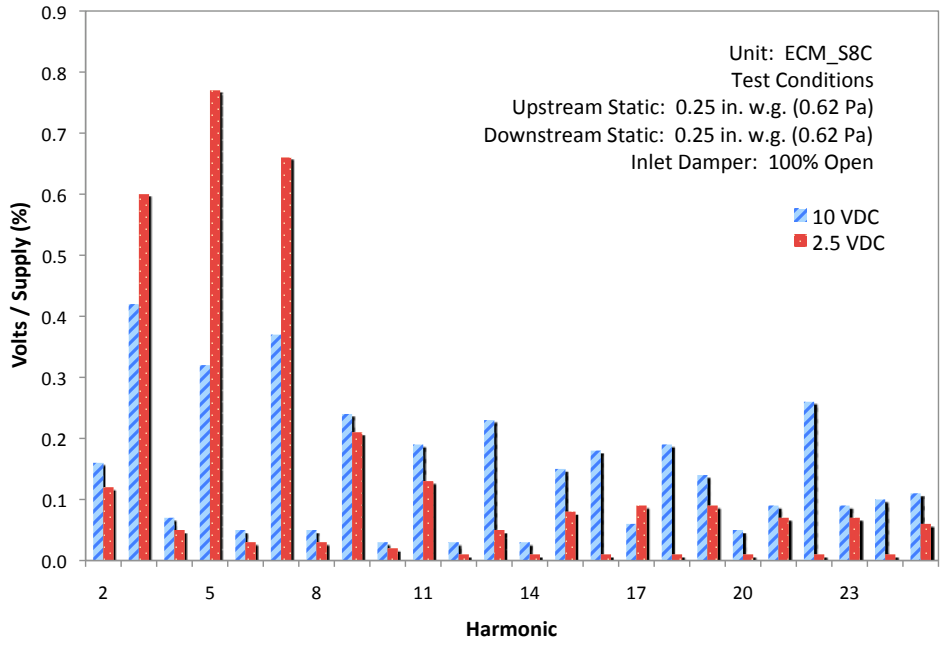

Figure A-3: ECM series percent voltage harmonics

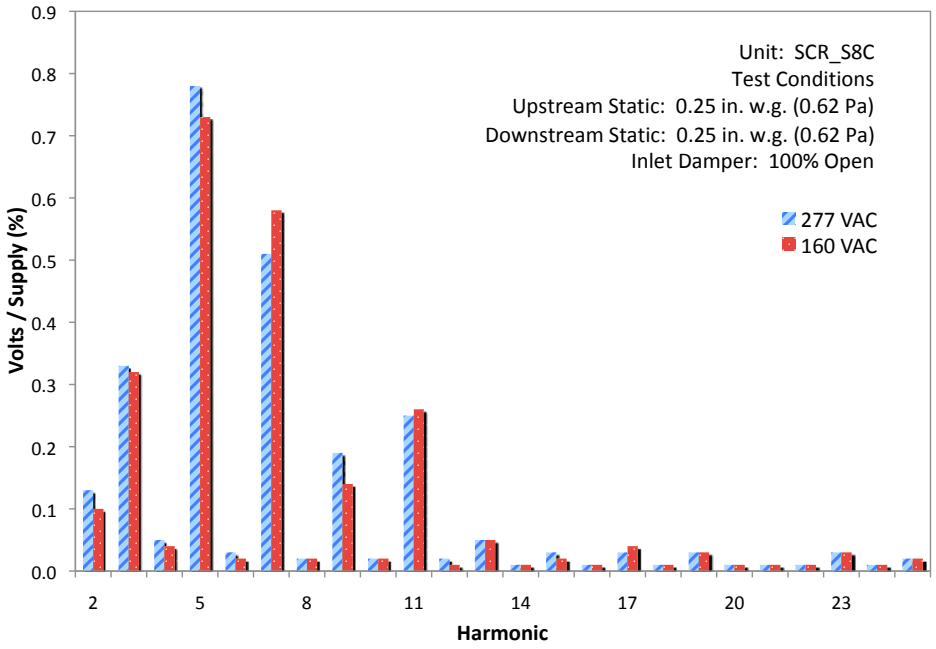

Figure A-4: SCR series percent voltage harmonics

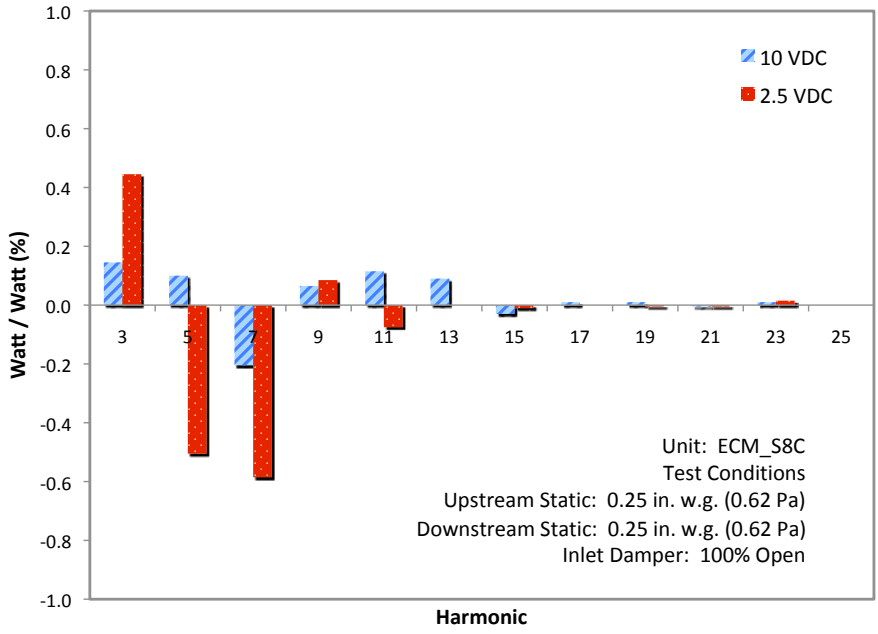

Figure A-5: ECM series percent real power harmonics

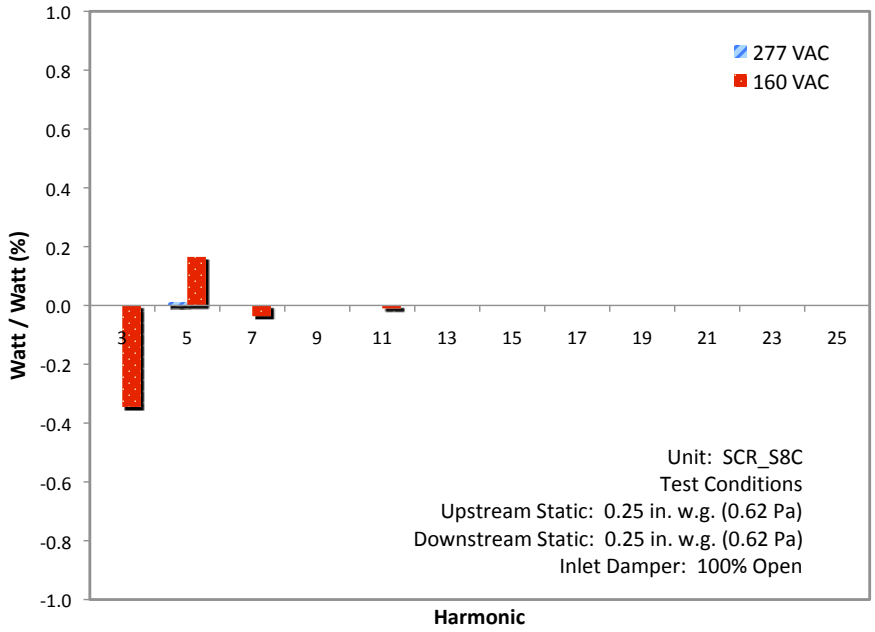

Figure A-6: SCR series percent real power harmonics

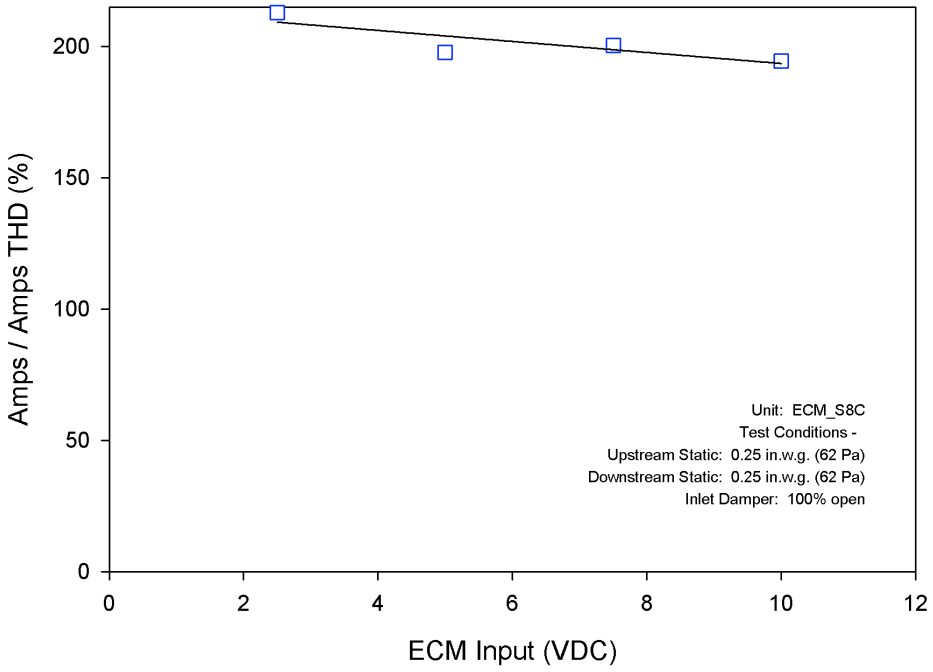

Figure A-7: Current THD for ECM series terminal units

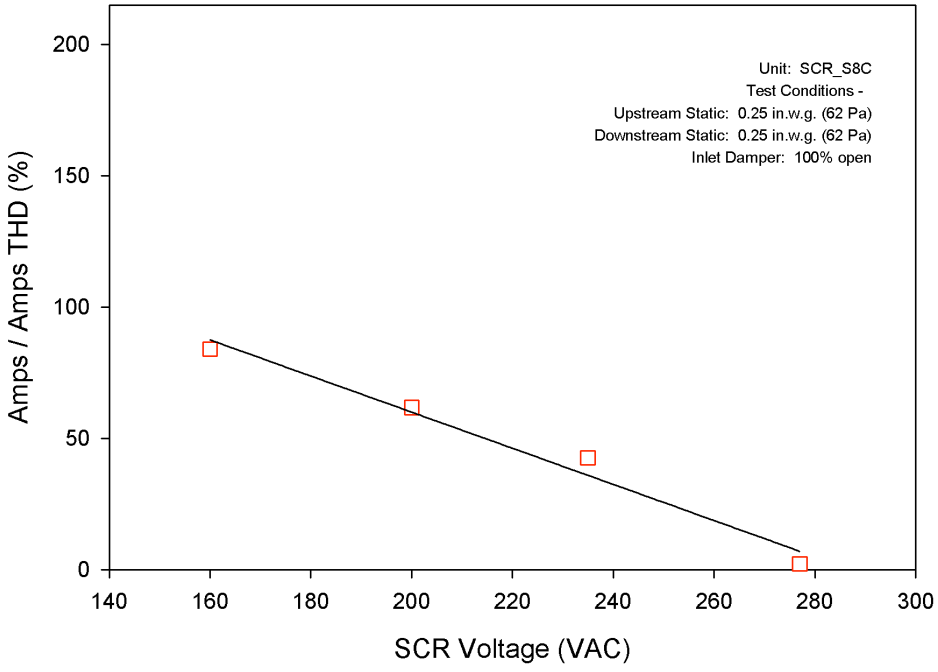

Figure A-8: Current THD for SCR series terminal units

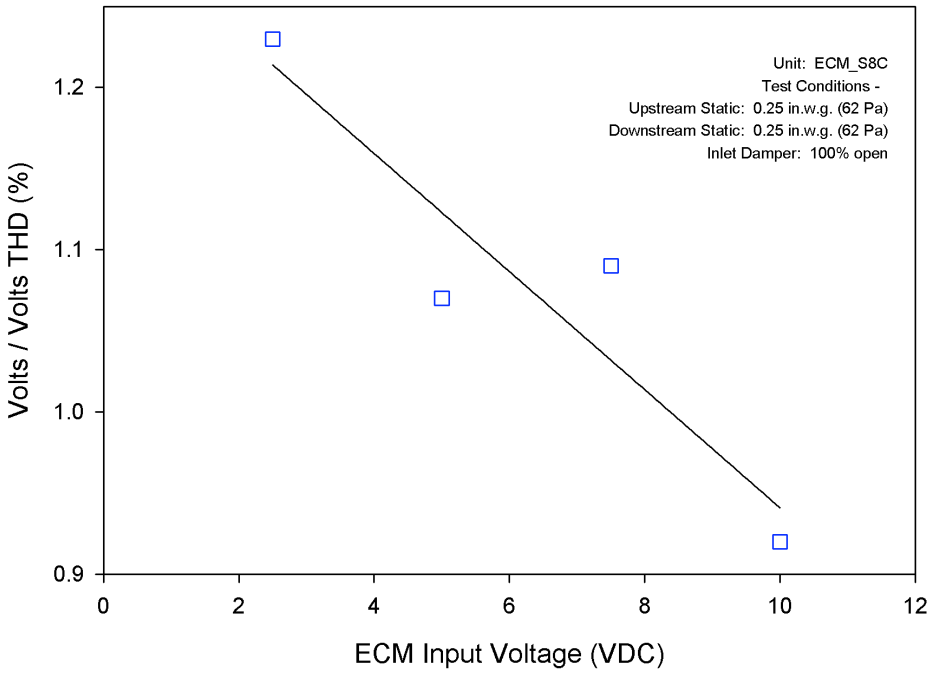

Figure A-9: Voltage THD for ECM series terminal units

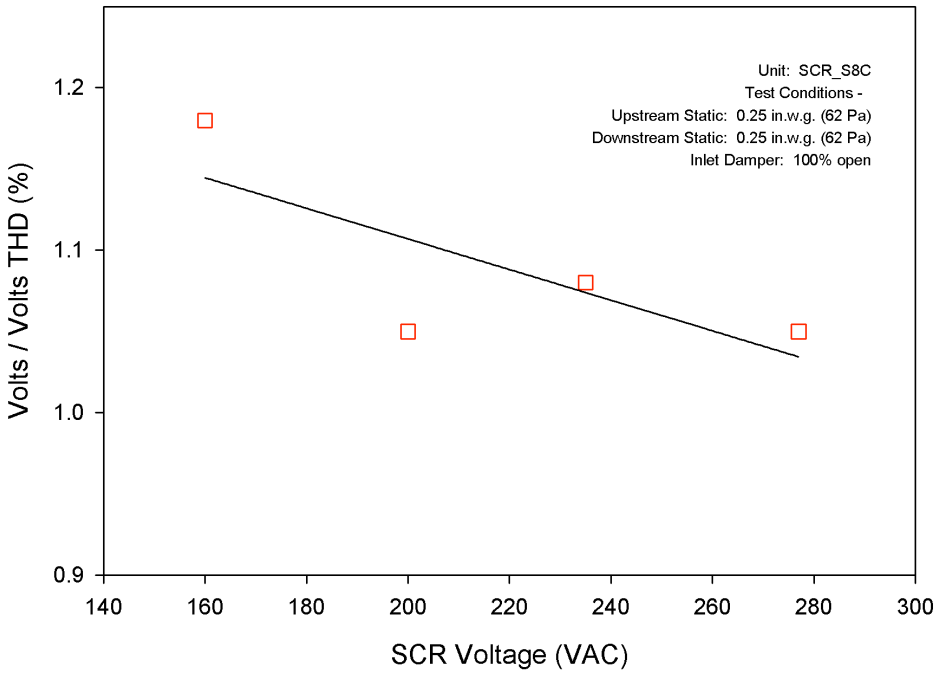

Figure A-10: Voltage THD for SCR series terminal units

APPENDIX B

PARALLEL DATA

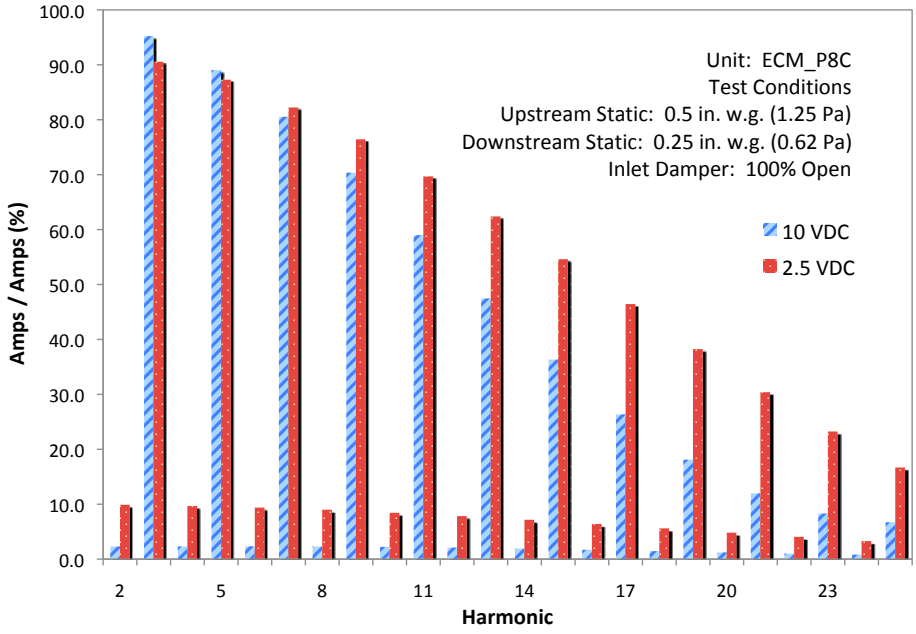

Figure B-1: ECM parallel percent current harmonics

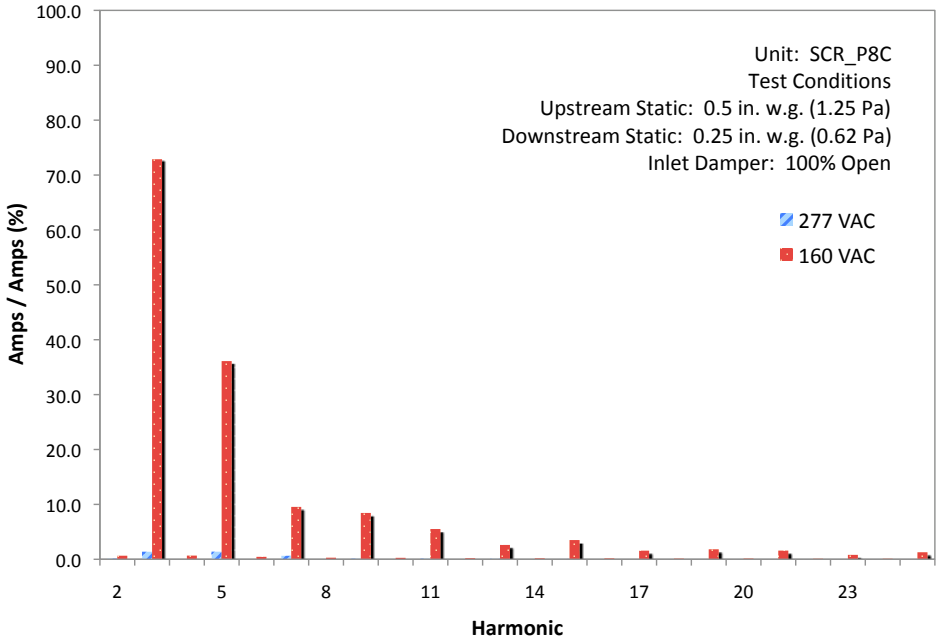

Figure B-2: SCR parallel percent current harmonics

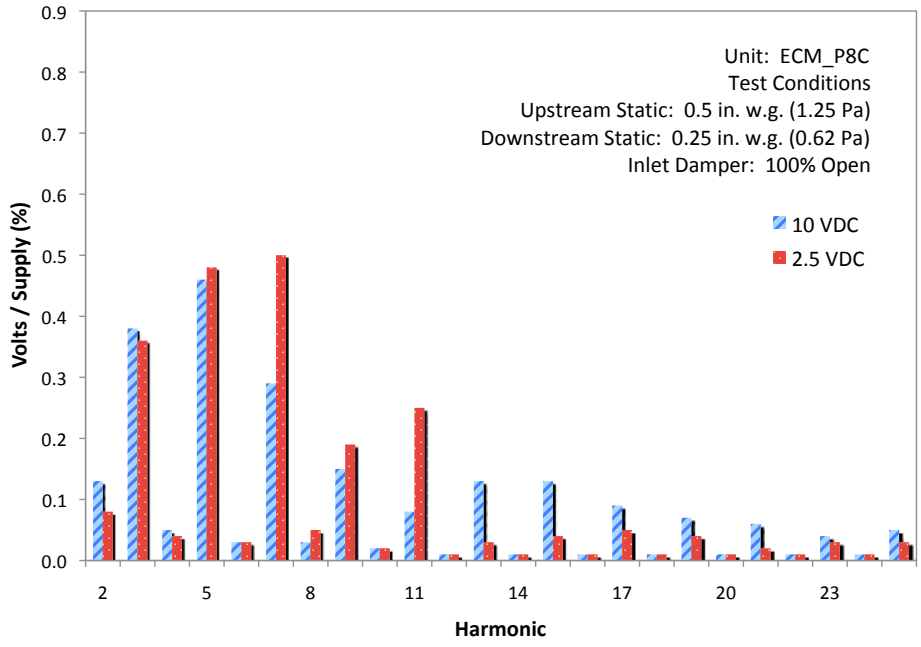

Figure B-3: ECM parallel percent voltage harmonics

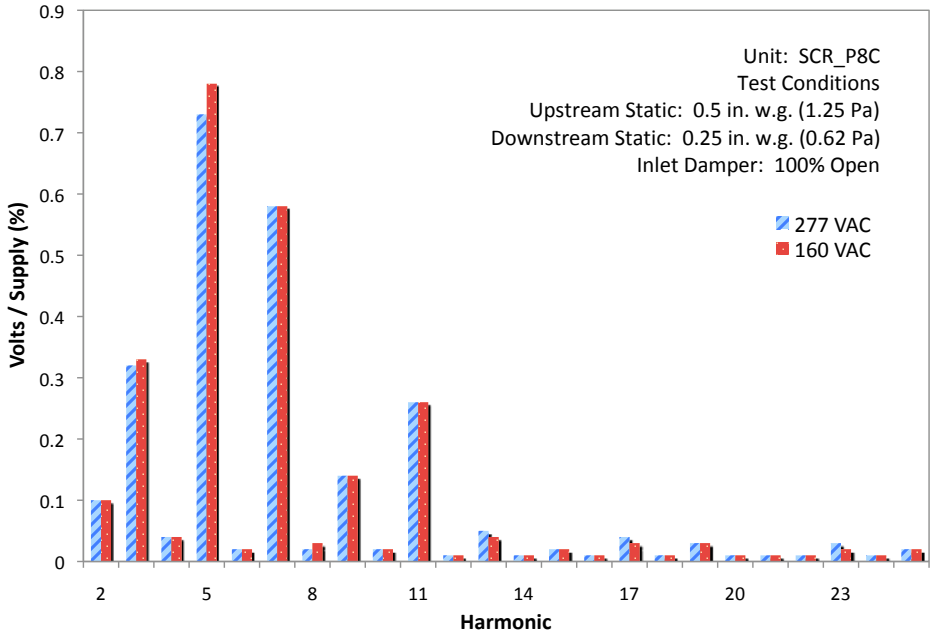

Figure B-4: SCR parallel percent voltage harmonics

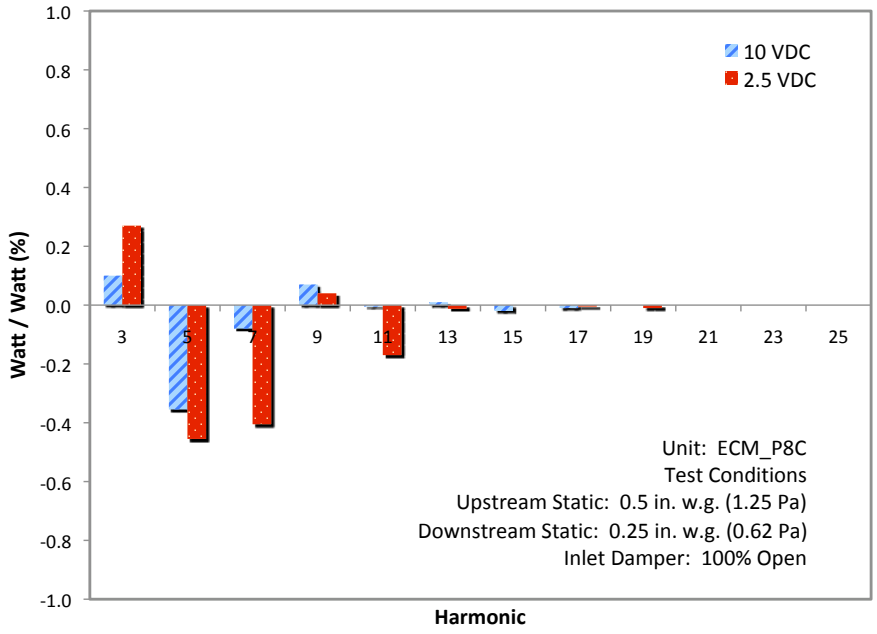

Figure B-5: ECM parallel percent real power harmonics

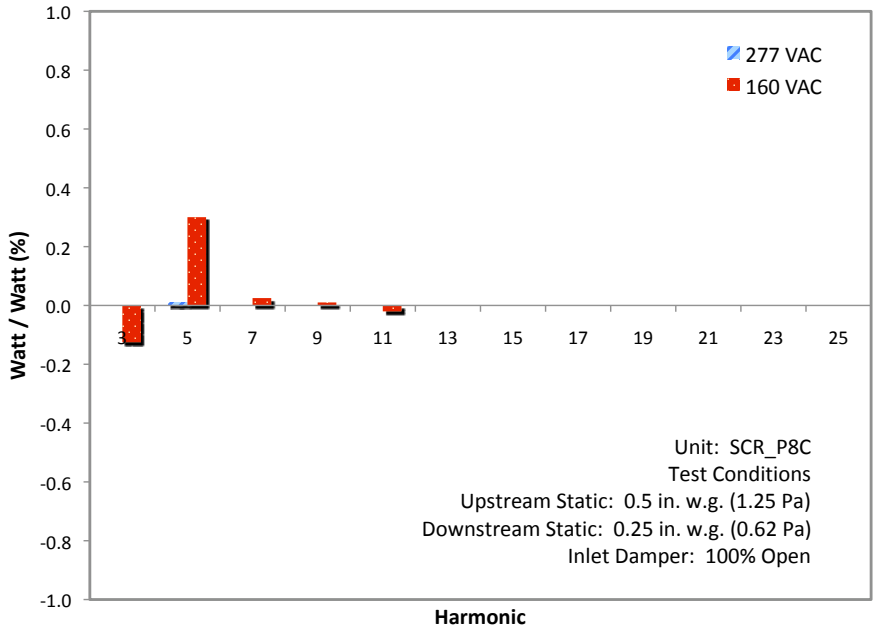

Figure B-6: SCR parallel percent real power harmonics

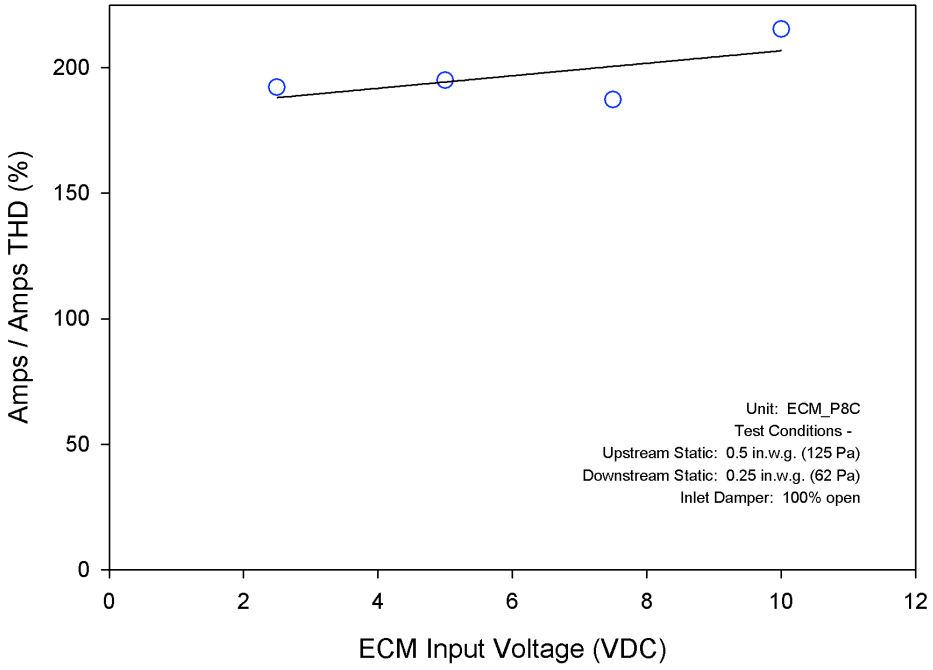

Figure B-7: Current THD for ECM parallel terminal units

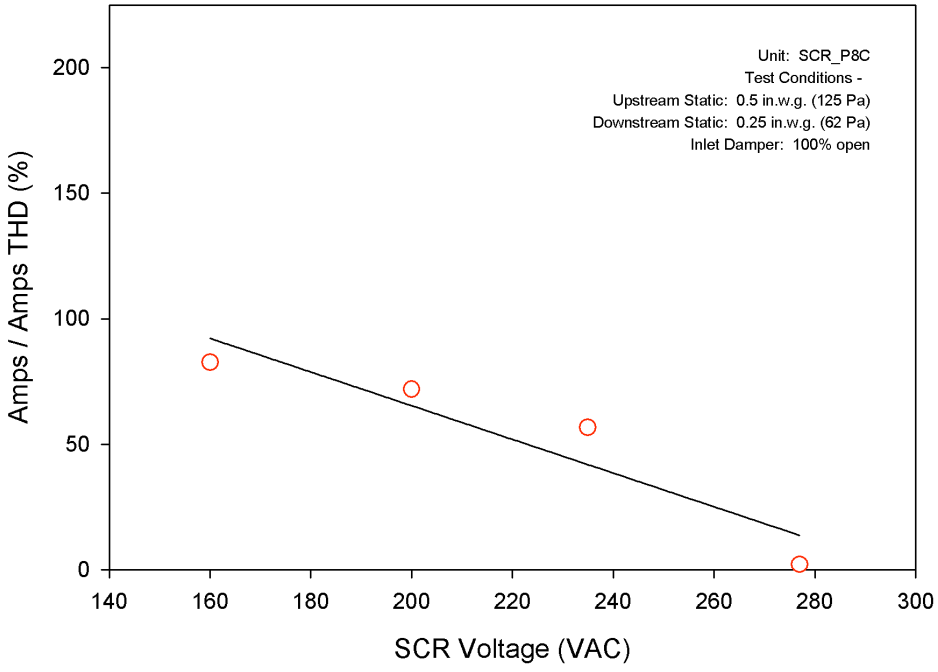

Figure B-8: Current THD for SCR parallel terminal units

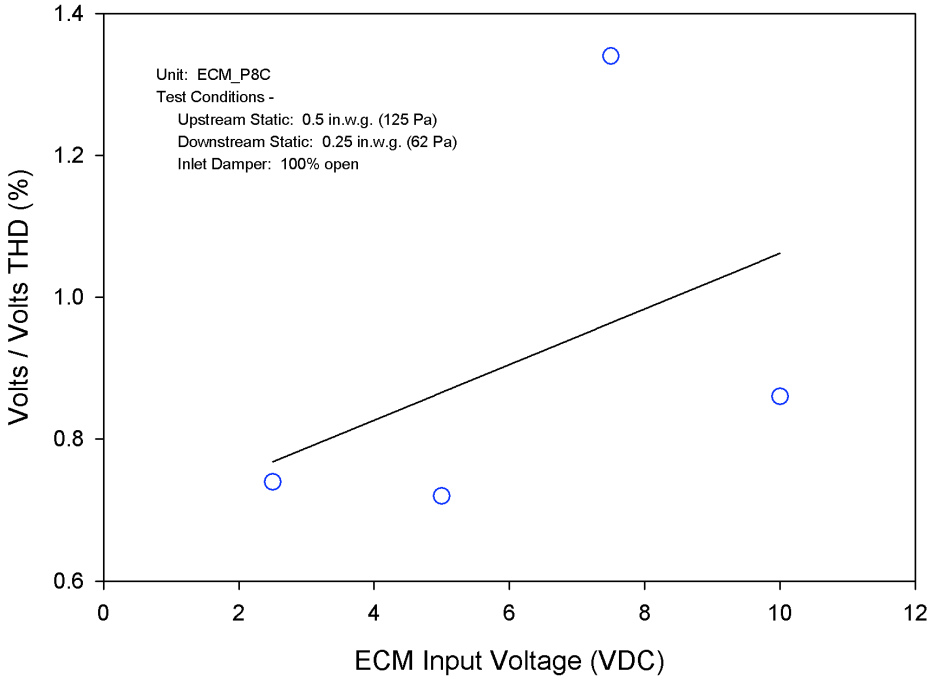

Figure B-9: Voltage THD for ECM parallel terminal units

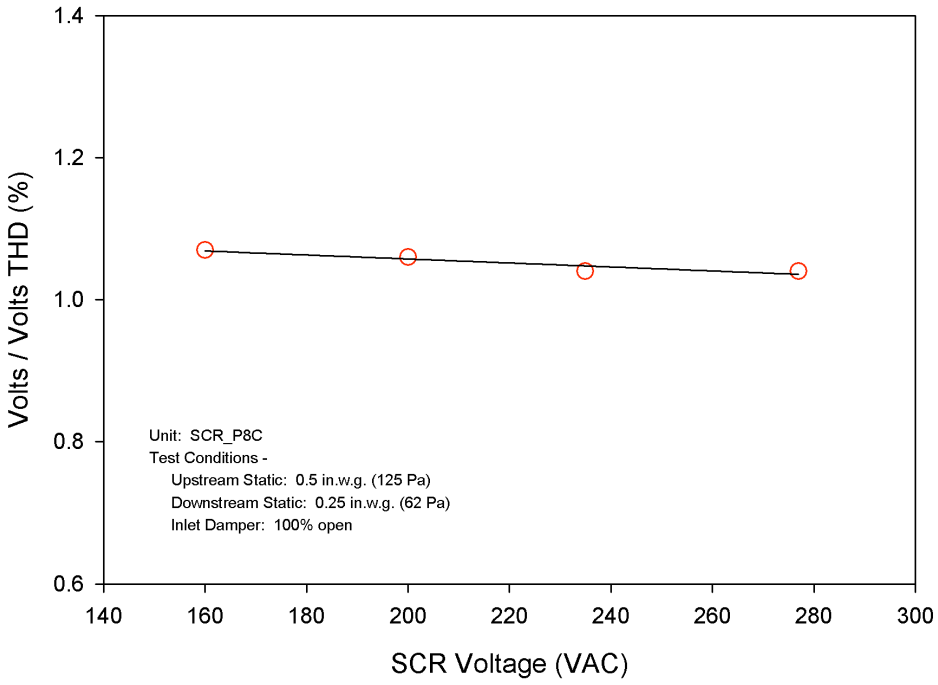

Figure B-10: Voltage THD for SCR parallel terminal units

APPENDIX C

EXPERIMENTAL APPARATUS

The "AMCA Figure 15" and "AMCA Figure 12" airflow chambers were connected directly together, without the fan powered terminal unit, in order to test the accuracy of the chambers against each other. The results of this test are presented in Table C-1.

Table C-1: AMCA flow chamber calibration

Test Point	**AMCA Figure 15** CFM (m^3/s)	**AMCA Figure 12** CFM (m^3/s)	**Difference** CFM (m^3/s)	**Percent Difference** (%)
1	270 (0.127)	280 (0.132)	-10 (-0.005)	-3.70 (-3.94)
2	499 (0.235)	484 (0.228)	15 (0.007)	3.01 (2.98)
3	747 (0.353)	722 (0.341)	25 (0.012)	3.35 (3.40)
4	1093 (0.516)	1090 (0.514)	3 (0.002)	0.27 (0.37)
5	1306 (0.616)	1304 (0.615)	2 (0.001)	0.15 (0.16)
6	1473 (0.695)	1474 (0.696)	-1 (-0.001)	-0.07 (-0.14)
7	1740 (0.822)	1745 (0.824)	-5 (-0.002)	-0.29 (-0.24)
8	1951 (0.921)	1950 (0.920)	1 (0.001)	0.05 (0.11)
9	2477 (1.169)	2474 (1.168)	3 (0.001)	0.12 (0.08)

The Fluke 435 Power Quality Analyzer was used for electrical data acquisition. The "Default 4" data logger preset was used from Table C-2 to simultaneously acquire the variables listed.

Table C-2: Fluke 435 variable list

Default 1 **Volt**	**Default 2** **Volt & Amp**	**Default 3** **Volt & Amp & Power**	**Default 4** **Volt & Amp & Power & Harm.**	**Default 5** **Monitor Readings**
V rms	V rms	V rms	V rms	V rms
V pk	V pk	V pk	V pk	A rms
CF Volt	CF Volt	CF Volt	CF Volt	THD
V ½ cycle	V ½ cycle	V ½ cycle	V ½ cycle	H1 ... H25
Frequency	A rms	A rms	A rms	Plt
	A pk	A pk	A pk	V ½ cycle
	CF Amp	CF Amp	CF Amp	A ½ cycle
	A ½ cycle	A ½ cycle	A ½ cycle	Unbalance
	Frequency	Watt	Watt	V3s signal 1
		VA	VA	V3s signal 2
		VAR	VAR	Frequency 10s
		PF	PF	
		DPF/cos φ	DPF/cos φ	
		Frequency	V H1 ... H25	
			A H1 ... H25	
			W H1 ... H25	
			K-factor A	
			K-factor W	
			THD V	
			THD A	
			THD W	
			Plt	
			Pst	

The damper actuator used to control the various FPTU inlet air dampers had the following linear calibration between input voltage and rotational position (Table C-3). The usage variables “S” and “P” represent the respective series and parallel FPTUs.

Table C-3: Damper actuator calibration

Input Voltage	**Angle**	**Usage**
0.00	0º	S/P
1.25	11.25º	S
2.50	22.5º	S/P
3.75	33.75º	S
5.00	45º	P
7.50	67.5º	P

The series designed fan powered terminal units tested in this study were supplied by with the following calibration table (Table C-4) from "Manufacturer C." The parallel FPTUs did not come with similar documentation.

Table C-4: "Manufacturer C" ECM_S8C calibration table

CFM	0-10 VDC REF.	CFM	0-10 VDC REF.	CFM	0-10 VDC REF.	CFM	0-10 VDC REF.
0	0.00	390	2.72	720	5.16	1031	7.61
191	0.34	400	2.79	729	5.24	1040	7.68
191	0.41	410	2.86	738	5.31	1048	7.76
191	0.48	419	2.93	748	5.38	1057	7.83
191	0.56	429	3.00	757	5.45	1065	7.90
193	0.63	439	3.08	766	5.52	1074	7.97
195	0.70	449	3.15	776	5.60	1082	8.04
197	0.77	458	3.22	785	5.67	1091	8.12
200	0.84	468	3.29	794	5.74	1099	8.19
204	0.92	478	3.36	803	5.81	1107	8.26
208	0.99	488	3.44	813	5.88	1115	8.33
212	1.06	498	3.51	822	5.96	1123	8.40
217	1.13	508	3.58	831	6.03	1130	8.48
222	1.20	517	3.65	840	6.10	1138	8.55
228	1.28	527	3.72	850	6.17	1145	8.62
234	1.35	537	3.80	859	6.24	1152	8.69
240	1.42	547	3.87	868	6.32	1159	8.76
247	1.49	557	3.94	877	6.39	1166	8.84
253	1.56	566	4.01	886	6.46	1173	8.91
261	1.64	576	4.08	896	6.53	1179	8.98
268	1.71	586	4.16	905	6.60	1185	9.05
276	1.78	596	4.23	914	6.68	1191	9.12
284	1.85	605	4.30	923	6.75	1197	9.20
292	1.92	615	4.37	932	6.82	1202	9.27
300	2.00	625	4.44	941	6.89	1207	9.34
308	2.07	634	4.52	950	6.96	1211	9.41
317	2.14	644	4.59	959	7.04	1216	9.48
326	2.21	653	4.66	968	7.11	1219	9.56
335	2.28	663	4.73	977	7.18	1223	9.63
344	2.36	672	4.80	986	7.25	1226	9.70
353	2.43	682	4.88	995	7.32	1229	9.77
362	2.50	691	4.95	1004	7.40	1231	9.84
372	2.57	701	5.02	1013	7.47	1232	9.92
381	2.64	710	5.09	1022	7.54	1234	10.00

VITA

Name: Andrew Cramlet

Address: 2815 St Rt 555
Little Hocking, OH 45742

Email: cramlet@gmail.com

Education: B.S., Mechanical Engineering, The Ohio State University, 2002
M.S., Mechanical Engineering, Texas A&M University, 2008